



INTERNATIONAL ENERGY AGENCY
Energy conservation in buildings and
community systems programme

Technical Note AIVC **59**

Parameters for the design of demand controlled hybrid ventilation systems for residential buildings



Air Infiltration and Ventilation Centre
Operating Agent and Management
INIVE EEIG
Boulevard Poincaré 79
B-1060 Brussels
Belgium

INTERNATIONAL ENERGY AGENCY
Energy Conservation in Buildings and
Community Systems Programme

Technical Note AIVC 59

**Parameters for the design of demand
controlled hybrid ventilation systems for
residential buildings**

**Viktor Dorer
Andreas Pfeiffer
Andreas Weber**

March 2005

Copyright INIVE EEIG 2005

All property rights, including copyright are vested in the Operating Agent ([INIVE EEIG](#)) on behalf of the International Energy Agency.

In particular, no part of this publication may be reproduced, stored in a retrieval system or transmitted in any form or by any means, electronic, mechanical, photocopying, recording or otherwise, without prior written permission of the Operating Agent.

This report is part of the work of the IEA Energy Conservation in Buildings & Community Systems Programme - Annex V Air Infiltration and Ventilation Centre

Publication prepared by:

- Viktor Dorer
- Andreas Pfeiffer
- Andreas Weber

EMPA Swiss Federal Laboratories for Materials Testing and Research
Laboratory for Energy Systems and Building Equipment
CH-8600 Dübendorf, Switzerland

Acknowledgement

This report was written as part of the EU project RESHYVENT, Cluster Project on Demand Controlled Hybrid Ventilation in Residential Buildings with Specific Emphasis on the Integration of Renewables
Contract No: ENK6-CT2001-00533
WP 5 Design parameters

Document AIC-TN59
ISBN 2-9600355-7-7

Annex V Participating Countries:

Belgium, Czech Republic, France, Greece, Netherlands, Norway, and the United States of America.

Preface

International Energy Agency

The International Energy Agency (IEA) was established in 1974 within the framework of the Organisation for Economic Co-operation and Development (OECD) to implement an International Energy Programme. A basic aim of the IEA is to foster co-operation among the twenty-four IEA Participating Countries to increase energy security through energy conservation, development of alternative energy sources and energy research development and demonstration (RD&D).

Energy Conservation in Buildings and Community Systems

The IEA sponsors research and development in a number of areas related to energy. In one of these areas, energy conservation in buildings, the IEA is sponsoring various exercises to predict more accurately the energy use in buildings, including comparison of existing computer programs, building monitoring, comparison of calculation methods as well as air quality and studies of occupancy.

The Executive Committee

Overall control of the programme is maintained by an Executive Committee, which not only monitors existing projects but also identifies new areas where collaborative effort may be beneficial.

To date the following have been initiated by the Executive Committee (completed projects are identified by *):

- 1 Load Energy Determination of Buildings *
- 2 Ekistics and Advanced Community Energy Systems *
- 3 Energy Conservation in Residential Buildings *
- 4 Glasgow Commercial Building Monitoring *
- 5 Air Infiltration and Ventilation Centre
- 6 Energy Systems and Design of Communities *
- 7 Local Government Energy Planning *
- 8 Inhabitant Behaviour with Regard to Ventilation *
- 9 Minimum Ventilation Rates *
- 10 Building HVAC Systems Simulation *
- 11 Energy Auditing *
- 12 Windows and Fenestration *
- 13 Energy Management in Hospitals*
- 14 Condensation *
- 15 Energy Efficiency in Schools *
- 16 BEMS – 1: Energy Management Procedures *
- 17 BEMS – 2: Evaluation and Emulation Techniques *
- 18 Demand Controlled Ventilation Systems *
- 19 Low Slope Roof Systems *
- 20 Air Flow Patterns within Buildings *
- 21 Thermal Modelling *
- 22 Energy Efficient communities *
- 23 Multizone Air Flow Modelling (COMIS)*
- 24 Heat Air and Moisture Transfer in Envelopes *
- 25 Real Time HEVAC Simulation *
- 26 Energy Efficient Ventilation of Large Enclosures *
- 27 Evaluation and Demonstration of Residential Ventilation Systems *
- 28 Low Energy Cooling Systems *

29	Daylight in Buildings *
30	Bringing Simulation to Application *
31	Energy Related Environmental Impact of Buildings *
32	Integral Building Envelope Performance Assessment *
33	Advanced Local Energy Planning *
34	Computer-aided Evaluation of HVAC Systems Performance *
35	Design of Energy Hybrid Ventilation (HYBVENT) *
36	Retrofitting of Educational Buildings *
36 WG	Annex 36 Working Group Extension 'The Energy Concept Adviser'
37	Low Exergy Systems for Heating and Cooling of Buildings *
38	Solar Sustainable Housing
39	High Performance Insulation systems (HiPTI)
40	Commissioning Building HVAC Systems for Improved Energy Performance
41	Whole Building Heat, Air and Moisture Response (MOIST-EN)
42	The Simulation of Building-Integrated Fuel Cell and Other Cogeneration Systems (COGEN-SIM)
43	Testing and Validation of Building Energy Simulation Tools
44	Integrating Environmentally Responsive Elements in Buildings
45	Energy-Efficient Future Electric Lighting for Buildings
46	Holistic Assessment Tool-kit on Energy Efficient Retrofit Measures for Government Buildings (EnERGo)

Annex V: Air Infiltration and Ventilation Centre

The Air Infiltration and Ventilation Centre was established by the Executive Committee following unanimous agreement that more needed to be understood about the impact of air change on energy use and indoor air quality. The purpose of the Centre is to promote an understanding of the complex behaviour of air flow in buildings and to advance the effective application of associated energy saving measures in both the design of new buildings and the improvement of the existing building stock.

The Participants in this task are Belgium, Czech Republic, France, Greece, Netherlands, Norway, and the United States of America.

Disclaimer

AIVC has compiled this publication with care. However, AIVC does not warrant that the information in this publication is free of errors. No responsibility or liability can be accepted for any claims arising through the use of the information contained within this publication. The user assumes the entire risk of the use of any information in this publication.

Content

SCOPE	1
NOMENCLATURE	2
1. INTRODUCTION	5
1.1. THE RESHYVENT PROJECT	5
1.2. THE FOUR RESIDENTIAL HYBRID VENTILATION SYSTEMS DEVELOPED IN THE FRAME OF THE RESHYVENT PROJECT	6
1.2.1. System 1 for cold climate (Sweden)	7
1.2.2. System 2 for moderate climate (The Netherlands)	8
1.2.3. System 3 for warm climate (Belgium/France)	9
1.2.4. System 4 for severe cold climate (Norway)	11
2. WIND EFFECTS IN THE BUILT ENVIRONMENT	13
2.1. STATE-OF-THE-ART, PRESENT KNOWLEDGE	13
2.1.1. From the undisturbed wind to the pressure acting on a façade element	13
2.1.2. Boundary layers, wind profiles	13
2.1.3. From meteo wind to wind on site	14
2.1.4. Shielding effect	16
2.1.5. Air flow in road canyons	16
2.1.6. Wind pressure distribution on building envelope	17
2.1.7. Methods of wind pressure determination	18
2.1.8. Cp-values on openings	19
2.1.9. Impact of balconies on Cp-values	20
2.1.10. Impact of wind fluctuations	20
2.1.11. How to handle the intrinsic uncertainties	21
2.2. ON WIND DATA IN METEO FILES	21
2.3. WIND EFFECTS IN THE URBAN ENVIRONMENT	21
3. COWL PERFORMANCE AND ABOVE ROOF AIR FLOW FIELDS	22
3.1. COWL PERFORMANCE	22
3.1.1. Pressure difference on cowls	22
3.1.2. Characteristics of different cowl types	22
3.1.3. Using experimental data	24
3.2. FROM EXPERIMENTAL DATA TO PRESSURE DIFFERENCES OF COWLS ON THE ROOF	25
3.2.1. CFD-calculations of air flow patterns around buildings	26
3.2.2. Using CFD results for cowl performance calculation	32
3.2.3. How to model cowl performance with TRNSYS?	38
4. INFLUENCE OF BUILDING LEAKAGE ON PRESSURE LEVELS AND OUTDOOR AIR FLOW RATES	40
4.1. BUILDING LEAKAGE	40
4.2. BUILDING LEAKAGE DISTRIBUTION	41
4.2.1. Pressure difference due to stack	41
4.2.2. Pressure difference due to wind	41
4.2.3. Combination of stack and wind differential pressure	42
4.2.4. Influence of wind and stack effect on the air change (COMIS calculations)	44
5. PRESSURE DIFFERENCE ACROSS FAÇADES, EXHAUST GRIDS AND FAN	46
5.1. GENERIC RESULTS OF COMIS SIMULATION FOR SYSTEM 2	46
5.1.1. Building	46
5.1.2. System	46
5.1.3. Outdoor climate	46
5.1.4. Presentation of results	48
5.1.5. General characteristics of the cumulative diagrams	48
5.1.6. Impact of the building leakage	48
5.1.7. Impact of imbalance	50
5.1.8. Impact of the self regulating supply grids	51
5.1.9. Impact of resistances of exhaust ducts	53
5.1.10. Conclusions	54

6.	EFFECT OF OUTDOOR AIR TRANSFER DEVICES ON ROOM AIR FLOW AND THERMAL COMFORT	55
6.1.	INTRODUCTION	55
6.2.	EXPERIMENTAL INVESTIGATIONS	55
6.2.1.	<i>Overview of the investigated outdoor air transfer devices</i>	<i>55</i>
6.2.2.	<i>Draft risk</i>	<i>56</i>
6.2.3.	<i>Occupied zone</i>	<i>56</i>
6.2.4.	<i>Experiments in the room climate laboratory of EMPA</i>	<i>56</i>
6.2.5.	<i>Influence of the ATD geometry</i>	<i>57</i>
6.2.6.	<i>Influence of the installation position of the ATD</i>	<i>58</i>
6.2.7.	<i>Influence of a convective heating element</i>	<i>59</i>
6.2.8.	<i>Influence of obstacles</i>	<i>60</i>
6.2.9.	<i>Influence of net curtains</i>	<i>60</i>
6.2.10.	<i>Influence of the air supply temperature</i>	<i>61</i>
6.2.11.	<i>Conclusions</i>	<i>62</i>
6.3.	THEORY OF AIR JETS APPLIED TO THE FLOW FIELD OF ATD	63
6.3.1.	<i>Archimedes-number [Recknagel 2001]</i>	<i>63</i>
6.3.2.	<i>Basic equations for the flat free jet [Recknagel 2001]</i>	<i>63</i>
6.3.3.	<i>Coanda Effect</i>	<i>64</i>
6.3.4.	<i>Non-isothermal horizontal flat free jet [Recknagel 2001]</i>	<i>65</i>
6.3.5.	<i>Theory of displacement ventilation according to [Heiselberg 2001]</i>	<i>65</i>
6.3.6.	<i>Displacement flow characteristic values of ATD</i>	<i>66</i>
6.4.	COMFORT EVALUATION USING CFD	68
6.4.1.	<i>Boundary conditions for the CFD calculations</i>	<i>68</i>
6.4.2.	<i>Geometry and simplifications</i>	<i>69</i>
6.4.3.	<i>Heat sources</i>	<i>69</i>
6.4.4.	<i>Calculation grid</i>	<i>70</i>
6.4.5.	<i>Evaluation of draft risk and comparison with measurements W-R-OS (case 1)</i>	<i>72</i>
6.4.6.	<i>Evaluation of draft risk at a supply temperature of –10 °C W-R-OS (case 2)</i>	<i>73</i>
6.4.7.	<i>Evaluation of draft risk at a supply temperature of –10 °C and convective heating element W-R-OS (case 3)</i>	<i>74</i>
6.5.	ATD WITH SUPPLY AIR PREHEATING CAPABILITY	75
6.5.1.	<i>Technical principle</i>	<i>75</i>
6.5.2.	<i>Water supply of the heat exchanger</i>	<i>75</i>
6.5.3.	<i>Generic results of simulation work for system 1</i>	<i>75</i>
7.	IAQ RELATED FACTORS	80
7.1.	POLLUTANT SOURCES DUE TO HUMAN METABOLISM	80
7.1.1.	<i>CO₂ production rates</i>	<i>80</i>
7.1.2.	<i>Water vapour release</i>	<i>81</i>
7.1.3.	<i>Situation in dwellings</i>	<i>81</i>
7.2.	INTERNAL POLLUTANT SOURCES	81
7.2.1.	<i>Water vapour release</i>	<i>81</i>
7.2.2.	<i>Smoking</i>	<i>82</i>
7.2.3.	<i>Gas cooking</i>	<i>82</i>
7.2.4.	<i>Material related sources</i>	<i>83</i>
7.2.5.	<i>Ground related sources</i>	<i>84</i>
7.3.	OCCUPANT PRESENCE AND ACTIVITY SCHEDULES	85
7.3.1.	<i>Stochastic occupancy model</i>	<i>85</i>
8.	APPLICATION POSSIBILITIES AND LIMITS OF CFD	87
8.1.	MODELLING OF AIR FLOWS AROUND BUILDINGS	87
8.1.1.	<i>General modelling guidelines from literature</i>	<i>87</i>
8.1.2.	<i>Comparison and verification with literature</i>	<i>89</i>
8.1.3.	<i>Three dimensional air flow around a cubic building</i>	<i>89</i>
8.1.4.	<i>Two and three dimensional air flow around a glass house with pitched roof</i>	<i>99</i>
8.1.5.	<i>Typical flow phenomena</i>	<i>104</i>
9.	REFERENCES	106

Scope

This AIVC Technical Note has been produced in the frame of the EU RESHYVENT project, conducted from January 2002 to December 2004. An outline of this project is given in the introduction of this report. The report initially was aimed at the project participants; however, many information may also be of general interest to manufacturers and designers of hybrid residential ventilation systems. Therefore it has been made available to a wider audience by publication as an AIVC TN.

For the design of demand controlled hybrid ventilation systems for residential buildings, the report gives detailed background information on topics which are not sufficiently covered by existing literature (e.g. wind pressures or thermal comfort evaluation by CFD simulation). The report also gives detailed information on input data necessary to perform computer simulations for the performance analysis of systems.

Within RESHYVENT, the information and data given in this report were aimed at the industrial consortia for the development and analysis of their systems and performance assessment simulations. Parts of this report were also used for the preparation of the RESHYVENT source book on residential hybrid ventilation.

Nomenclature

Variables

A	area	$[m^2]$
C_d	discharge coefficient	$[-]$
C_p	wind pressure coefficient	$[-]$
$C_{p/V=0}$	value of C_p when $V=0$ (velocity in the duct)	$[-]$
C_Q	flow velocity coefficient	$[-]$
C_{Qp}	predicted C_Q	$[-]$
DR	draft risk	$[\%]$
d	zero plane displacement	$[m]$
Fr	Froude number	$[-]$
g	acceleration of gravity	$[m/s^2]$
h	height	$[m]$
I_w	wind performance indicator	$[-]$
L	length	$[m]$
m	mixing number	$[m]$
p_d	dynamic pressure	$[Pa]$
p_s	static pressure	$[Pa]$
$p_{s,r}$	static reference pressure in undisturbed wind at the same height	$[Pa]$
$p_{s,cowl}$	static pressure in wind tunnel at cowl position	$[Pa]$
$p_{t,duct}$	total pressure in the duct	$[Pa]$
p_w	wind pressure on the building façade	$[Pa]$
Δp_w	wind induced pressure difference on the terminal (cowl)	$[Pa]$
Δp_i	wind and duct flow interaction pressure loss	$[Pa]$
Δp_{loss}	pressure loss due to the air flow in the duct	$[Pa]$
Q	air flow	$[m^3/s]$
S	shelter factor	$[-]$
T	absolute temperature	$[K]$
Tu	turbulence	$[\%]$
U	local wind speed at cowl position	$[m/s]$
u	normalized local wind speed at cowl position	$[-]$
U_{10}	undisturbed wind speed at 10 m height	$[m/s]$
U_r	undisturbed wind speed at building reference height	$[m/s]$
V	air flow velocity in the duct	$[m/s]$
v	wind speed	$[m/s]$
v	local air velocity	$[m/s]$
$(V/U)_{C_p=0}$	ratio V/U when $C_p=0$	$[-]$
\dot{V}	volume flow	$[m^3/s]$
x_0	fictive origin of the jet	$[m]$
z	height	$[m]$
z_r	building reference height	$[m]$
α	roof pitch angle	$[^\circ]$
α	wind profile exponent	$[-]$
β	wind direction angle	$[^\circ]$
φ	vertical wind incidence angle	$[^\circ]$
Φ	porosity	$[-]$
ρ	air density	$[kg/m^3]$
ϑ_L	local air temperature	$[^\circ C]$
ζ	dynamic loss coefficient	$[-]$

Indices

<i>0</i>	aerodynamic roughness
<i>1</i>	position 1
<i>2</i>	position 2
<i>act</i>	actual
<i>b</i>	building
<i>J</i>	jet
<i>m</i>	meteo
<i>o</i>	opening
<i>ref</i>	reference
<i>R</i>	room
<i>s</i>	sheltered
<i>u</i>	boundary layer
<i>w</i>	wind
<i>w</i>	wall
<i>x,y,z</i>	x-, y-, z- direction

1. Introduction

1.1. The RESHYVENT project

From January 2002 to December 2004 the EU RESHYVENT was executed within the EU Fifth Framework Programme on the investigation and development of demand controlled hybrid ventilation systems in residential buildings. The project is a clustering of four industrial consortia with a multi-disciplinary scientific consortium. Each of these industrial consortia has developed a working prototype of a hybrid ventilation system for a specific climate. A scientific group with 12 partners from research institutes, consultants and universities has carried out the scientific research work for the development of these systems.

The key elements of the RESHYVENT project are reflected in the subtitle of the project “Cluster Project on Demand Controlled Hybrid Ventilation in Residential Buildings with specific emphasis of the Integration of Renewables”.

Hybrid Ventilation

Hybrid ventilation is defined in accordance with the IEA Annex 35 project “Hybrid ventilation for offices and schools” as a two-mode system that is controlled to minimise the energy consumption while maintaining acceptable indoor air quality and thermal comfort. The two modes refer to natural and mechanical driving forces.

Hybrid ventilation systems must provide air for indoor air quality, thermal conditioning and thermal comfort. A control system has to establish the desired air flow rate and pattern at the lowest energy consumption possible. This means:

- air flows will be exactly controlled to the actual needs, based on thermal comfort and IAQ;
- using natural driving forces as long as possible, using mechanical forces when necessary

Demand Controlled Ventilation

Ventilation is exactly tuned to the demands of the users, in terms of IAQ and thermal comfort under all climatic conditions. This means in general the use of sensors and developing ventilation and control strategies. The control system is the heart of the whole system.

Integration of Renewables

Within the RESHYVENT project there was specific emphasis on the application of renewables. Despite the hybrid character of the system auxiliary energy is needed for running the fans, the sensors and the control system. This energy is, as far as possible, be generated by sustainable technologies, such as PV and wind energy. Besides that renewable energy is used for optimising wind and solar effects. In this case wind-optimised cowls and solar chimneys are technologies which were developed.

Residential Buildings

The scope of the project was residential buildings, single family houses as well as multifamily houses in the new build sector and the existing sector. The hybrid ventilation systems were developed for different climates, ranging from (sever) cold, moderate, mild to warm. Specific attention was paid to the thermal comfort conditions during winter (draught) for the cold and moderate climates and for the thermal conditions during summer (overheating) for the mild and warm climates.

Project organisation and deliverables

The RESHYVENT project was a clustering of four industrial consortia with a multi-disciplinary scientific consortium. The industrial consortia were served and supported by scientific Support Units corresponding with the defined tasks in the work packages. Each of the four Industrial Consortia had a "scientific coach". Their task was to coach the industries in their RTD work and to operate as an intermediary to the scientific partners and the co-ordinator.

To come to the final output and deliverables of the practical and generic part a number of supporting research activities were undertaken in the scientific support units. The scientific research work was organised in a number of work packages. The industrial partners could consult these work packages.

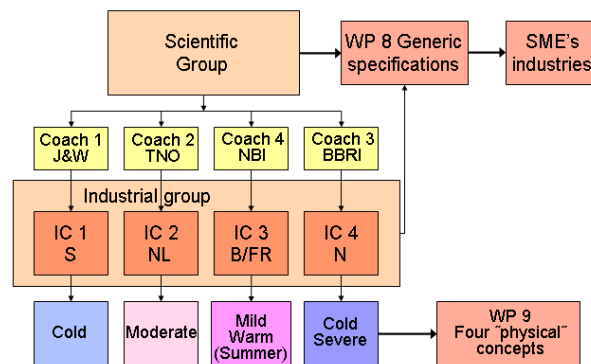


Figure 1.1: The organisation structure of RESHYVENT

The project had two types of deliverables:

- A practical part, i.e. the development and construction of components, products and systems, to be demonstrated after completion of the project and, later, commercially exploited and launched on the market by industries.
- A generic part, i.e., all developed knowledge, (technical, economical, social etc.) as well as all supporting tools, instruments and documents will be disposable for EU industries.

Work package 5 dealt with design parameters, sensitivity analyses and design constraints, focusing on essential elements like wind effects in the built environment and modelling air flows in spaces. The project results are documented in this AIVC TN.

More information of the RESHYVENT project can be found on the website: www.reshyvent.com

1.2. The four residential hybrid ventilation systems developed in the frame of the RESHYVENT project

In the RESHYVENT project four industrial consortia (IC) were formed, each containing a number of industrial partners. Each IC addressed a defined task to develop and construct a demand controlled hybrid ventilation system. Each industrial consortium focused on a specific application field (climate, building and application of renewables). This had consequences on the significance of thermal comfort in summer and winter conditions and ventilation components for supply and exhaust, see table 1.1.

Table 1.1: Application fields of the four hybrid ventilation systems developed within RESHYVENT

	IC 1 – Sweden	IC 2 – Netherlands	IC 3 – Belgium/France	IC 4 – Norway
Climate	Cold	Moderate	Mild and warm	Severe
Building type	Apartments	Dwellings Apartments	Dwellings	Dwellings
Renewables	PV, Wind. Heat recovery optional	PV Wind	PV	Wind Heat recovery
Summer Comfort	No	Limited	Crucial	No
Winter Comfort	Important	Important	Important	Crucial
Supply	Crucial	Important	Important	Crucial
Exhaust	Crucial	Crucial	Crucial	Crucial

Ventilation in apartments

- one self regulated flow constant volume flow EC fan per apartment
- exhaust air terminal devices in bathroom, lavatory and kitchen
- outdoor air inlets with back flow damper, in façade of bedroom and living room
- pre-adjusted normal ventilation as a function of number of persons, the number can be set by the user
- high efficiency cooker hood with manually forced ventilation with timer
- Lowered ventilation when no one at home, manual or automatic (controlled by burglar lock of entrance door or pre-set timer) control. The fan can be turned off.
- lowered ventilation at night in living room, manual or automatic (pre-set timer) control
- relative humidity controlled ventilation in bathroom i.e. preventing lowered ventilation if high humidity level and no one at home

Ventilation of common areas

- demand controlled ventilation of common areas like stairwell, bicycle storeroom, apartment storerooms, laundry room, technical rooms or central air-to-air heat recovery from exhaust air to supply air (to some of the common rooms)

Space heating apartments

- supply air to bedrooms pre-heated by supply air radiator
- bedrooms heated by radiator
- supply air to living room pre-heated to 18 °C by special convector with back draft damper
- living room heated by radiator and convector
- indoor temperature 19 °C – 23 °C

1.2.2. System 2 for moderate climate (The Netherlands)

The Dutch consortium had elaborated two concepts: one for 2004 (ready at end of the project) and one for 2010. The 2004 concept is a fully hybrid demand controlled system with de-central supply from the facade and a coupled hybrid central mechanical extract. A characteristic development in this concept is an extreme low-resistance ductwork ($< 2 \text{ Pa}$ at $56 \text{ dm}^3/\text{s}$) based on the experiences and components developed within the EC TIPVENT project. A special fan is developed using 2 Watt at $56 \text{ dm}^3/\text{s}$ at 20 Pa . This extreme low fan power is possible by a combination of the low pressure duct work and wind optimised cowls ($< 1 \text{ Pa}$ at $56 \text{ dm}^3/\text{s}$). Supply grilles are actively controlled with compensation for cross flow and infiltration. The advanced control system is being developed in close co-operation with WP7. The prototype was tested in 2003 in laboratory. In 2004 the system was installed in a newly build test house at the by Brno University of Technology Czech Republic and since then has been extensively tested.

System description

Figure 1.1 gives an overview of the system. A single-family house is shown, with the living room and the kitchen at the ground floor and the bathroom and the bedrooms at the first floor. To reduce the flow resistance the exhaust is lined up under the roof outlet.

The ventilation flow is demand controlled. For the living room and the bedrooms CO_2 sensors are foreseen. Also other sensors to detect the presence of persons like infrared (IR) can be used. A central control unit receives information from these sensors and gives set points to the self-regulating inlets and vents and, if necessary, starts and controls the fan. The nominal total flow rate is $56 \text{ dm}^3/\text{s}$. However the maximum flow rate is foreseen at $100 \text{ dm}^3/\text{s}$, which can be used during cooking, showering and for passive cooling.

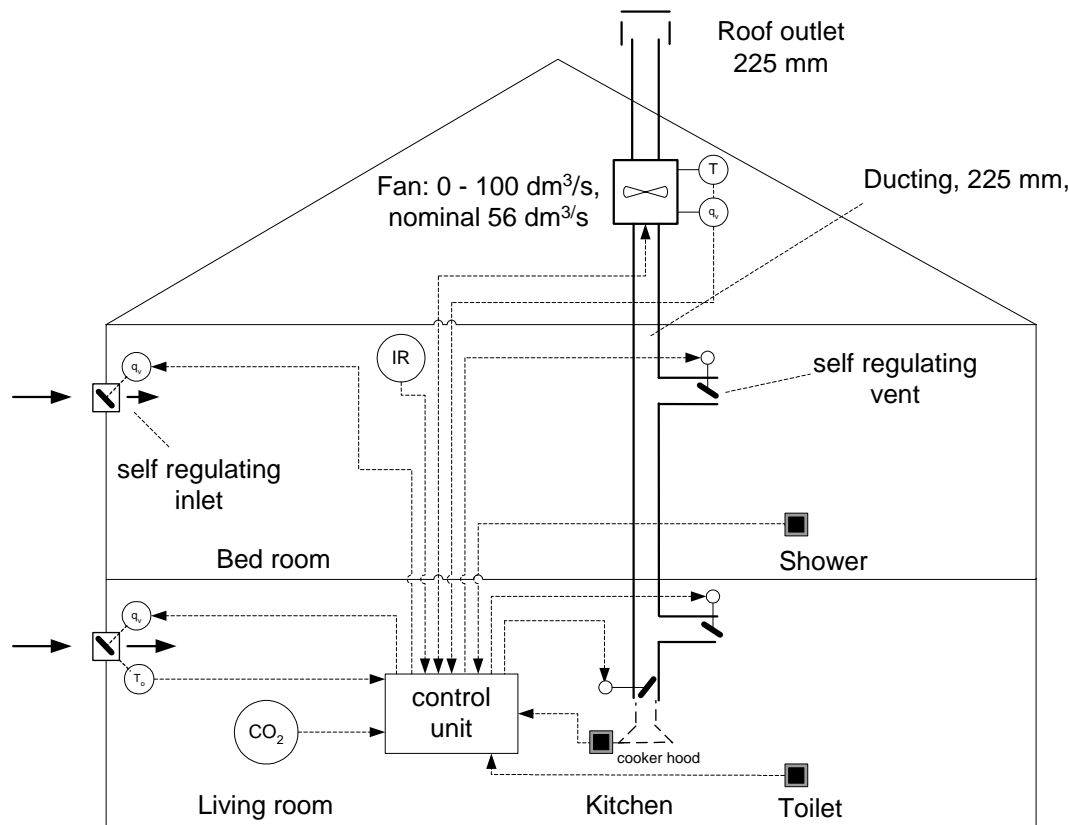


Figure 1.3: The demand controlled hybrid ventilation system for moderate climate

Supply

The supply inlets comply with the following requirements:

- Self-regulating inlets;
- Placement in window frame;
- Draught correction (comfort);
- Allow for (separate) cooker hood, compensation of supply during use of hood by control unit;
- Possibility for passive cooling (through ventilation) through extra fixed inlet with larger geometric aperture;
- Building leakage compensation on inlets.

Distribution

The distribution components will comply with the following requirements:

- Pressure drop over ducting @ 56 dm³/s maximum 2 Pa;
- Ducting round maximum 225 mm;
- Improved coupling fittings;
- Limited noise propagation (cross transmission of noise) especially with regard to fan;
- Special fittings for apartments with individual units on central exhaust;
- Development self-regulating vents at approximate 5 Pa pressure difference with controllable flow rate.

1.2.3. System 3 for warm climate (Belgium/France)

The purpose of the Belgian/French system is to provide one improved ventilation system allowing significant good indoor air quality, heating (and cooling) energy savings and acceptable thermal comfort on summer, by using especially renewable energy.

This concept is based on sensors measuring relative humidity in bathroom and kitchen, occupancy in bedrooms and toilet, and agitation (i.e. the number of people) in the living room.

Driving forces are as much as possible natural ones (thermal stack effect, and wind induction), assisted with a photovoltaic supplied “roof cowl fan” whose speed is adapted to only compensate natural stack effect deficiency in the hotter times.

According to total ventilation forces evaluation, motorised inlets and extract grilles are driven in order to ensure suitable air renewal in each room, in correlation with need measurements.

In case of very hot times, a “night cooling” mode consist in an “over-ventilation”(maximum fan assistance) and in the opening of motorised windows, during summer nights, when outdoor temperature is colder than indoor.

System concept

The concept, developed for mild and moderate climates, is a demand controlled ventilation system based on sensors for presence detection, agitation detection, relative humidity and temperature. The summer comfort issue is specially handled by the integration of intensive ventilation devices into the system. A first version of this system has been developed during the EU SAVE project Photovent. This system was not yet a two mode system at that time and the aspect of summer comfort was not yet integrated. It has been farther developed into a hybrid system during the RESHYVENT project, among other thanks to the development of the fan.

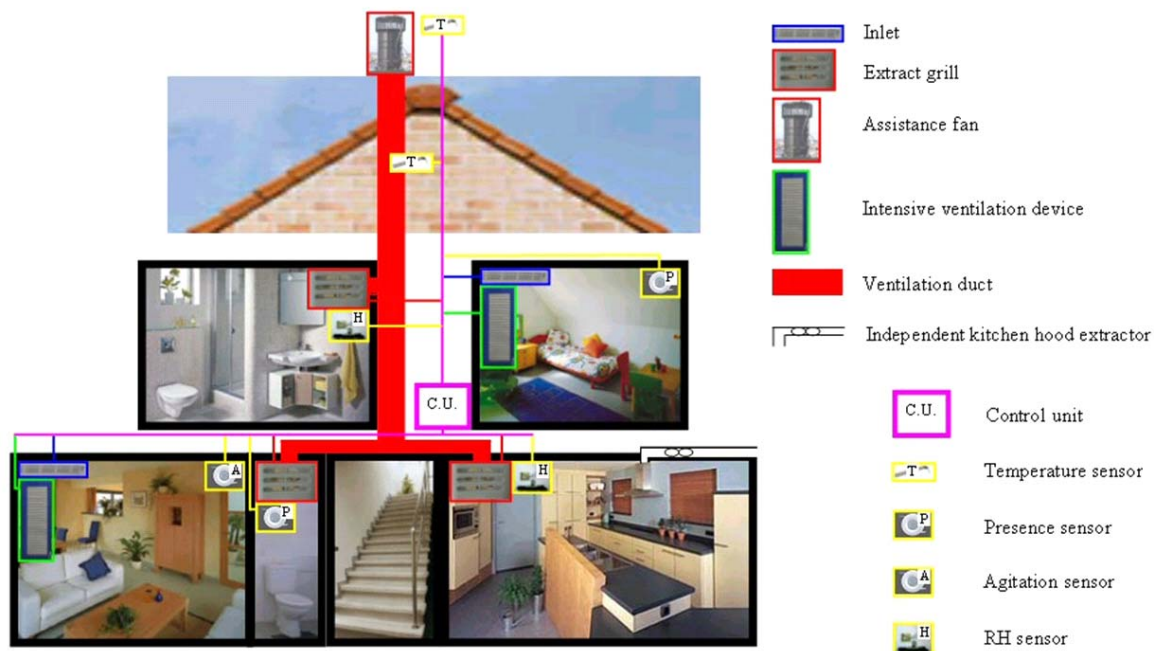


Figure 1.4: Concept of the system 3 for warm climate (Belgium/France)

All the ventilation devices such as air inlets, outlets and intensive ventilation device are motorised and these devices as the fan are piloted by a central control unit, determining the airflow in each room, speed of the fan and the opening of some windows. The balance between supply and exhaust is continuously guaranteed by the central control unit which makes the needed adjustment to the system. Air supply is provided by naturally dimensioned motorised inlets. Air exhaust is provided by naturally dimensioned motorised outlets. The exhaust is a fan-assisted low resistance air duct (160 mm square duct) equipped with low resistance connection fittings. The airflows in the kitchen and bathroom are regulated by relative humidity controlled devices when no presence is detected and by the presence detection otherwise. The airflow in the dry rooms (living room, bedrooms) is controlled by presence and agitation detection. Minimal airflows are realised when no presence is detected.

A crucial part of the system is the fan (figure 1.5). It has been specially developed to allow natural ventilation when it is switched off. The development of this fan is described in the proceedings of the 2001 AIVC conference. The pressure losses due to the fan are lower than 1Pa for airflows of 70dm³/s.

The fan, placed on the roof, has also been optimised (a.o. via wind tunnel testing) to act as roof cowl to benefit of the wind effect. The energy consumption of the fan is 2W at 6Pa or 70dm³/s. Prototype of PV-supply of the fan is now available.

The hybrid character of the system comes from the fact that the fan is switched off when the outdoor conditions are favourable which makes this system a two-mode system and not a low-consuming mechanical system. The integration of the night-cooling mode into the system could be considered as a third mode-system.

The communication between the components of the system can occur via wires or via a wireless solution. The wireless solution (433 MHz radio-commanded) makes this system particularly convenient for refurbishment applications.

The system has been optimised to insure a good thermal comfort during summer conditions. Motorised windows equipped with intensive natural ventilation louvres or solar shading are part of the system. These louvres allow the application of night cooling strategies in the building.



Figure 1.5: Exhaust fan used for the system3:

- power consumption: 2W at 6Pa or 70dm³/s
- acting as roof cowl when switched off
- pressure loss (switched off): <1 Pa for 70dm³/s

1.2.4. System 4 for severe cold climate (Norway)

The Norwegian concept is being developed for extreme cold climates. For these conditions heat recovery is necessary for preheating and to recover energy. The System 4 concept is an attempt to unite the benefits of heat recovery with very low pressure drop systems. It has the following features:

- Balanced ventilation with a modular packaged air handling unit (AHU) with minimal air flow resistance, and the following components: 2 efficient axial fans with EC motors, air-to-air heat exchanger (rotary), electrostatic air filter (washable metal filter).
- Natural ventilation assistance with a roof-mounted wind cowl (integrated inlet and exhaust cowl). The concept system is dimensioned such that the system can operate on full natural ventilation when the building is unoccupied, since the required flow rate can be allowed to drops from 0.5 air changes per hour to approx 0.2 air changes per hour when the building is unoccupied. The system is dimensioned such that the system pressure drop is 5 Pa at 0.2 air changes, which is the same as the available natural driving forces.
- Demand-controlled ventilation:
 - The ventilation flow rate is controlled according to a CO₂ or RH sensor (or both) placed in the exhaust air side of the ventilation unit. The air flow rate is controlled to keep the concentration below a certain value (PI-controller). When the building is normally occupied, the fan power is 25 W (an additional 5 W is provided by natural driving forces). When the building is unoccupied over long periods, the fan power can drop to 0 W, since the natural driving forced alone are sufficient for the required 5 Pa.

- A motorized damper is placed in the air supply duct to the living room. The damper is controlled by an IR-sensor in the living room. When the living room is vacated, more of the supply air is diverted to the bedrooms.
- All components are designed for low pressure losses: Shorter wider ducts that permit easier inspection and cleaning, low velocity air supply/exhaust terminals (thus low noise generation, the low velocity promoting displacement ventilation in bedrooms).

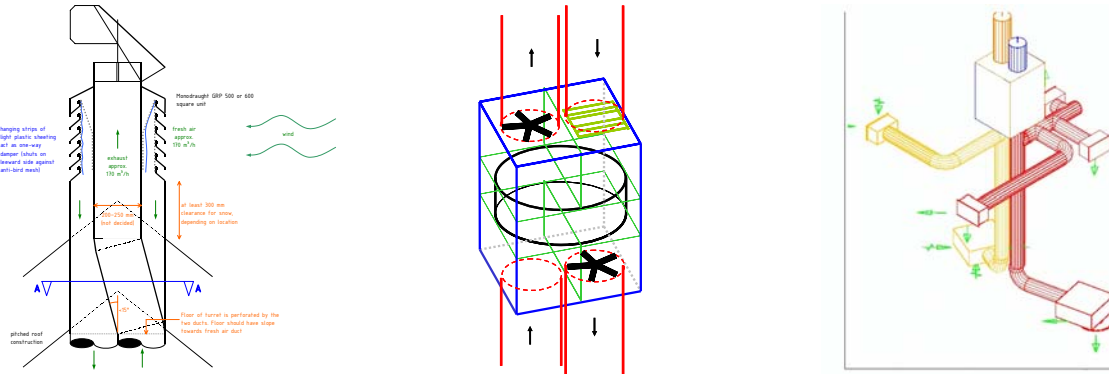


Figure 1.6: Parts of the system: the wind vane with the wind augmented inlet, the rotary heat exchanger and the duct system.

2. Wind effects in the built environment

2.1. State-of-the-art, present knowledge

2.1.1. From the undisturbed wind to the pressure acting on a façade element

The wind pressure acting on the façade of a building is dependent on wind speed and direction, topography and roughness of the terrain upstream, location of the building relative to other structures or vegetation and building shape. With reference to the static pressure in the free stream at the same height, wind pressure on the building surface can be determined for individual façade elements with:

$$p_w = p - p_{s,r} = C_p \frac{\rho}{2} v_{ref}^2 \quad (1)$$

Several methods are available for the determination of the wind pressure coefficients. Wall averaged C_p -values for simple building shapes in isolated terrain can be found in literature. Tools for the statistical regression of wind tunnel data sets have been developed and can be used in a wider range of application (limits of applicability to be checked for the individual tools). Specific wind tunnel tests or CFD analysis must be applied for unusual building geometry or specific situations of surrounding structures. Wind pressure coefficients have to be determined for several individual wind directions, usually in regular increments of 30° to 45°. Values for intermediate wind directions can be interpolated from this data.

Usually there is no measured wind speed data available exactly from the building site and at the building reference height. Therefore, a transfer method for the wind data from the nearest meteorological station must be applied.

2.1.2. Boundary layers, wind profiles

The wind speed profile in the boundary layer is dependent on the upstream terrain roughness and can be described with different models.

Power law

$$\frac{U_2}{U_1} = \left(\frac{z_2}{z_1}\right)^\alpha \quad (2)$$

Logarithmic law

$$\frac{U_2}{U_1} = \frac{\ln(z_2 / z_0)}{\ln(z_1 / z_0)} \quad (3)$$

Table 2.1 shows values for the profile exponent α and the roughness height z_0 for different terrain roughness classes

Table 2.1: Terrain roughness classes and the according profile exponent α , roughness height z_0 , and thickness of the boundary layer z_u [Wolfenseher 1978]

class	terrain description	α	z_0	z_u
1	sea, flat terrain without obstacles	0.1 - 0.15	0.005 - 0.05	240 - 320
2	open terrain with isolated obstacles	0.15 - 0.25	0.05 - 0.5	320 - 400
3	wood, small city, suburb	0.25 - 0.35	0.5 - 1.5	400 - 480
4	city centre	0.35 - 0.45	1.5 - 3	480 - 550

Wind profile in urban areas

In urban areas, the above described speed profile is shifted upwards with the zero-plane-displacement d :

$$\frac{U_2}{U_1} = \left(\frac{z_2 - d}{z_1 - d} \right)^\alpha \quad (4)$$

or

$$\frac{U_2}{U_1} = \frac{\ln((z_2 - d) / z_0)}{\ln(z_1 - d / z_0)} \quad (5)$$

According [Grimmond and Oke 1999], for d a value of 0.7 of the average height h_b of the buildings in the surrounding area can be taken, if $0.3 \leq \lambda_p \leq 0.5$ and $0.1 \leq \lambda_f \leq 0.3$. Here the two parameters used are the non-dimensional front-area $\lambda_f = A_f / A_T$, and the non-dimensional plan-area, $\lambda_p = A_p / A_T$, where A_T denotes the total area, A_p is the area occupied by buildings, and A_f is the frontal area of the buildings (calculated as the product from the average height and the average width). If the above conditions are not fulfilled (in particular, if the density of buildings is low), the method given by [Kutzbach 1961] may be used:

$$d = \lambda_p^{0.29} h_b, \quad \lambda_p \leq 0.29 \quad (6)$$

[Santamouris 2000] describes the wind speed in the obstructed sublayer between ground and building height with an exponential profile:

$$U = U_0 e^{z/Z_0} \quad (7)$$

Where U_0 is a constant reference speed and Z_0 is the roughness length of the obstructed sublayer and can be approximated for the city:

$$Z_0 = 0.1 h_b^2 / z_0 \quad (8)$$

The zero-displacement-plane d in equation (5) and the reference speed U_0 in equation (7) are then determined by the requirement that the wind speed at the building height must be equal in both profiles.

2.1.3. From meteo wind to wind on site**Simple method**

The transfer of wind speed data from meteo location to the building site with the simple method uses only the wind profile from both locations. It may be applied for flat topography without any hill or mountain between the two places and building locations not too far from measurement site. This method has been implemented in the multizone air flow model COMIS.

With the profile of the meteorological station site undisturbed wind speed v_u above boundary layer can be calculated. Therefore the height of the weather-pylon z_M and the thickness of the boundary layer z_u must be known. Thickness of boundary layer z_u is dependent on the terrain roughness. Values are given in table 2.1.

It is assumed that the undisturbed wind speed is the same above meteo station and above building site. The speed profile of the building location can be used to calculate the speed v_{ref} at building reference height.

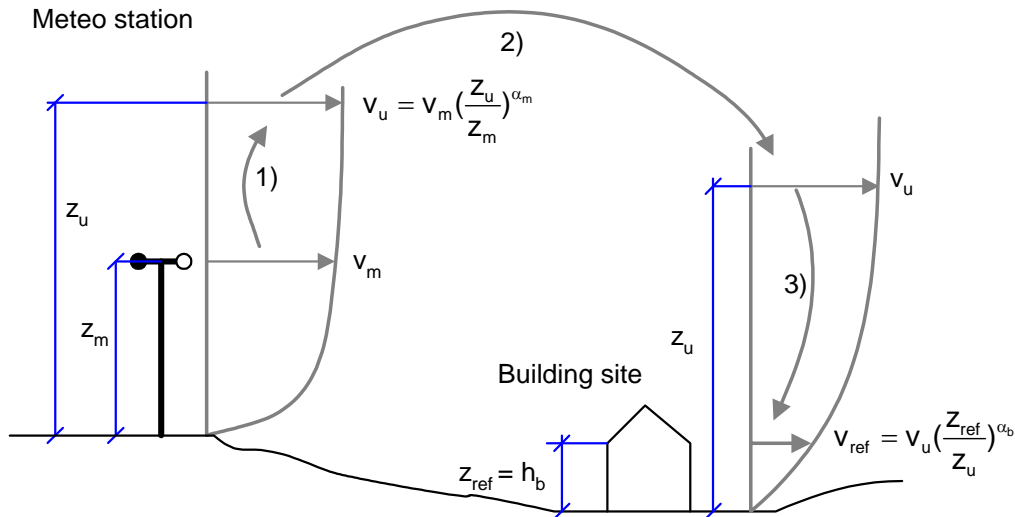


Figure 2.1: Transfer of wind speed data from meteo location to building location in flat topography with the simple method using the two local wind profiles

Advanced Method

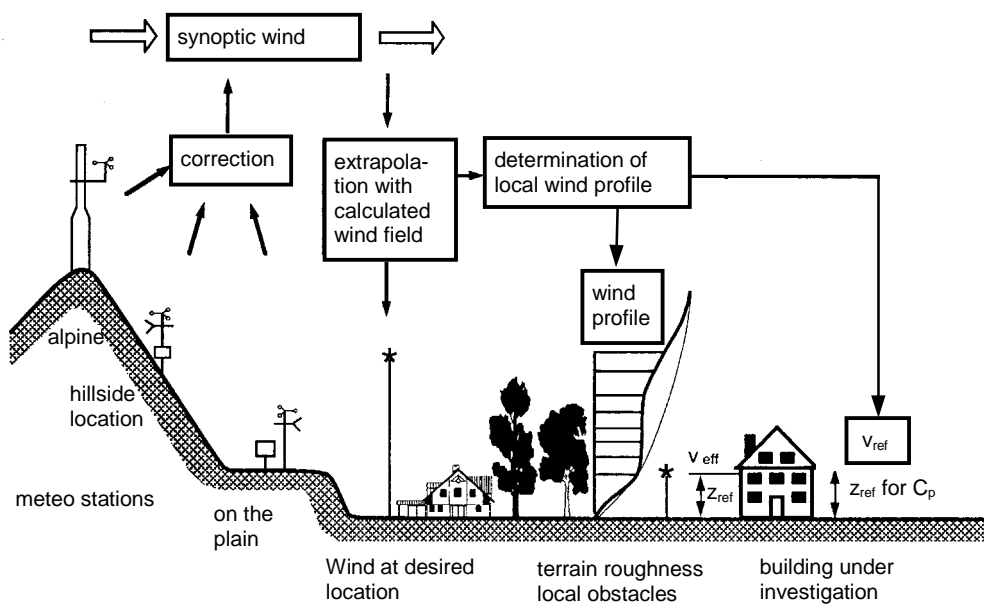


Figure 2.2: Transfer of wind speed data from meteo location to building location in complex topography with the advanced method using a meso-scale model of the concerning region

For complex topography, such as a hill country or a mountainous region, an advanced method [Hertig 1990 and 1993] for the wind data transfer must be applied:

- 1) Determination of the synoptic wind in the free atmosphere above the weather station taking into account:
 - Error of measuring instruments and influencing of mast and neighbour measuring instruments
 - Local obstacles and buildings
 - Local terrain roughness
 - regional topography

- 2) Extrapolation of the wind in the free atmosphere above the building location (The topographical influence is taken into account by a transfer matrix, which has been calculated with a mesoscale model of the concerning region)
- 3) Calculation of the local wind at building reference height with the local wind speed profile

Unfortunately, up to now, this method has not been implemented in a software tool for practical applications. In the field of wind energy use similar methods has been developed. The user friendly software tool Wind Atlas and Application Program WAsP [Bowen 1996], developed and distributed by Wind Energy Department at Risø National Laboratory in Denmark, is used to predict mean power production at a desired wind turbine site from measurements made at another location in the same region. It has to be sorted out whether this tool might be useful for wind data transfer for the purpose of wind pressure calculation.

A similar statistical wind model for rugged topography, such as the Swiss Alps, is presented by [Meteotest 2002]. In this model the wind in the height of 50 m is calculated from the 2D wind field at 1000 m above sea level, corrected with the effective altitude of the terrain and 2D fields of correction coefficients, taking into account the influence of the topography. The model has been developed to determine yearly averaged wind speed at any point of the modelled region in order to estimate the wind energy potential at any desired location.

2.1.4. Shielding effect

Shielding effect from surrounding structures must be taken into account for the determination of the wind pressure coefficients. That means wind speed v_{ref} at reference height has to be available from a place outside the disturbed area but with the same wind profile.

[Wiren 1985] measured the change in C_p with wind angle and building separation for a building with identical buildings to either side. With flow along the building row and decreasing separation, pressure becomes more uniform for all walls ($C_p = -0.15$) except the front wall ($C_p = 0.15$). It is concluded that only the nearest ring of obstacles dominates the building sheltering, and that additional rings do not significantly contribute to the sheltering effect. Several tables and figures with values for wall averaged C_p 's showing this context are given in [Walker 1992].

[Walker 1996] introduced a wind shadow model to account for the sheltering effect of upwind obstacles. A shelter factor which is depending on the dimension and the distance of the obstacle is used to calculate the wind speed reduction in the wake.

$$v_s = Sv \tag{9}$$

2.1.5. Air flow in road canyons

The air flow field in a road canyon is depending on the following three main parameters:

- canyon geometry, described with mean height of buildings h_b , canyon width w , and length l
- wind characteristics (speed and direction) above the canyon
- temperature distribution inside the canyon

For wind perpendicular to the road, three different flow regimes depending on building separation can be distinguished according to [Hussain and Lee 1980] (figure 2.3):

- a) isolated roughness flow ($w/h_b > 2.5$):
buildings are far enough apart that each building acts in isolation.
- b) wake interference flow ($2.5 > w/h_b > 1.5$):
buildings are closer together and front separation region of the downwind building is met before reattachment
- c) skimming flow ($w/h_b < 1.5$):
a stable vortex is established in the canyon and the bulk of the flow does not enter it.

[Santamouris 2000] suggests a model for flow speed in the canyon depending on free stream wind above the canyon:

For wind speed above the canyon < 4 m/s, a chaotic flow with maximum speed of 0.5 m/s will occur inside the canyon. There is more or less no coupling between wind speed and direction above and inside the canyon.

For wind speed above the canyon > 4 m/s the flow speed inside is linearly correlated to the wind speed above. For each of the following three different cases regarding incident angle of the wind [Santamouris 2000] gives coefficients depending on canyon geometry:

- parallel incidence (incidence angle 0° or $180^\circ \pm 30^\circ$): Flow along the canyon axis with an exponential profile.
- vertical incidence (incidence angle 90° or $270^\circ \pm 30^\circ$): Flow with one or two vortices are developed depending on h/w .
- oblique wind all (other cases): Flow with a cork-screw type of vortex along the canyon.

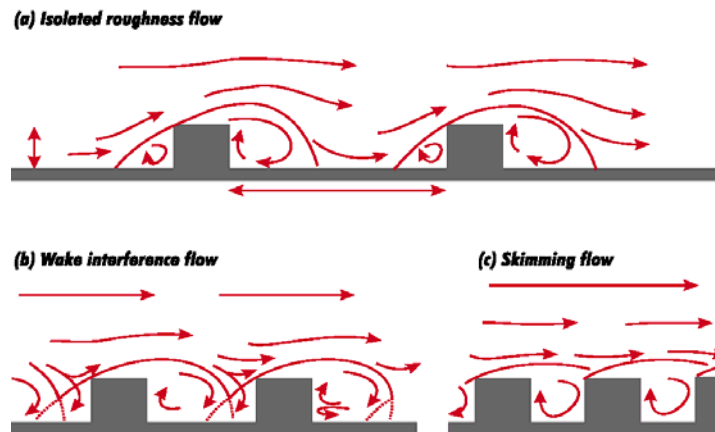


Figure 2.3: Flow regimes for wind perpendicular to the road axis depending on building separation - (a) Isolated roughness flow – (b) Wake interference flow – (c) Skimming flow [Santamouris 2001]

As described above the speed in the canyon is not in the whole range linearly correlated to the free stream speed. This leads to C_p -values depending on velocity because shielding effects have to be included in the C_p -values (see previous chapter). In current air infiltration analysis tools the C_p -values can only be input depending on wind direction but not on velocity.

2.1.6. Wind pressure distribution on building envelope

As spatial wind pressure distribution on building surface is not uniform, a façade can be subdivided in several façade elements. For each element an individual value represents the spatial average C_p of the corresponding area. The C_p denotes the relation of the wind pressure to the dynamic pressure at building reference height (see equation (1)). Thus the velocity profile of the upstream wind influences the C_p -values of the individual façade elements (figure 2.4). In other words, data sets of C_p -values must be given together with the corresponding upstream velocity profile or terrain roughness parameter. As already described earlier, also the shielding effects has to be included in the C_p -values.

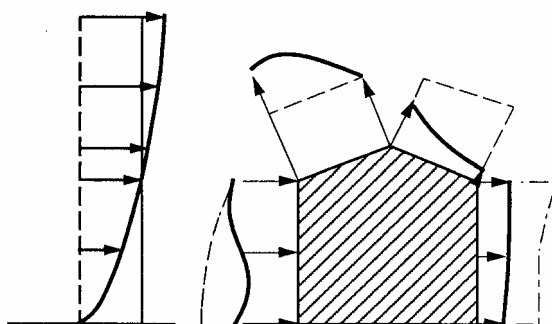


Figure 2.4:
Pressure distribution on building surface:

- with wind profile
- - - - without wind profile

2.1.7. Methods of wind pressure determination

Wind tunnel test

Wind tunnel testing is needed for unusual building geometry or specific situations of surrounding structures. Therefore a scale model of the building and surrounding environs has to be placed in a wind tunnel that can accurately represent the lower levels of the turbulent boundary layer. Pressure taps, connected via plastic tubes are placed on each façade element of the model for the pressure distribution determination. The model needs to be placed on a turn-table so that pressure can be analysed for the complete spectrum of wind direction. To achieve the correct wind velocity profile, the upwind roughness has to be modelled using arrays of cubic blocks.

[Hertig 1994] shows the results of an investigation on scale models of some typical Swiss houses, first without environs and second with a full scale proximity model radius of 200 m.

Extensive data is given for two different reference velocities:

- 1) reference height at roof height, measured in the undisturbed stream
- 2) reference height at roof height, measured on the roof

Statistical regression of wind tunnel data sets

With the software tool C_p -Generator [Knoll 1995], statistical regression of extensive wind tunnel data sets can be performed. Parameters describing the building geometry are used for the regression. With the same method the C_p -values of an upstream obstacle are determined. These values are used together with the distance of the obstacle to calculate a correction term which considers the shielding effect of the obstacle on the C_p -values of the building under investigation.

CPCALC+ [Grosso 1995] is a similar tool. Here the surrounding buildings are described with the two parameters plan area density and surrounding building height. The shielding effect can be taken into account for each calculated wind direction separately.

Wall averaged C_p -values

For low rise buildings up to three storeys with simple building geometry and uniform surrounding environs, wall averaged C_p -values fulfil with sufficient accuracy the requirements of air flow calculation models. In [Orme 1994] data for different length to width ratios, wind shielding conditions and roof pitch angles can be found. Direction dependence of wind shielding effects is not taken into account. Other sources for wall averaged C_p -values are [Bassett 1990], [ASHRAE 2001].

Wall averaged values vs. statistical regression

[Wong 2001] made an evaluation exercise of wind pressure data produced with CPCALC+ and wall averaged values. Data from wind tunnel tests on a scale model of the investigated building including the surrounding buildings are used as reference. C_p -values of the front side façade were compared. A good correlation to the reference values was found for most wind directions. The correlation coefficients of the wall averaged method were slightly closer to 1 than those of the values from CPCALC+.

Wind from 90° was sheltered by a building close to the investigated one. As mentioned above, for the wall averaged values from literature, the shielding effect is uniform for all wind directions, thus the correlation for 90° was poor. As in this exercise the same shielding parameters have been used for all wind direction, the results from CPCALC+ had also a bad correlation for wind from 90°, but this is rather a consequence of inadequate input data than of a shortcoming of the tool.

In this exercise also the influence of the inaccurate C_p -values on the resulting air flows has been investigated using a multizone airflow model. In this case, the errors of the air flows were much smaller than those of the C_p -values.

CFD calculation of building environment

In several studies CFD calculation technique has been used to investigate airflow patterns around buildings and wind pressure distribution on building surface. An advantage of this method is that experiments can be performed without the expense of the construction of scale models of the building and environs and without the need to take many time consuming measurements. The velocity profile can either be defined as boundary condition at the inflow into the computational domain or it can be obtained by modelling a long enough upstream distance with the corresponding terrain roughness.

[Cooper 1992] used two and three dimensional CFD-models to predict the pressure coefficients on all faces of a sheltered building. The influence of the distance and the form of an upwind obstacle has been investigated. Results from wind tunnel tests showed a good agreement of the characteristics of the pressure distributions, although different in terms of numerical values.

Also [Mikkelsen 1995] compared results from CFD calculations using a $K-\varepsilon$ turbulence model with those from wind tunnel tests and full scale measurements on a cube and on a simple house. Computed pressure coefficients on the cube indicated slightly higher values than those obtained by wind tunnel tests. On upwind faces the characteristics of the pressure distribution calculated with the model showed a good agreement with the measurements. As $K-\varepsilon$ models cannot correctly predict the reverse flow after separation on the roof surface and the side walls, the computed C_p -values in the separation zones are considerably affected by the boundary conditions, therefore they can have larger differences to the measurements. Modelling unsteady state turbulent flow with large eddy simulation (LES) method the flow separation can be predicted correctly. As this method needs finer grid arrangement it takes much more computational time than the $K-\varepsilon$ model.

A dynamical effect of the fluctuating wind direction on the pressure in the separation area can also only be predicted correctly with LES [Jiang 2002]. With a fixed wind direction, large recirculation zones may be formed behind the building. A fluctuating wind direction destroys these large recirculation zones and leads to much smaller eddies. The difference in the air flow pattern causes a different pressure distribution on building surface. C_p -values from LES with a varied wind direction showed a good agreement with onsite measurement, whereas values from LES with a fixed wind direction correspond to measurements performed in wind tunnel experiments, where the wind direction was fixed as well.

[Zhou 1997] showed a significant improvement of the predicted C_p -values using a combination of the $K-\varepsilon$ model in fully turbulent regions with a one-equation model in near wall areas. The general agreement between numerical results from this so called two layer method and experimental data is reasonable, also on the roof surface and the side walls.

2.1.8. C_p -values on openings

The flow through a large opening can be calculated with:

$$Q = C_d \cdot A_o \cdot \sqrt{\frac{2 \cdot \Delta p}{\rho}} \quad (10)$$

Where A_o is the opening area and Δp is the pressure difference across the opening. With the following two assumptions C_p -values of the completely sealed building and C_d -values from literature can be used:

- 1) The flow trough the large opening does not disturb the flow pattern around the building.
- 2) The discharge coefficient C_d for an opening is dependent only on the geometry and is not affected by the external flow field

[Vickery 1987] compared flow estimates computed with these assumptions with values measured in wind tunnel experiments on a model of a building with two porous side walls, where pressure loss of the external openings dominate (i.e. no internal flow path with considerable resistance). Measured flow was expressed in dimensionless form using a flow velocity coefficient C_Q .

$$C_Q = \frac{Q}{A_w \cdot v_{ref}} \quad (11)$$

With the two assumptions given above this coefficient can be predicted for a single wall

$$C_{Qp} = \Phi \cdot C_d \cdot \sqrt{C_p} \quad (12)$$

Where the porosity is defined as $\Phi = A_o/A_w$ (A_o is the opening area and A_w the wall area). The inaccuracy of C_{Qp} increases with porosity and thus with C_Q and with the wind angle. The ratio of the predicted to the anticipated coefficient C_Q is for a single wall approximately:

$$\frac{C_{Qp}}{C_Q} = \frac{1}{\sqrt{(1 - 1.5C_{Qp})(1 + 0.45C_{Qp})}} \quad (13)$$

With $C_d=0.6$ and $C_p=1.2$ and wind normal to the wall.

Depending on wind angle and C_Q , this ratio is in the same order of magnitude for a building with openings in the windward and leeward walls and no considerable internal flow resistance.

In conclusion, for wall porosity of less than about 23% on two opposite faces and wind not strongly inclined (wind angle below 45°) to the vented faces, internal flow rates can be predicted with moderate accuracy (about $\pm 10\%$) from a knowledge of the external pressure distribution on solid model. The accuracy will be better if the flow is dominated by internal flow resistances.

2.1.9. Impact of balconies on C_p -values

Wind tunnel tests have shown the following changes of pressure distribution due to the installation of balconies [Chand 1998]:

- no significant changes on the leeward wall
- on the windward wall with perpendicular wind the pressure is:
 - reduced at ground floor and at the space covered by the balconies on the top floor
 - increased at near the top of the building
 - increased at the wall ends on all intermediate floors
 - increased at the middle section on the mid-height level balcony space
 - not significantly changed at all other positions
- on windward wall with oblique wind:
 - on the upwind end of the wall, the pressure change is similar to the change on the windward wall a with perpendicular wind
 - on the downwind end of the wall, the pressure above the topmost balcony is increased and reduced at all positions below, with negative pressures at ground floor and at space covered by the topmost balcony

2.1.10. Impact of wind fluctuations

Natural wind varies in speed and direction due to its gustiness. In addition, vortices are generated in the upstream surroundings. Also thermal effects can cause wind fluctuations. This causes a fluctuation of the wind pressures on building surface. The distribution of the pressure fluctuation does not correlate with the distribution of the time averaged values. That means that a position at the envelope with a low average pressure does not have low pressure fluctuation.

The simulation with time averaged C_p -values has proven to be useful but has known limitations. As a numerical effect based on the nonlinear equation systems used in multizone airflow models, there will be more or less difference between results from simulation with hourly averaged values and those from simulation with fluctuating pressures in time [Phaff 1992].

But also physical effects of wind fluctuation have an influence on the air infiltration rate. The two main effects are known as (1) pulsation flow and (2) penetrating eddies. Pulsation flow means a variation in pressure at the opening, inducing a fluctuation flow due to the compressibility of the air in the internal space. The flow depends on the magnitude of the fluctuating pressure and the size of the enclosure.

Penetrating eddies have higher frequency fluctuations that induce an air exchange at the opening due to smaller scale turbulence, with eddy sizes comparable with or smaller than the opening size. Thus a turbulent diffusion of air through the opening is produced.

[Haghighat 2000] shows a review of existing fluctuating infiltration models. Some models are described in the frequency domain and others in the time domain. Empirical correlations expressing mean airflow rate through an opening as a function of temperature difference, wind velocity and fluctuating terms are another type of model. None of the current multizone airflow calculation programs includes such a fluctuating infiltration model. For this a higher degree of generalisation, i.e. an extension to n openings and m enclosures inside an arbitrary oriented building, is necessary.

[Etheridge 2000] presents a fluctuating infiltration model described in the time domain, which additionally takes into account the inertia of the accelerated mass of the air in the opening.

2.1.11. How to handle the intrinsic uncertainties

The sensitivity of airflow modelling results on C_p -values depends on air tightness of the building, distribution of leakage, ventilation system, ventilation network and the flow exponents of the airflow components. In conclusion the sensitivity is different in each individual case [Phaff 1992]. Therefore, no rules of thumb can be given. For a correct handling of uncertainties of C_p -values, a sensitivity analysis has to be performed in each case.

Airflow results are more influenced by the variation of C_p -values in buildings with wind dominated ventilation and in airtight buildings. Here the use of inaccurate C_p -data is more critical for the uncertainty of the result than in other cases.

2.2. On wind data in meteo files

Often wind climate data is not measured directly at the building location. Wind data from the nearest meteo station is not in any case a useful basis for the determination of the wind situation at the site of interest, because the wind speed and direction is very much depending on the surrounding terrain. Only in flat topography the direction may be assumed similar on both meteo station and site locations. In this case the wind speed may be transferred using the two wind profiles (see chapter 2.1.3 From meteo wind to wind on site). This method is not applicable for the conversion of wind data from a near by station, positioned in a rural terrain, to urban data. The urban canopy is the atmospheric layer that extends from ground level to above roof level in the urban area. A reduction of 20% to 30% is often observed in the average wind speed within this layer, from suburban to urban areas, and with the turbulence intensity increased by 50% to 100%. Moreover, in lighter wind conditions there is an increase in urban wind speeds due to pressure gradients created by the urban heat island effect. (see also chapter 2.1.5 Air flow in road canyons).

Hourly weather data sets which are used for dynamic thermal building simulation or solar system simulation sometimes are generated from monthly averaged values using stochastic models. This practise has been proven for air temperature and radiation data, but not for wind data. Therefore hourly measured data should be used.

2.3. Wind effects in the urban environment

Wind effects in the urban environment have been studied in several projects, previous and in parallel to the RESHYVENT project. Measurements and wind speed in urban canyons have been carried since the 1930. Especially the National and Kapodistrian University of Athens, Greece, has performed many modelling and experimental validation work on the topic of wind speed distribution in urban canyons [Santamouris 2001a], [Santamouris 2001b], [Allard 2004], also in the frame of RESHYVENT [Niachou 2004].

3. Cowl performance and above roof air flow fields

3.1. Cowl performance

3.1.1. Pressure difference on cowls

Wind arriving at the end of a cylindrical exhaust duct produces a suction effect based on the locally accelerated air flow around the duct. In order to increase the up-draught in a stack duct or to prevent wind induced flow reversal in the duct, roof cowls are used to enhance the suction effect and to shelter the duct from rain.

The aerodynamic characteristics of cowls and roof outlets are determined by experimental measurements according to [CEN EN 13141-5]. The device is exposed in a wind tunnel considering also an exhaust air flow. The pressure difference across the device is measured for different wind and exhaust flow velocities. Vertical as well as horizontal wind angles can be simulated by tilting and rotating the duct in the wind tunnel, as shown in figure 3.1.

With the total pressure in the duct $p_{t,duct}$ and the wind velocity U , the wind pressure coefficient $C_{p,cowl}$ can be calculated from the measured static pressure in the wind tunnel $p_{s,cowl}$ in function of wind angle and velocity ratio of wind and exhaust flow. The wind pressure coefficient is defined as:

$$C_{p,cowl} = \frac{2(p_{t,duct} - p_{s,cowl})}{\rho U^2} = \frac{2\Delta p_w}{\rho U^2} \quad (14)$$

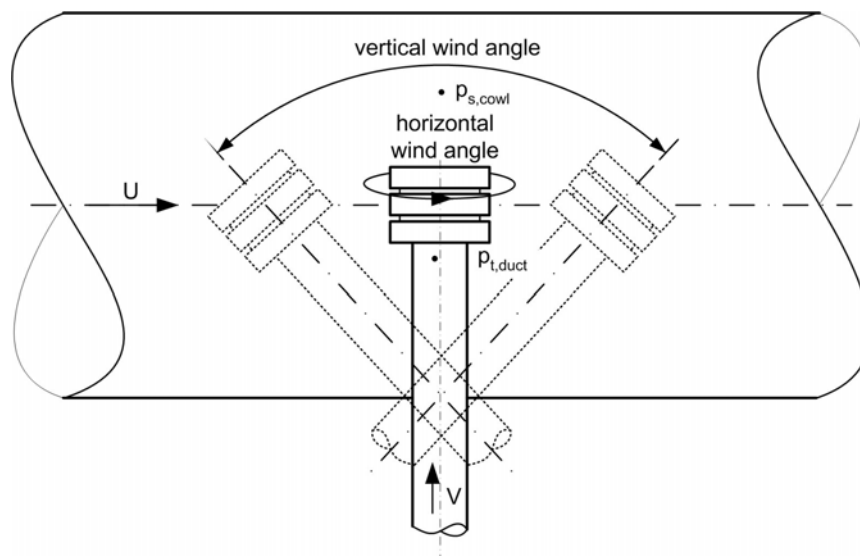


Figure 3.1: Experimental measurement of C_p -value of a cowl according to [CEN EN 13141-5]. The cowl can be rotated to simulate varying vertical and horizontal wind incident angles.

3.1.2. Characteristics of different cowl types

In several investigations the performance of usual and new developed cowls has been studied. A short summary is given below:

[De Gids and den Ouden 1987] investigated the behaviour of thirteen different cowl types in a wind tunnel and compared them with an open duct. The measured pressure coefficients are shown in dependency of the vertical wind approach angle φ (from perpendicular descending to perpendicular ascending) and of the air flow velocity ratio V/U where V is the velocity in the duct and U is the wind velocity. Compared to an open duct the investigated cowls can be divided into three groups:

- cowls which produce an improvement of the pressure and the stability

- cowls which work worse
- cowls which have a positive influence in certain circumstances and in other cases a negative effect. These cowls generally have a favourable effect in presence of descending winds but an unfavourable effect with rising winds.

[Welsh 1994] showed a method for the rating of the cowl performance. Three factors are used, which are described below (1-3):

1. Loss coefficient

The loss coefficient ζ describes the ratio between the pressure loss Δp_{loss} due to the air flow in the duct and the dynamic pressure in the duct:

$$\zeta = \frac{2\Delta p_{loss}}{\rho V^2} \quad (15)$$

The loss coefficient of the investigated terminal types are shown in *table 3.1* in descending order of performance with the least restrictive first.

Table 3.1: loss coefficient of the investigated terminal types

Terminal type 100 mm	loss coefficient ζ	Terminal type 150 mm	loss coefficient ζ
Open pipe	1.0	Open pipe	1.0
Mushroom cap	2.1	Chinese hat	1.1
Balloon	2.2	Rotating cowl 1	1.1
H pot 1	2.7	Rotating cowl 2	1.3
Gas flue	3.2	Gas flue	2.0
Hpot 2	4.7	Aero-dynamic cowl	2.3
Grey vane	6.7		

2. Wind performance indicator

The wind performance indicator describes the extractive performance caused by the wind. An approximate quadratic relation for the C_p -value was found:

$$C_{p,cowl} = \frac{2\Delta p_w}{\rho U^2} = C_{p|V=0} + (\zeta - 1)(V/U)^2 + \frac{2\Delta p_i}{\rho U^2} \quad (16)$$

The three terms in this equation describe the suction effect of the wind, the flow resistance in the duct terminal and the interaction between wind and duct flow. $C_{p|V=0}$ is the wind pressure coefficient of the cowl, when the flow in the duct is zero. The pressure loss coefficient ζ is defined in eq. (15) and can be measured when the wind speed is zero.

$C_{p|V=0}$ and the interaction pressure Δp_i are dependent on the terminal geometry, the wind direction and on the wind angle to the vertical. Δp_i also changes with the ratio of the two flow velocities. Therefore [Gonzales 1984] used for the interaction term a constant B :

$$C_{p,cowl} = \frac{2\Delta p_w}{\rho U^2} = C_{p|V=0} + (\zeta - 1)(V/U)^2 + B \cdot [(V/U)^2]^n \quad (17)$$

[Millet 1998] puts: $n = 0.5$ and $B = \sqrt{C_{p|V=0} \cdot \zeta}$

The wind performance indicator is defined by [Welsh 1994] as the product of the average values of $C_{p|V=0}$ and $(V/U)_{C_p=0}$. The associated error band (standard deviation) defines the range of the performance indicator depending on wind direction and wind angle.

$$I_w = C_{p|V=0} \cdot (V/U)_{C_p=0} \quad (18)$$

The following table shows the measured wind performance indicators together with the standard deviation.

Table 3.2: measured wind performance indicator

Terminal type 100 mm	Wind performance indicator	Terminal type 150 mm	Wind performance indicator
H pot 1	-0.23 ± 0.22	Rotating cowl 1	-0.53 ± 0.50
Balloon	-0.16 ± 0.09	Rotating cowl 2	-0.12 ± 0.07
H pot 2	-0.16 ± 0.13	Gas flue	-0.07 ± 0.04
Gas flue	-0.11 ± 0.11	Aero-dynamic cowl	-0.03 ± 0.04
Grey vane	-0.09 ± 0.04		

3. Flow-reversal potential

The flow-reversal potential gives an indication, whether flow-reversal can occur. If the maximum value of $C_{p/V=0}$ is positive, or if the derivative $d(\Delta p_w)/dU$ is positive in the case of $V = 0$, then flow reversal is possible.

Depending on the application the priority of these rating factors is varying.

The examined terminals can be divided in three groups:

- 1) Terminals with large loss factors: "Gas flue", "H pot 2" and "Grey vane"
- 2) Terminals good at inducing up-draught: "Rotating cowl 1", "H pot 1"
- 3) Terminals which may cause flow-reversal: open pipe, "Mushroom cap", "Chinese hat"

3.1.3. Using experimental data

Cowl performance data measured according to [CEN EN 13341-5] includes values for $C_{p,cowl}$ as a function of the vertical wind approach angle φ and the duct air speed V . The wind speed used in the experiment is the reference wind speed U_{ref} , which is in general $U_{ref} = 8\text{ m/s}$. According to the similitude law $C_{p,cowl}$ remains the same if the ratio V/U does not change (see also eq. (17)). Therefore the $C_{p,cowl}$ - values at the reference wind speed U_{ref} can be used for an actual wind speed U_{act} as follows:

$$C_{p,cowl}(U_{ref}, V) = C_{p,cowl}(U_{act}, V \cdot \frac{U_{act}}{U_{ref}}) \quad (19)$$

The maximum air speed in the duct is limited in the experiment to V_{max} (e.g. $V_{max} = 16\text{ m/s}$). Therefore only $C_{p,cowl}$ -values for V/U ratios up to V_{max}/U_{ref} are available from the experiment. At the end, for a high duct air speed V and a low wind speed U , the pressure difference is equal to the one given by the pressure loss coefficient ζ eq. (15).

The curve of the pressure difference Δp as a function of the duct air speed V can be determined for an actual wind speed $U_{act} < U_{ref}$ using the following methodology:

- 1) Eq. (14) together with the similitude law can be applied for air duct speeds lower than V_1 with:

$$V_1 = U_{act} \cdot \frac{V_{max}}{U_{ref}} \quad (20)$$

- 2) For air duct speeds higher than V_1 , it is important to make a transition to the curve with no wind eq. (15) by keeping a monotonous curve. To do so, it is recommended to search for a duct air speed V_2 where the pressure difference according to eq (15) $\Delta p_{loss}(V_2)$ is higher than the pressure difference at V_1 according to eq (14) $\Delta p_w(U_{act}, V_1)$. This can be done by first trying $V_2 = 2 V_1$ then $V_2 = 3 V_1$

For V_2 , the pressure difference $\Delta p_{loss}(V_2)$ is calculated using eq. (15)

- 3) For duct air speeds between V_1 and V_2 , the curve is a linear interpolation between the two points
- 4) For duct air speeds higher than V_2 : the curve is the $\Delta p_{loss}(V)$ according to eq. (15)

Example of application

A cowl was tested at the reference wind velocity $U_{ref} = 8$ m/s with duct air speeds up to a maximum of $V_{max} = 4$ m/s.

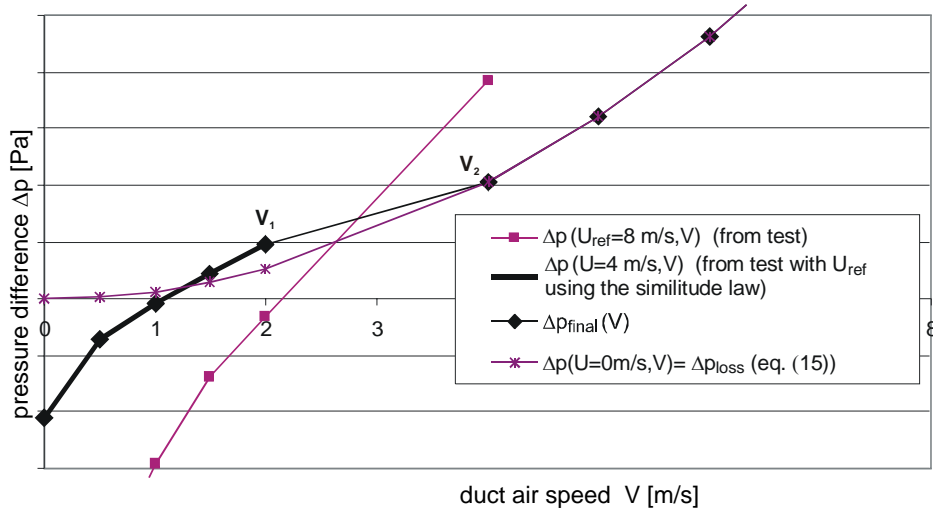


Figure 3.2: Cowl pressure difference as a function of the duct air speed for an actual wind speed of 4 m/s derived from test data at reference wind speed $U_{ref} = 8$ m/s

For $U_{act} = 4$ m/s:

- 1) $V_1 = U_{act} \cdot V_{max} / U_{ref} = 4 \text{ m/s} \cdot 4 \text{ m/s} / 8 \text{ m/s} = 2 \text{ m/s}$
From $V = 0$ m/s to $V_1 = 2$ m/s: Δp is calculated using eq. (14) with $C_{p,cowl}$ -values taken from the test with U_{ref} according to the similitude law (eq. (19)).
- 2) For $V_2 = 2 V_1 = 4$ m/s: $\Delta p(U = 0, V_2)$ is higher than $\Delta p(U = 4 \text{ m/s}, V_1) \rightarrow V_2 = 4$ m/s
- 3) A linear interpolation is made between V_1 and V_2
- 4) For $V > V_2$: $\Delta p(U = 0, V) = \Delta p_{loss} \text{ (eq(15))}$ is applied

3.2. From experimental data to pressure differences of cowls on the roof

As shown in equation (14), the C_p value of a cowl is defined as the ratio of the cowl pressure difference to the local dynamic wind pressure near the device. The value is depending on the velocity and the vertical incidence angle of the local wind flow. Both, the velocity as well as the incidence angle at the cowl position above the roof are influenced by the building. Therefore a function has to be found to transfer the reference wind velocity U_r at the building reference height z_r to the velocity U and vertical incidence angle φ at the cowl position (see figure 3.3). The building ridge height is defined as the building reference height in the cases shown in this section. CFD calculations of the air flow around buildings can be used to find such functions.

With the CFD calculation results the correct $C_{p,cowl}$ can be selected from the experimental data and the pressure difference can be calculated with the local velocity. For simplification purposes, the cowl performance is assumed to be independent of the horizontal wind incidence angle (valid for axial symmetric or wind aligned cowls).

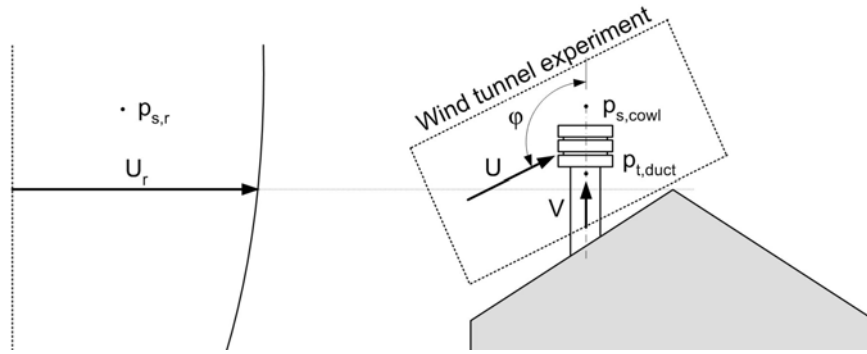


Figure 3.3: Link between wind tunnel measurements of cowls and CFD calculations.

3.2.1. CFD-calculations of air flow patterns around buildings

In this section the CFD-calculations for some typical sites and building shapes are documented. Some of the results have been used to evaluate the data for the above described transfer of wind data.

On the topic of C_p -values above roof and walls, many measurements and calculations have already been carried out. Unfortunately the airflow pattern above roof level has seldom been documented in detail. Even though many useful hints on how to model flow fields around buildings using CFD can be found in earlier work (for references see chapter 8.1).

Calculated cases

The flow field pattern above a building roof is highly dependent on building geometry, roof shape and wind direction. In this investigation by CFD calculations using FLOVENT, up to seven different parameters shall be varied. Because all possible combinations would lead to an extensive amount of cases, only few typical flow situations are calculated at present. Moreover, the influence of certain parameters like wind profile, building geometry and roof shapes are investigated with two dimensional calculations. For the three dimensional simulation two common building shapes, one with flat roof and one with a pitched roof, have been selected. figure 3.4 shows the definition of wind incident angle and roof pitch angle.

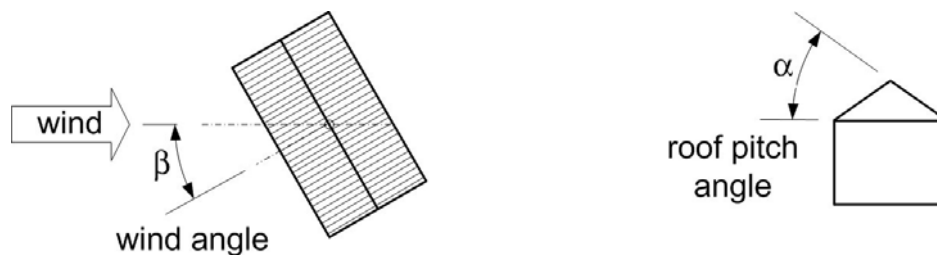


Figure 3.4: Definition of wind incident angle and roof pitch angle of the building

The boundary condition of the wind is defined by several air outlets placed at the windward boundary of the calculation domain. Each outlet has a predefined air velocity which equals to a logarithmic wind profile with a certain surface roughness parameter. In most cases a roughness parameter of 0.05, which corresponds to a site with open terrain and only few isolated obstacles, is used. Because the flow pattern (especially the reattachment zone behind the building) around a building is not independent of wind speed, see [Smith et al., 2001], the influence of two typical wind velocities is evaluated, based on two dimensional computations. Table 3.3 and table 3.4 below give an overview of the configurations which have been investigated by CFD.

Calculation domain

Dependent on the dimensionality and building geometry, the size of the domain has been chosen according to the literature discussed in chapter 8.1.1, as well as to the experience gained by calculating the validation cases in chapter 8.1. The downstream boundary is an open face, the top and vertical sides of the domain have symmetry conditions. The upstream boundary is defined by twelve air outlets with predefined air speed leading to a logarithmic wind profile with wind speed and roughness parameter corresponding to table 3.3 and table 3.4. The ground is assumed to be a flat plate with a surface roughness of zero.

Table 3.3: 2D flow cases calculated by CFD

¹⁾ This case has been calculated but is not documented here

²⁾ This case has not been calculated

Case	Dim	Building geometry				Wind			CFD	Notes
		H [m]	S [m]	α [°]	z_r [m]	U_{10} [m/s]	z_0 [m]	U_r [m/s]		
1.1a	2D	6	6	0	6	2	0.05	1.81	✓	Influence of wind parameters: Wind velocity and roughness for a flat roof building.
1.1b	2D	6	6	0	6	2	0.35	1.70	✓	
1.1c	2D	6	6	0	6	10	0.05	9.04	✓	
1.2	2D	6	12	0	6	2	0.05	1.81	✓ ¹⁾	Influence of building geometry: Height and length.
1.3	2D	6	30	0	6	2	0.05	1.81	✓ ¹⁾	
1.4	2D	12	12	0	12	2	0.05	2.07	✓ ²⁾	
1.5	2D	12	30	0	12	2	0.05	2.07	✓ ²⁾	Influence of roof geometry: pitch angle and wind velocity in combination with pitch roof building.
2.1	2D	6	12	10	7.1	2	0.05	1.87	✓ ¹⁾	
2.2	2D	6	12	20	8.2	2	0.05	1.92	✓ ²⁾	
2.3	2D	6	12	30	9.5	2	0.05	1.98	✓ ²⁾	
2.4	2D	6	12	40	11.0	2	0.05	2.04	✓ ²⁾	

Table 3.4: 3D Flow cases calculated by CFD

¹⁾ This case has been calculated but is not documented here

²⁾ This case has not been calculated

case	Dim	Building geometry					Wind				CFD	Notes
		H [m]	S [m]	B [m]	α [°]	z_r [m]	β [°]	U_{10} [m/s]	z_0 [m]	U_r [m/s]		
3.1a	3D	6	12	12	0	6	0	2	0.05	1.81	✓ ²⁾	Variation of wind direction for a flat roof building with two different building shapes.
3.1b	3D	6	12	12	0	6	45	2	0.05	1.81	✓ ²⁾	
3.2a	3D	12	12	30	0	12	0	2	0.05	2.07	✓ ²⁾	
3.2b	3D	12	12	30	0	12	45	2	0.05	2.07	✓ ²⁾	
3.2c	3D	12	12	30	0	12	90	2	0.05	2.07	✓ ²⁾	
4.1a	3D	6	12	12	30	9.5	0	2	0.05	1.98	✓	Variation of wind direction for a pitched roof building with two different building shapes.
4.1b	3D	6	12	12	30	9.5	45	2	0.05	1.98	✓	
4.1c	3D	6	12	12	30	9.5	90	2	0.05	1.98	✓	

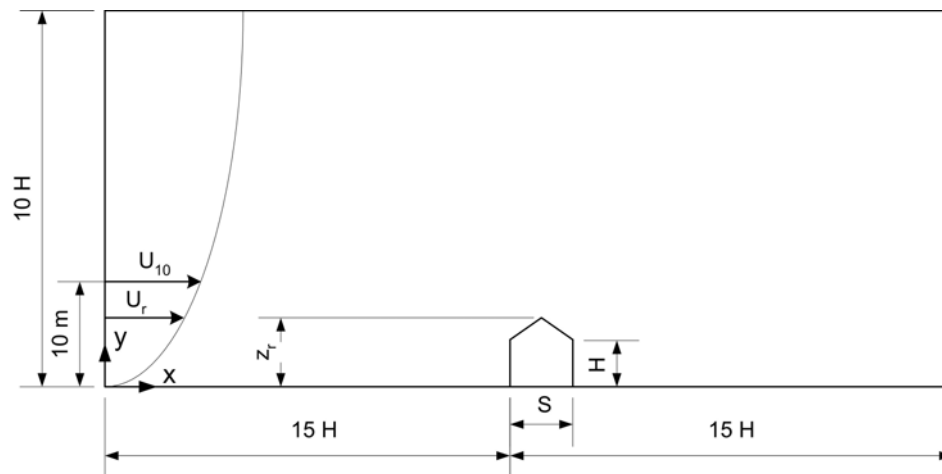


Figure 3.5: Minimal domain size for two dimensional calculations.

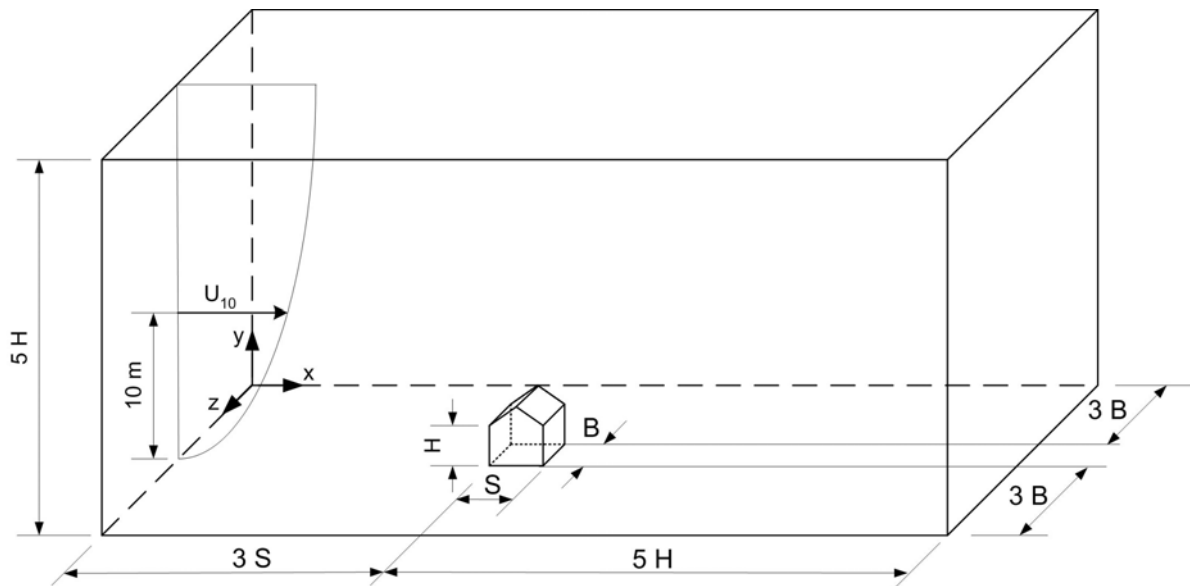


Figure 3.6: Minimal domain size for three dimensional calculations. Because of the lower blockage effect a smaller domain is needed for 3D simulations in order to get domain size independent results.

Mesh design

In accordance with the calculations in chapter 8.1 and hints from literature the grid has been designed individually for each case. The smallest cells were placed in regions of high gradients in particular on the building roof and walls. Table 3.5 gives an overview of the meshes and the exact domain size used in the computations. NX, NY and NZ refer to the number of nodes in the x, y and z directions, respectively. NC refers to the total number of control volumes located within the flow domain and dx_{min} , dy_{min} and dz_{min} refer to the size (normalised with H) of the smallest grid spacing in the x, y and z directions respectively.

Table 3.5: Domain size and grid lay-out for two and three dimensional calculations

Case	Domain size [m]			Number of grid cells			Total	Smallest grid cells		
	X	Y	Z	NX	NY	NZ	NC	dx _{min}	dy _{min}	dz _{min}
1.1a-c	180	60	-	127	66	-	8'382	0.029	0.012	-
1.2	180	60	-	149	67	-	9'983	0.026	0.012	-
1.3	180	60	-	185	69	-	12'765	0.024	0.012	-
2.1	180	60	-	198	87	-	17'226	0.013	0.012	-
4.1a-c	108	60	84	136	90	100	1'224'000	0.080	0.072	0.020

Results from CFD calculations

The results from CFD calculations were analysed focusing on the determination of C_p -values in cowls. Therefore, the flow field above roof was visualised by iso-plots of air speed and flow-angle. The air speeds were normalised to the undisturbed upstream wind velocity at building reference height (ridge-height). The normalised air speed can be calculated according to equation (21).

$$u = \frac{U}{U_r} = \frac{\sqrt{U_x^2 + U_y^2 + U_z^2}}{U_r} \quad (21)$$

The definition the flow angle is shown in figure 3.7.

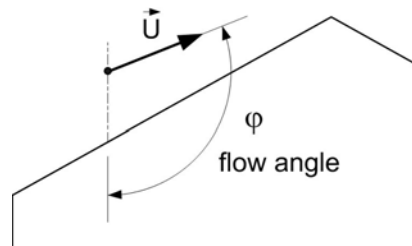


Figure 3.7: Definition of air flow angle above roof

To gain an overview of the pressure situations in the vicinity of the building, the C_p -value-field is evaluated additionally. This may also help to verify experimental data of similar flow cases if available. The C_p -value is calculated according to equation (22) and takes into account the static pressure difference (difference between static pressure in each cell and free stream static pressure at the same height), air density and wind velocity at building reference height (ridge-height).

$$C_p = \frac{2(p_s - p_{s,r})}{\rho U_r^2} \quad (22)$$

Case 1.1a

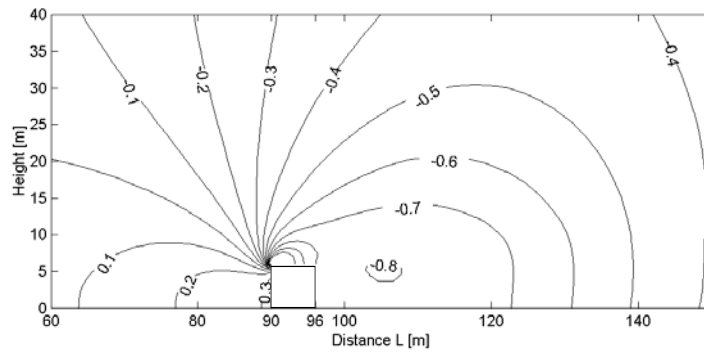


Figure 3.8: C_p -value field around building, two dimensional CFD calculation

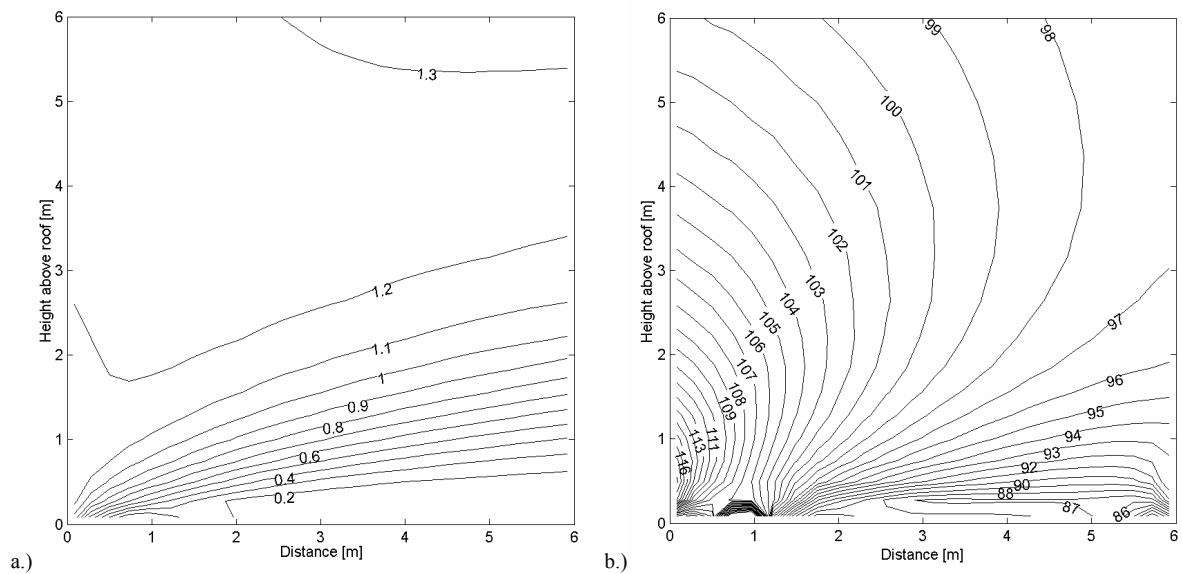


Figure 3.9: Two dimensional computed air flow field above a flat roof building with the dimension of 6 x 6 m

- a.) Air speed 0 to 6 m above roof level, normalised with wind speed on ridge height.
 b.) Air velocity angle 0 to 6 m above roof level.

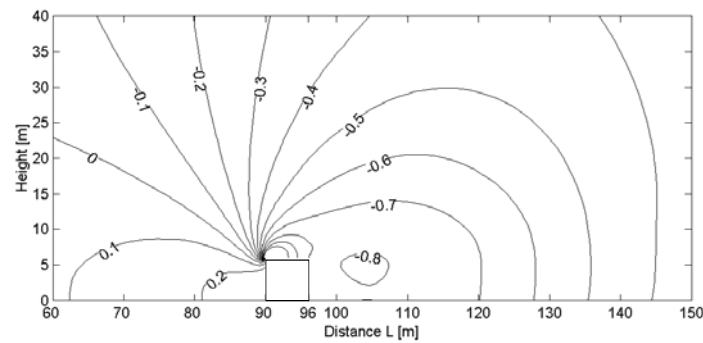
Case 1.1b

Figure 3.10: Two dimensional CFD calculation of the C_p -value field.

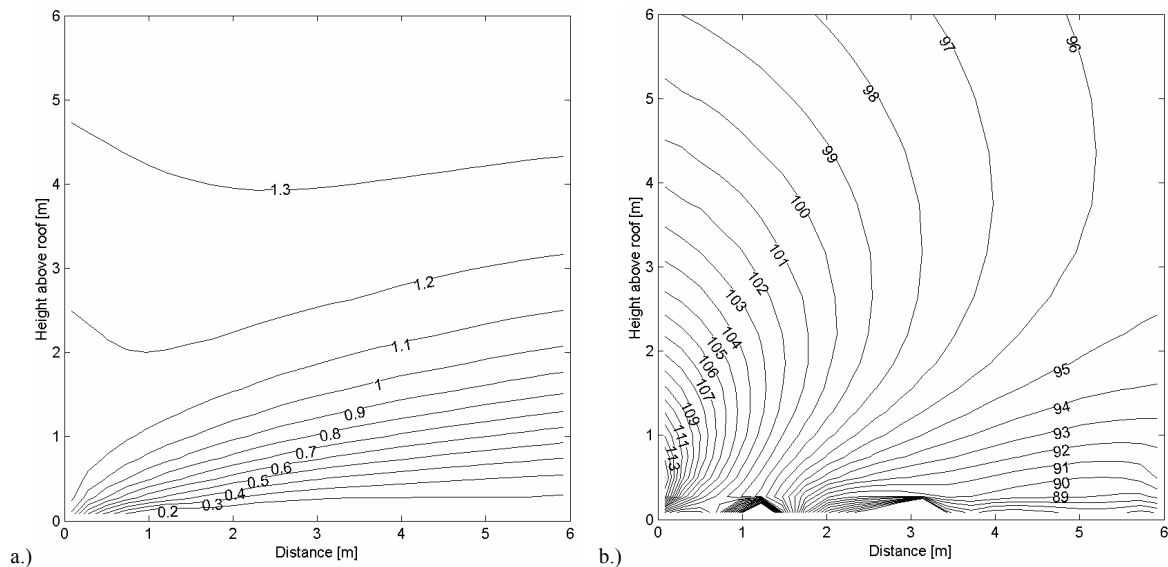


Figure 3.11: Two dimensional computed air flow field above a flat roof building with the dimension of 6 x 6 m

a.) Air speed 0 to 6 m above roof level, normalised with wind speed on ridge height.

b.) Air velocity angle 0 to 6 m above roof level.

Influence of the roughness parameter z_0 for flat roof building

By comparing case 1.1a with 1.1b it can be seen that the C_p -values are very similar. The more wind sheltered site in case 1.1b leads to lower C_p -values on the windward wall because of smaller air velocities near the ground. The normalised air speed above roof is slightly higher above and slightly lower below 10 m height above ground. This is caused by the two different wind profiles which have an intersection at the height of 10 m above ground level. The discrepancies of the flow angle can be described by the same phenomena.

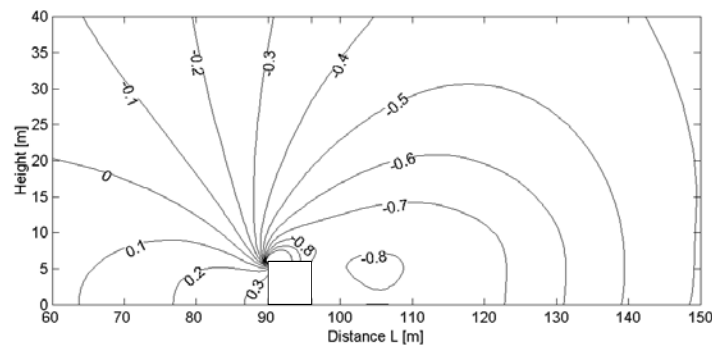
Case 1.1c

Figure 3.12: Two dimensional CFD calculation of the C_p -value field.

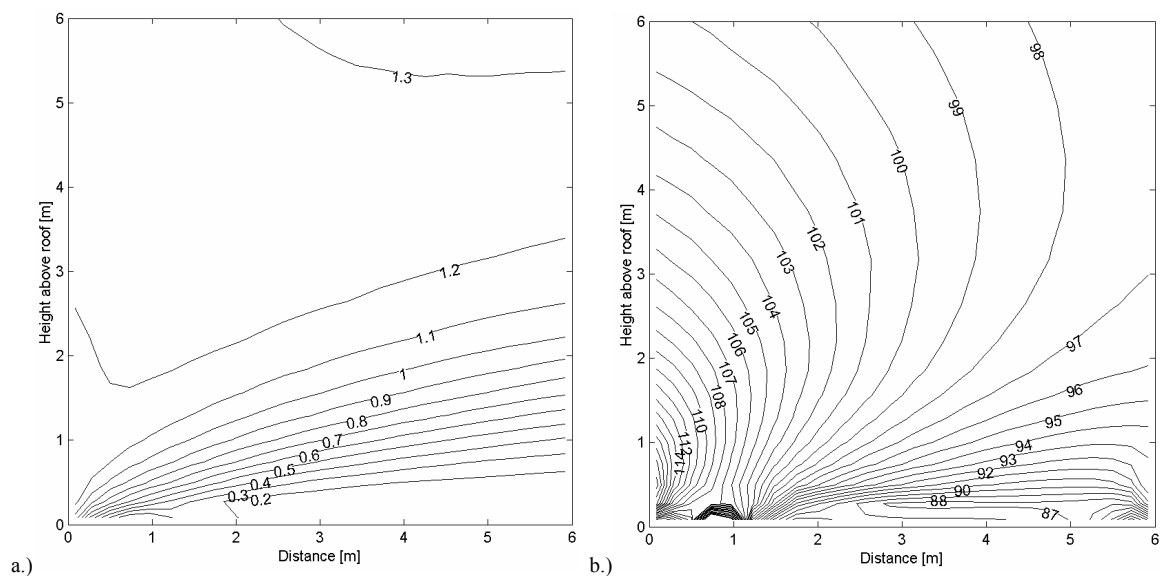


Figure 3.13: Two dimensional computed air flow field above a flat roof building with the dimension of 6 x 6 m

a.) Air speed 0 to 6 m above roof level, normalised with wind speed on ridge height.

b.) Air velocity angle 0 to 6 m above roof level.

Influence of wind velocity level for flat roof building

For both normalised wind speed and flow angle a satisfactory agreement can be found by comparing case 1.1a with 1.1c. Only the C_p -value in the near surroundings of the building are not exactly identical. Even though it can be stated, that the normalised speed and flow angle above a flat roof building are nearly independent of wind velocity level.

3.2.2. Using CFD results for cowl performance calculation

Both speed and flow angle are needed to select the correct $C_{p,cowl}$ from measurement data. The C_p at the cowl position above the roof is needed to calculate the static pressure $p_{s,cowl}$. With $p_{s,cowl}$, the local speed U and $C_{p,cowl}$ the total pressure in the duct $p_{t,cowl}$ can be calculated according to eq. (14). Because these variables are highly dependent on wind direction and building geometry, a large amount of data will be needed to properly predict the pressure situation in cowls. Therefore two different approaches could be considered to carry out transient simulations of ventilation systems including cowls:

1. Calculation of a project specific case

If the geometry of the building and position of the cowl is already defined the normalised speed, the vertical flow angle and the C_p is mainly a function of the wind direction which can be determined for a certain position above roof.

2. Establishment of a database

In this case we do not know anything about the building and the position of the cowl in advance. With a huge amount of computations the three dimensional data field could be parameterised with building geometry, cowl position and wind direction.

As an example of the first approach, the wind direction dependent values of local flow angles, velocity ratios and C_p values have been evaluated for the case 4.1 of table 3.4. The dimensions of the building are 6 m x 12 m x 12 m and the roof pitch angle is 30 degrees.

The air flow around the building has been calculated with CFD for different wind directions in 45 degrees interval. To reduce the number of calculation cases the influence of the wind speed level on the air flow pattern is neglected. Hence, the investigation has been done for a wind speed of 2 m/s which corresponds with an average wind speed in Switzerland. From the comprehensive numerical results only the data near the cowl are of interests and have been evaluated.

The results are given in table 3.6, table 3.7 and figure 3.8 for the 45 cowl positions indicated in figure 3.14., figure 3.15 and figure 3.16 show the results for one cowl position in three different heights. The normalised speed and the vertical incidence flow angle are shown as a function of the wind direction. These functions have been found by interpolating the results of the 45 degrees intervals.

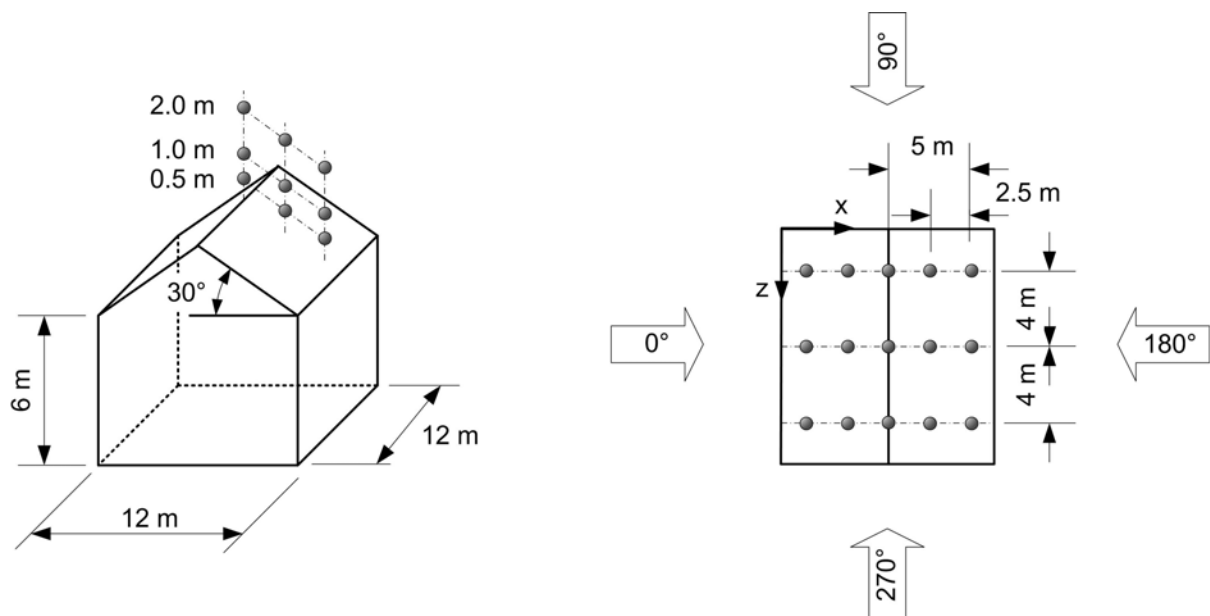


Figure 3.14: Definition of the example building. Evaluation of the flow field for 45 cowl positions with three CFD calculations.

Table 3.6: Results from CFD calculations: vertical incidence flow angle φ for all cowl positions.

position			wind direction β [°]								
x [m]	z [m]	height above roof [m]									
			0	45	90	135	180	225	270	315	360
1.0	2.0	0.5	114.4	107.9	91.1	118.3	115.2	77.1	87.7	105.7	114.4
1.0	6.0	0.5	117.1	107.4	87.8	86.7	117.4	86.7	87.8	107.4	117.1
1.0	10.0	0.5	114.4	105.7	87.7	77.1	115.2	118.3	91.1	107.9	114.4
1.0	2.0	1.0	110.9	106.7	93.8	108.7	115.9	71.8	87.4	105.1	110.9
1.0	6.0	1.0	114.3	106.8	88.6	69.2	116.0	69.2	88.6	106.8	114.3
1.0	10.0	1.0	110.9	105.1	87.4	71.8	115.9	108.7	93.8	106.7	110.9
1.0	2.0	2.0	106.7	104.9	95.2	93.3	117.6	69.7	88.8	103.4	106.7
1.0	6.0	2.0	110.4	105.0	90.4	71.7	116.5	71.7	90.4	105.0	110.4
1.0	10.0	2.0	106.7	103.4	88.8	69.7	117.6	93.3	95.2	104.9	106.7
3.5	2.0	0.5	114.9	109.7	95.4	114.6	115.9	96.2	86.5	108.0	114.9
3.5	6.0	0.5	117.1	109.4	87.3	84.3	118.0	84.3	87.3	109.4	117.1
3.5	10.0	0.5	114.9	108.0	86.5	96.2	115.9	114.6	95.4	109.7	114.9
3.5	2.0	1.0	111.0	107.4	97.0	87.6	115.9	94.9	88.2	106.2	111.0
3.5	6.0	1.0	113.9	107.3	90.8	75.2	118.6	75.2	90.8	107.3	113.9
3.5	10.0	1.0	111.0	106.2	88.2	94.9	115.9	87.6	97.0	107.4	111.0
3.5	2.0	2.0	105.7	103.8	96.9	89.8	100.5	90.2	89.6	103.0	105.7
3.5	6.0	2.0	108.9	103.7	91.5	81.1	102.3	81.1	91.5	103.7	108.9
3.5	10.0	2.0	105.7	103.0	89.6	90.2	100.5	89.8	96.9	103.8	105.7
6.0	2.0	0.5	107.7	98.5	92.5	98.5	107.7	103.8	86.5	103.8	107.7
6.0	6.0	0.5	109.1	100.9	86.7	100.9	109.1	100.9	86.7	100.9	109.1
6.0	10.0	0.5	107.7	103.8	86.5	103.8	107.7	98.5	92.5	98.5	107.7
6.0	2.0	1.0	105.3	97.1	94.8	97.1	105.3	101.3	87.2	101.3	105.3
6.0	6.0	1.0	107.3	98.1	88.4	98.1	107.3	98.1	88.4	98.1	107.3
6.0	10.0	1.0	105.3	101.3	87.2	101.3	105.3	97.1	94.8	97.1	105.3
6.0	2.0	2.0	101.2	96.3	95.7	96.3	101.2	97.5	88.8	97.5	101.2
6.0	6.0	2.0	103.5	95.5	90.6	95.5	103.5	95.5	90.6	95.5	103.5
6.0	10.0	2.0	101.2	97.5	88.8	97.5	101.2	96.3	95.7	96.3	101.2
8.5	2.0	0.5	115.9	114.6	95.4	109.7	114.9	108.0	86.3	96.2	115.9
8.5	6.0	0.5	118.0	84.3	87.1	109.4	117.1	109.4	87.1	84.3	118.0
8.5	10.0	0.5	115.9	96.2	86.3	108.0	114.9	109.7	95.4	114.6	115.9
8.5	2.0	1.0	115.9	87.6	97.0	107.4	111.0	106.2	88.1	94.9	115.9
8.5	6.0	1.0	118.6	75.2	90.7	107.3	113.9	107.3	90.7	75.2	118.6
8.5	10.0	1.0	115.9	94.9	88.1	106.2	111.0	107.4	97.0	87.6	115.9
8.5	2.0	2.0	100.5	89.8	96.9	103.8	105.7	103.0	89.5	90.2	100.5
8.5	6.0	2.0	102.3	81.1	91.5	103.7	108.9	103.7	91.5	81.1	102.3
8.5	10.0	2.0	100.5	90.2	89.5	103.0	105.7	103.8	96.9	89.8	100.5
11.0	2.0	0.5	115.2	118.3	91.0	107.9	114.4	105.7	87.5	77.1	115.2
11.0	6.0	0.5	117.4	86.7	87.6	107.4	117.1	107.4	87.6	86.7	117.4
11.0	10.0	0.5	115.2	77.1	87.5	105.7	114.4	107.9	91.0	118.3	115.2
11.0	2.0	1.0	115.9	108.7	93.8	106.7	110.9	105.1	87.3	71.8	115.9
11.0	6.0	1.0	116.0	69.2	88.5	106.8	114.3	106.8	88.5	69.2	116.0
11.0	10.0	1.0	115.9	71.8	87.3	105.1	110.9	106.7	93.8	108.7	115.9
11.0	2.0	2.0	117.6	93.3	95.2	104.9	106.7	103.4	88.8	69.7	117.6
11.0	6.0	2.0	116.5	71.7	90.4	105.0	110.4	105.0	90.4	71.7	116.5
11.0	10.0	2.0	117.6	69.7	88.8	103.4	106.7	104.9	95.2	93.3	117.6

Table 3.7: Results from CFD calculations: normalised flow speed u for all cowl positions.

position			wind direction β [°]								
x [m]	z [m]	height above roof [m]									
			0	45	90	135	180	225	270	315	360
1.0	2.0	0.5	0.748	0.824	0.663	0.269	0.171	0.488	0.359	0.905	0.748
1.0	6.0	0.5	0.694	0.858	0.323	0.119	0.223	0.119	0.323	0.858	0.694
1.0	10.0	0.5	0.748	0.905	0.359	0.488	0.171	0.269	0.663	0.824	0.748
1.0	2.0	1.0	0.805	0.866	1.015	0.314	0.162	0.705	0.590	0.945	0.805
1.0	6.0	1.0	0.755	0.901	0.703	0.280	0.216	0.280	0.703	0.901	0.755
1.0	10.0	1.0	0.805	0.945	0.590	0.705	0.162	0.314	1.015	0.866	0.805
1.0	2.0	2.0	0.867	0.916	1.118	0.685	0.125	0.875	0.981	0.985	0.867
1.0	6.0	2.0	0.823	0.951	1.033	0.754	0.172	0.754	1.033	0.951	0.823
1.0	10.0	2.0	0.867	0.985	0.981	0.875	0.125	0.685	1.118	0.916	0.867
3.5	2.0	0.5	0.854	0.956	0.599	0.225	0.170	0.361	0.281	0.976	0.854
3.5	6.0	0.5	0.831	0.980	0.214	0.605	0.190	0.605	0.214	0.980	0.831
3.5	10.0	0.5	0.854	0.976	0.281	0.361	0.170	0.225	0.599	0.956	0.854
3.5	2.0	1.0	0.909	1.010	1.031	0.425	0.133	0.291	0.539	1.019	0.909
3.5	6.0	1.0	0.886	1.026	0.649	0.999	0.139	0.999	0.649	1.026	0.886
3.5	10.0	1.0	0.909	1.019	0.539	0.291	0.133	0.425	1.031	1.010	0.909
3.5	2.0	2.0	0.986	1.065	1.152	1.196	0.743	1.106	1.037	1.073	0.986
3.5	6.0	2.0	0.964	1.080	1.079	1.223	0.689	1.223	1.079	1.080	0.964
3.5	10.0	2.0	0.986	1.073	1.037	1.106	0.743	1.196	1.152	1.065	0.986
6.0	2.0	0.5	1.102	1.343	0.880	1.343	1.102	1.183	0.852	1.183	1.102
6.0	6.0	0.5	1.094	1.338	0.815	1.338	1.094	1.338	0.815	1.338	1.094
6.0	10.0	0.5	1.102	1.183	0.852	1.183	1.102	1.343	0.880	1.343	1.102
6.0	2.0	1.0	1.082	1.251	1.091	1.251	1.082	1.162	0.989	1.162	1.082
6.0	6.0	1.0	1.071	1.256	1.003	1.256	1.071	1.256	1.003	1.256	1.071
6.0	10.0	1.0	1.082	1.162	0.989	1.162	1.082	1.251	1.091	1.251	1.082
6.0	2.0	2.0	1.098	1.180	1.157	1.180	1.098	1.163	1.100	1.163	1.098
6.0	6.0	2.0	1.089	1.201	1.126	1.201	1.089	1.201	1.126	1.201	1.089
6.0	10.0	2.0	1.098	1.163	1.100	1.163	1.098	1.180	1.157	1.180	1.098
8.5	2.0	0.5	0.170	0.225	0.596	0.956	0.854	0.976	0.280	0.361	0.170
8.5	6.0	0.5	0.190	0.605	0.212	0.980	0.831	0.980	0.212	0.605	0.190
8.5	10.0	0.5	0.170	0.361	0.280	0.976	0.854	0.956	0.596	0.225	0.170
8.5	2.0	1.0	0.133	0.425	1.030	1.010	0.909	1.019	0.538	0.291	0.133
8.5	6.0	1.0	0.139	0.999	0.647	1.026	0.886	1.026	0.647	0.999	0.139
8.5	10.0	1.0	0.133	0.291	0.538	1.019	0.909	1.010	1.030	0.425	0.133
8.5	2.0	2.0	0.743	1.196	1.152	1.065	0.986	1.073	1.037	1.106	0.743
8.5	6.0	2.0	0.689	1.223	1.078	1.080	0.964	1.080	1.078	1.223	0.689
8.5	10.0	2.0	0.743	1.106	1.037	1.073	0.986	1.065	1.152	1.196	0.743
11.0	2.0	0.5	0.171	0.269	0.661	0.824	0.748	0.905	0.357	0.488	0.171
11.0	6.0	0.5	0.223	0.119	0.320	0.858	0.694	0.858	0.320	0.119	0.223
11.0	10.0	0.5	0.171	0.488	0.357	0.905	0.748	0.824	0.661	0.269	0.171
11.0	2.0	1.0	0.162	0.314	1.014	0.866	0.805	0.945	0.586	0.705	0.162
11.0	6.0	1.0	0.216	0.280	0.699	0.901	0.755	0.901	0.699	0.280	0.216
11.0	10.0	1.0	0.162	0.705	0.586	0.945	0.805	0.866	1.014	0.314	0.162
11.0	2.0	2.0	0.125	0.685	1.118	0.916	0.867	0.985	0.979	0.875	0.125
11.0	6.0	2.0	0.172	0.754	1.033	0.951	0.823	0.951	1.033	0.754	0.172
11.0	10.0	2.0	0.125	0.875	0.979	0.985	0.867	0.916	1.118	0.685	0.125

Table 3.8: Results from CFD calculations: C_p -values for all cowl positions.

position			wind direction β [°]								
x [m]	z [m]	height above roof [m]									
			0	45	90	135	180	225	270	315	360
1.0	2.0	0.5	0.18	0.15	-0.51	-0.56	-0.33	-0.47	-0.20	-0.08	0.18
1.0	6.0	0.5	0.25	0.03	-0.30	-0.53	-0.33	-0.53	-0.30	0.03	0.25
1.0	10.0	0.5	0.18	-0.08	-0.20	-0.47	-0.33	-0.56	-0.51	0.15	0.18
1.0	2.0	1.0	0.17	0.14	-0.47	-0.57	-0.33	-0.48	-0.20	-0.07	0.17
1.0	6.0	1.0	0.24	0.03	-0.30	-0.53	-0.33	-0.53	-0.30	0.03	0.24
1.0	10.0	1.0	0.17	-0.07	-0.20	-0.48	-0.33	-0.57	-0.47	0.14	0.17
1.0	2.0	2.0	0.15	0.12	-0.39	-0.56	-0.33	-0.48	-0.19	-0.07	0.15
1.0	6.0	2.0	0.21	0.01	-0.28	-0.50	-0.33	-0.50	-0.28	0.01	0.21
1.0	10.0	2.0	0.15	-0.07	-0.19	-0.48	-0.33	-0.56	-0.39	0.12	0.15
3.5	2.0	0.5	0.05	-0.06	-0.54	-0.67	-0.34	-0.55	-0.20	-0.17	0.05
3.5	6.0	0.5	0.08	-0.13	-0.31	-0.71	-0.33	-0.71	-0.31	-0.13	0.08
3.5	10.0	0.5	0.05	-0.17	-0.20	-0.55	-0.34	-0.67	-0.54	-0.06	0.05
3.5	2.0	1.0	0.03	-0.08	-0.50	-0.66	-0.34	-0.55	-0.20	-0.18	0.03
3.5	6.0	1.0	0.05	-0.15	-0.30	-0.70	-0.33	-0.70	-0.30	-0.15	0.05
3.5	10.0	1.0	0.03	-0.18	-0.20	-0.55	-0.34	-0.66	-0.50	-0.08	0.03
3.5	2.0	2.0	0.00	-0.10	-0.38	-0.51	-0.32	-0.48	-0.19	-0.19	0.00
3.5	6.0	2.0	0.02	-0.17	-0.27	-0.56	-0.32	-0.56	-0.27	-0.17	0.02
3.5	10.0	2.0	0.00	-0.19	-0.19	-0.48	-0.32	-0.51	-0.38	-0.10	0.00
6.0	2.0	0.5	-0.37	-0.87	-0.49	-0.87	-0.37	-0.54	-0.19	-0.54	-0.37
6.0	6.0	0.5	-0.37	-0.86	-0.29	-0.86	-0.37	-0.86	-0.29	-0.86	-0.37
6.0	10.0	0.5	-0.37	-0.54	-0.19	-0.54	-0.37	-0.87	-0.49	-0.87	-0.37
6.0	2.0	1.0	-0.27	-0.57	-0.43	-0.57	-0.27	-0.43	-0.19	-0.43	-0.27
6.0	6.0	1.0	-0.27	-0.61	-0.28	-0.61	-0.27	-0.61	-0.28	-0.61	-0.27
6.0	10.0	1.0	-0.27	-0.43	-0.19	-0.43	-0.27	-0.57	-0.43	-0.57	-0.27
6.0	2.0	2.0	-0.17	-0.32	-0.29	-0.32	-0.17	-0.31	-0.18	-0.31	-0.17
6.0	6.0	2.0	-0.18	-0.38	-0.24	-0.38	-0.18	-0.38	-0.24	-0.38	-0.18
6.0	10.0	2.0	-0.17	-0.31	-0.18	-0.31	-0.17	-0.32	-0.29	-0.32	-0.17
8.5	2.0	0.5	-0.34	-0.67	-0.55	-0.06	0.05	-0.17	-0.20	-0.55	-0.34
8.5	6.0	0.5	-0.33	-0.71	-0.31	-0.13	0.08	-0.13	-0.31	-0.71	-0.33
8.5	10.0	0.5	-0.34	-0.55	-0.20	-0.17	0.05	-0.06	-0.55	-0.67	-0.34
8.5	2.0	1.0	-0.34	-0.66	-0.50	-0.08	0.03	-0.18	-0.20	-0.55	-0.34
8.5	6.0	1.0	-0.33	-0.70	-0.30	-0.15	0.05	-0.15	-0.30	-0.70	-0.33
8.5	10.0	1.0	-0.34	-0.55	-0.20	-0.18	0.03	-0.08	-0.50	-0.66	-0.34
8.5	2.0	2.0	-0.32	-0.51	-0.38	-0.10	0.00	-0.19	-0.19	-0.48	-0.32
8.5	6.0	2.0	-0.32	-0.56	-0.27	-0.17	0.02	-0.17	-0.27	-0.56	-0.32
8.5	10.0	2.0	-0.32	-0.48	-0.19	-0.19	0.00	-0.10	-0.38	-0.51	-0.32
11.0	2.0	0.5	-0.33	-0.56	-0.51	0.15	0.18	-0.08	-0.20	-0.47	-0.33
11.0	6.0	0.5	-0.33	-0.53	-0.30	0.03	0.25	0.03	-0.30	-0.53	-0.33
11.0	10.0	0.5	-0.33	-0.47	-0.20	-0.08	0.18	0.15	-0.51	-0.56	-0.33
11.0	2.0	1.0	-0.33	-0.57	-0.47	0.14	0.17	-0.07	-0.20	-0.48	-0.33
11.0	6.0	1.0	-0.33	-0.53	-0.30	0.03	0.24	0.03	-0.30	-0.53	-0.33
11.0	10.0	1.0	-0.33	-0.48	-0.20	-0.07	0.17	0.14	-0.47	-0.57	-0.33
11.0	2.0	2.0	-0.33	-0.56	-0.39	0.12	0.15	-0.07	-0.19	-0.48	-0.33
11.0	6.0	2.0	-0.33	-0.50	-0.28	0.01	0.21	0.01	-0.28	-0.50	-0.33
11.0	10.0	2.0	-0.33	-0.48	-0.19	-0.07	0.15	0.12	-0.39	-0.56	-0.33

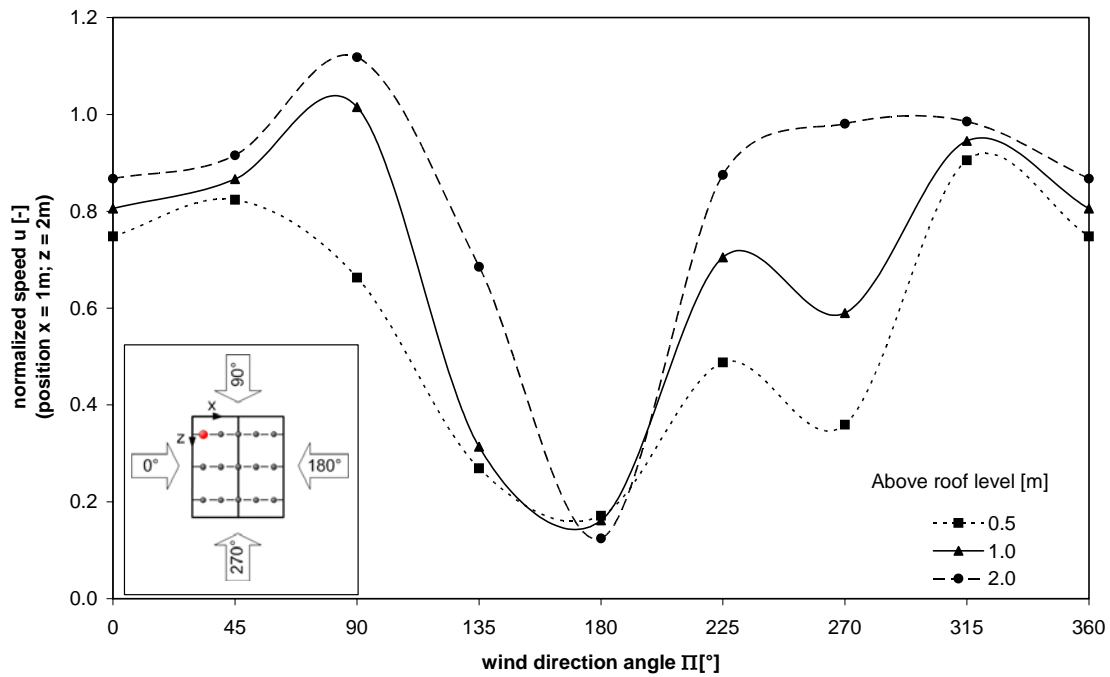


Figure 3.15: Normalised speed u depending on wind direction calculated from CFD results for one position in three different heights

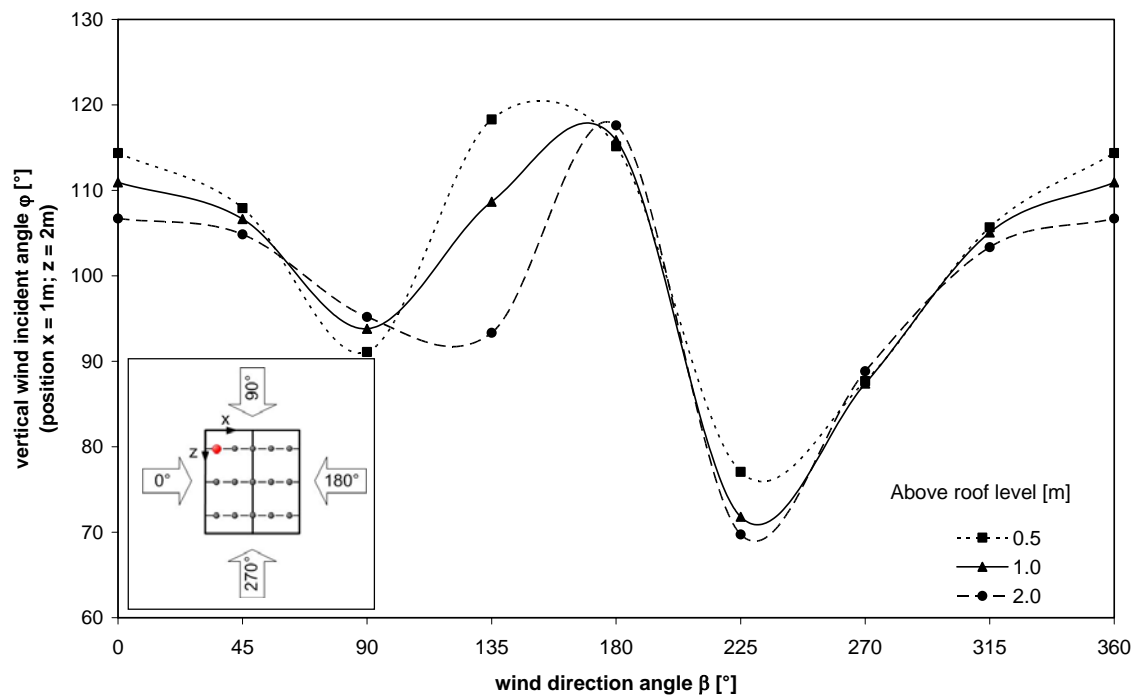


Figure 3.16: Vertical incidence flow angle depending on wind direction calculated from CFD results for one position in three different heights

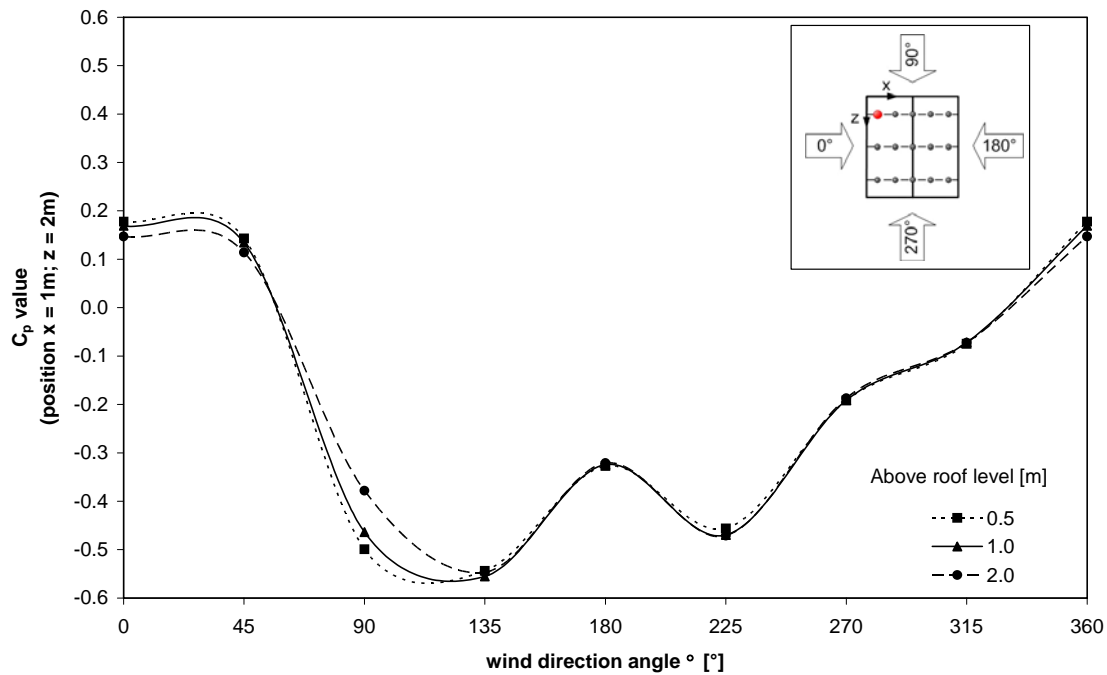


Figure 3.17: C_p value depending on wind direction calculated from CFD results for one position in three different heights

3.2.3. How to model cowl performance with TRNSYS?

Within the RESHYVENT project, the building and system simulation program TRNSYS [Klein 2000] has been used for the performance assessment of the four systems. TRNFLOW is the complete integration of the multizone air flow and pollutant transport model COMIS [Feustel 2001] into the thermal multizone building module TRNSYS.

Figure 3.18 shows a proposal how cowls could be modelled in TRNSYS by using TRNFLOW and a new separate Type for the cowl model. This proposed type has to be fed with wind data, CFD results of the specific building as shown in table 3.6, table 3.7 and table 3.8 and with the wind channel test data of the cowl. Because the cowl characteristic is highly dependant on the duct mass flow an iterative calculation is necessary. The new type carries out the interpolation of the CFD data according to the actual wind direction. The results of this interpolation are the C_p -value at the cowl position above the roof, the local wind speed and the vertical incident angle at the cowl position. The C_p -value is used to calculate the static pressure $p_{s,cowl}$ at the cowl position according to equation (22). The speed and the incident angle together with the velocity in the duct is used to determine the cowl pressure difference from the test data using equation (14) and the methodology described in chapter 3.1.3. The resulting total pressure $p_{t,duct}$ at the end of the duct is then the input for TRNFLOW.

TRNFLOW has to be adapted in the way that the pressure of an external node can be defined as an input. This is not a feature of the current version of TRNFLOW; it has to be implemented if the proposed method should be applied.

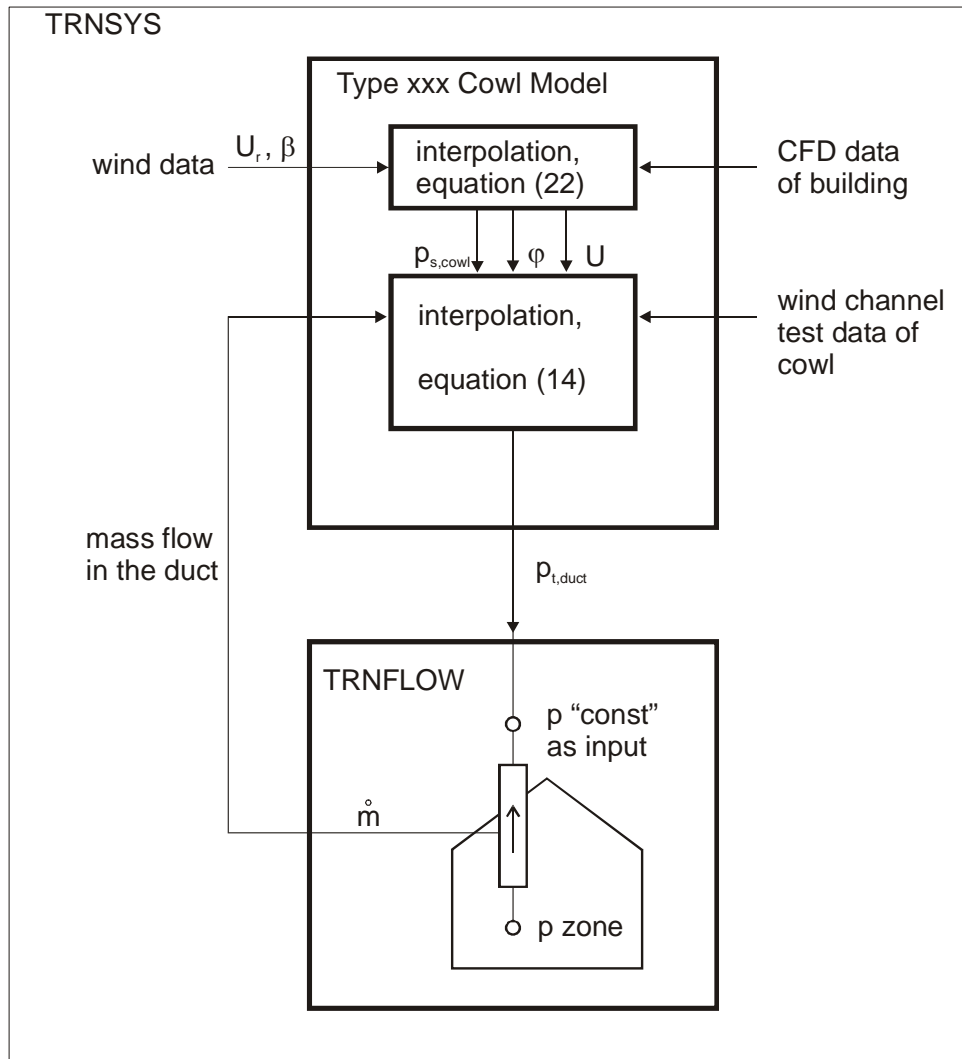


Figure 3.18: Modelling of cowls in TRNSYS

4. Influence of building leakage on pressure levels and outdoor air flow rates

4.1. Building leakage

Compared to ducts, filters and heat exchangers, pressure drops in external and internal air transfer devices (ATD) are very small. Likewise, natural forces induce low pressures in the range of a few Pascal. Therefore, the exhaust flow in an exhaust ventilation system is hardly affected by these external factors, also for axial fans with flat pressure –flow characteristic.

But on the other hand, the supply flow through the ATD is very much affected by small pressure changes and natural forces have great influence. Further more, even at these low pressures, a significant amount of the outdoor air is not entering the building through the ATD, but through leaks in the building envelope itself. These effects are outlined in more detail below.

How much outdoor air is supplied by the ATD and how much is delivered by infiltration? This is illustrated in figure 4.1 for three building air tightness levels. The assumed air flow exponents are 0.7 for the building leakage and 0.52 for the ATD.

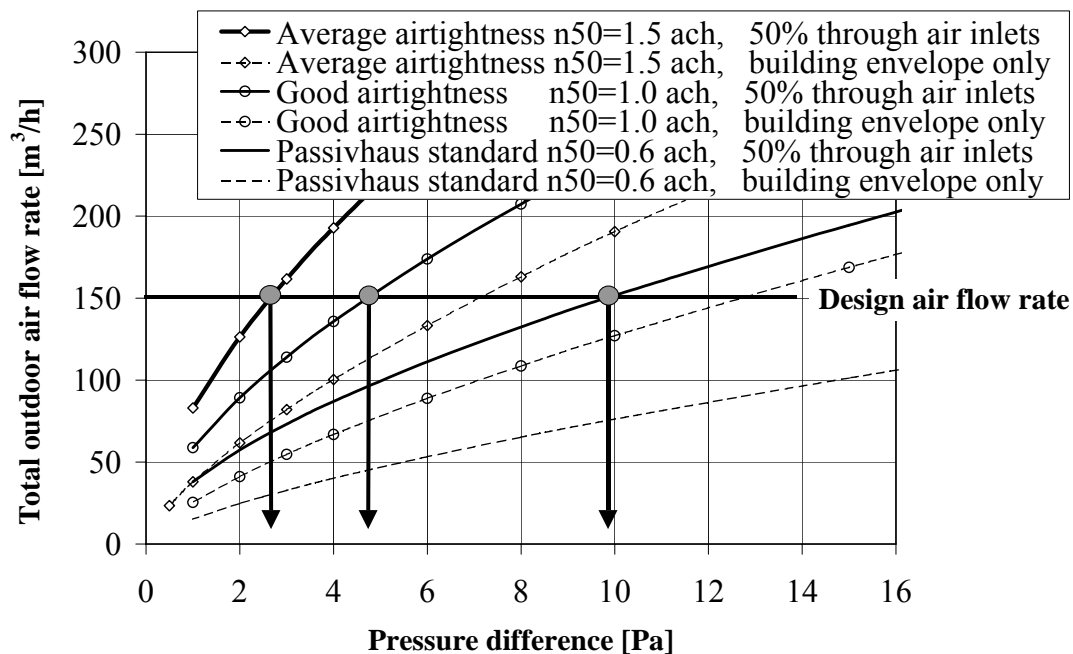


Figure 4.1: Pressure-outdoor flow characteristic for single family houses with different air tightness levels. The ATD are dimensioned such, that 50% of the nominal outdoor air flow rate is delivered by the ATD and the other 50% by infiltration.

Figure 4.1 shows, that for an outdoor air flow rate of 150 m³/h ($n = 0.38 \text{ h}^{-1}$) and for an average tight building (air leakage $n_{50} = 1.5 \text{ h}^{-1}$) already at approx. 2.5 Pa pressure difference 50 % of the outdoor air enters by infiltration. For 80 % supply by the ATD, pressure level must be reduced to 1 Pa.

For a very airtight building (e.g. according to the Passivhaus standard, $n_{50} = 0.6 \text{ h}^{-1}$) also at 10 Pa pressure difference, still more than 50 % of the outdoor flow can be supplied through the ATD.

These examples highlight the high importance of the building air tightness for extract systems. Only in very airtight buildings, reasonable amount of the outdoor air can be supplied through the ATD as intended. In all other cases, outdoor air is supplied mainly by infiltration, despite the fact that low pressure ATDs are installed.

4.2. Building leakage distribution

4.2.1. Pressure difference due to stack

Pressures induced by stack are in the same pressure range as the design pressures for the ATD. The flow through the ATD is influenced by natural forces accordingly. Figure 4.2 gives cumulative frequency of the thermal induced pressure difference during the heating period for the location Zurich for different stack heights. A constant indoor temperature of 20°C is assumed.

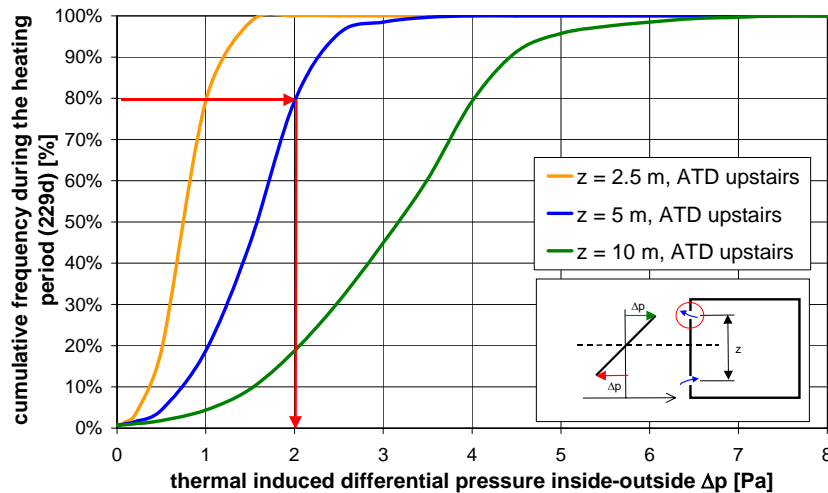


Figure 4.2: Cumulative frequency of the thermal induced pressure difference during the heating period for the location Zurich.

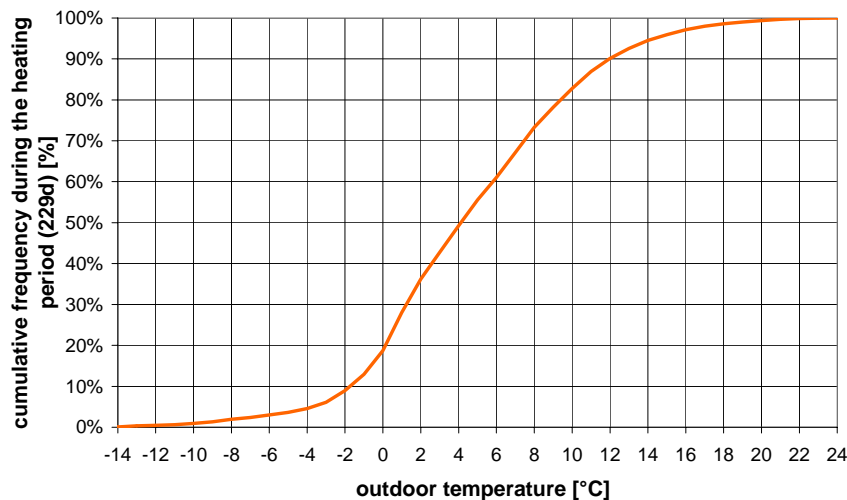


Figure 4.3: Cumulative frequency of the outdoor temperature during the heating period for the location Zurich.

4.2.2. Pressure difference due to wind

The wind induced pressure difference between outside and inside has been calculated using a simple flow network according to Figure 4.4. The total flow through each facade (50 % leakage - plus 50% ATD- flows) is represented by one airflow component with a resulting flow exponent of 0.62. The air flow coefficients of these four components are assumed to be equal. Figure 4.4 gives the cumulative frequency of the wind induced pressure difference for the façades 1 to 4 during the heating period for the location Zurich, assuming a constant wind direction. The cumulative frequency of the wind velocity during the heating period in Zurich is given in figure 4.5.

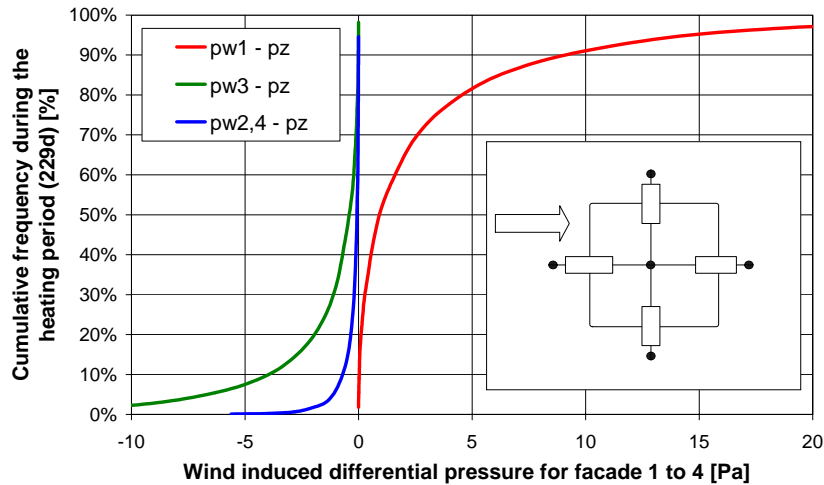


Figure 4.4: Cumulative frequency of the wind induced pressure difference for façade 1 to 4 during the heating period for the location Zurich.

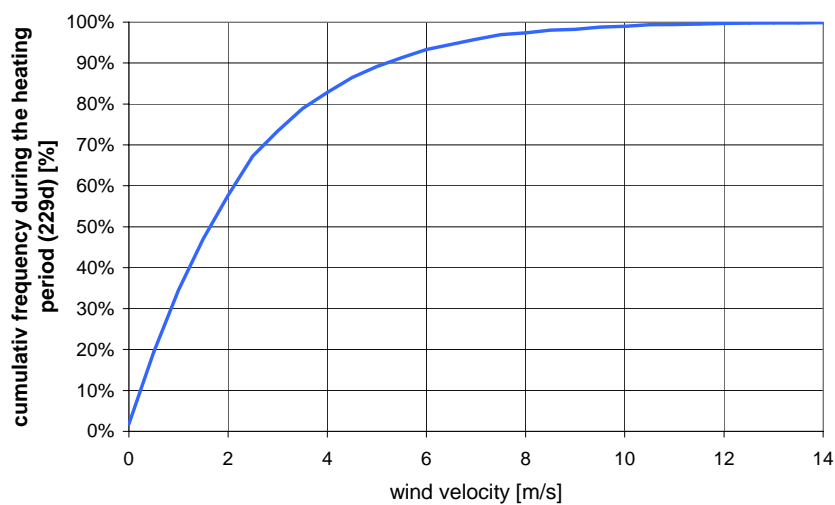


Figure 4.5: Cumulative frequency of the wind velocity during the heating period for the location Zurich

4.2.3. Combination of stack and wind differential pressure

Figure 4.6 and figure 4.7 give the cumulative frequency of the wind and thermal induced pressure difference across the façade during the heating period for the location Zurich, for the windward and the leeward façade respectively. A constant difference of 0 Pa to the ambient barometric pressure is assumed in the middle of the effective stack height which only can be achieved with additional in- respectively outflows (q_a) e.g. through leakages or other ATDs.

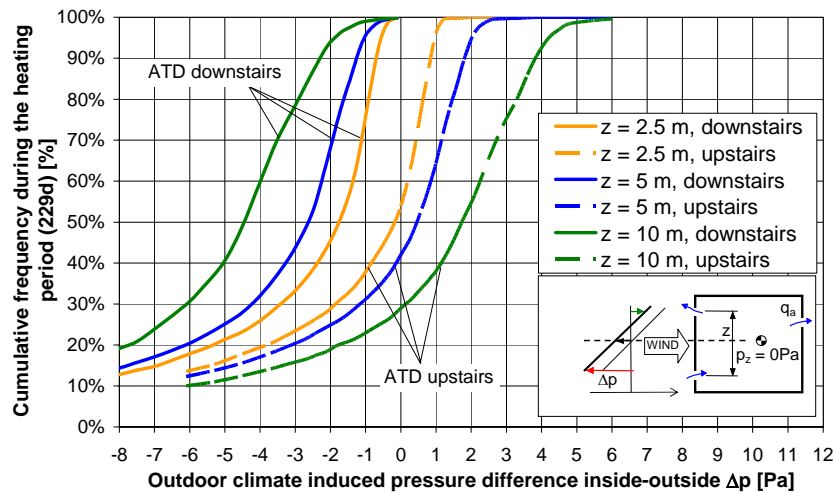


Figure 4.6: Cumulative frequency of the wind and thermal induced pressure difference during the heating period for the location Zurich. Pressure differences are only valid for the windward façade.

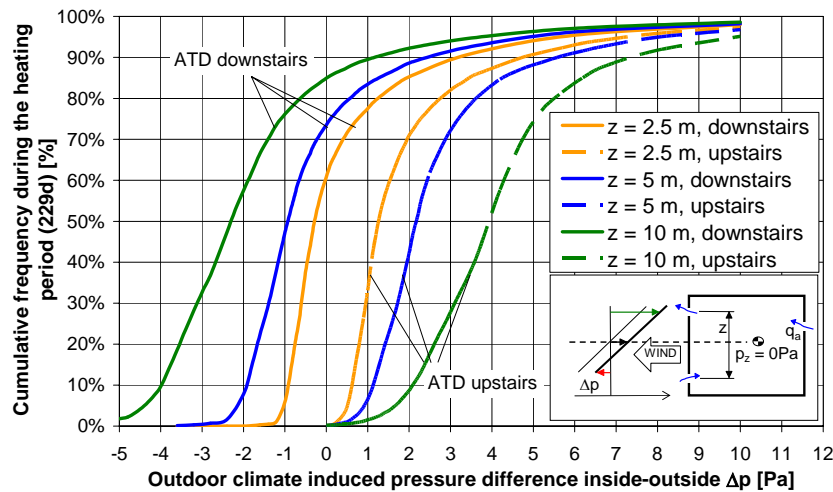


Figure 4.7: Cumulative frequency of the wind and thermal induced pressure difference during the heating period for the location Zurich. Pressure differences are only valid for the leeward façade.

4.2.4. Influence of wind and stack effect on the air change (COMIS calculations)

The influence of wind and stack effect on the air change has been investigated by COMIS simulations [Feustel 2001] on the example of a two-storey row-house with an exhaust system in the ground floor. The flow network of the building is shown in figure 4.8.

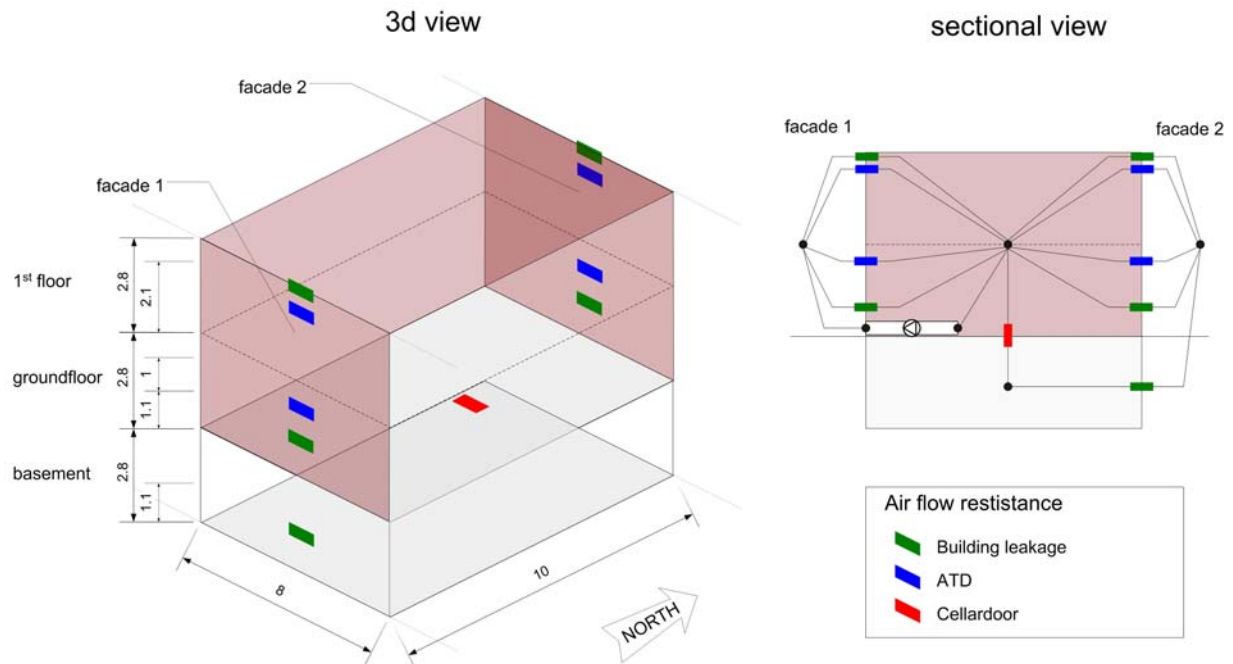


Figure 4.8: COMIS node model for the air flow calculation of a residential natural and exhaust ventilation system

Table 4.1: C_p -values for façade 1 and 2

Wind direction	0°	90°	180°	270°
C_p façade 1	0.5	-0.1	-0.3	-0.1
C_p façade 2	-0.3	-0.1	0.5	-0.1

Resulting air flows are again calculated for the heating period in Zurich, using DRY weather data. Wind pressure coefficients for a free standing building according to table 4.1 have been used. Figure 4.9 shows the cumulative frequency of the outdoor air change rate for the situation without the exhaust system. Due to the stack effect the major part of the outdoor air enters the building through the ATDs in the ground floor and leaves through the ATDs in the 1st floor. Dependent on the number of ATDs, the air enters the building between 75% and 85% of the time exclusively in the ground floor.

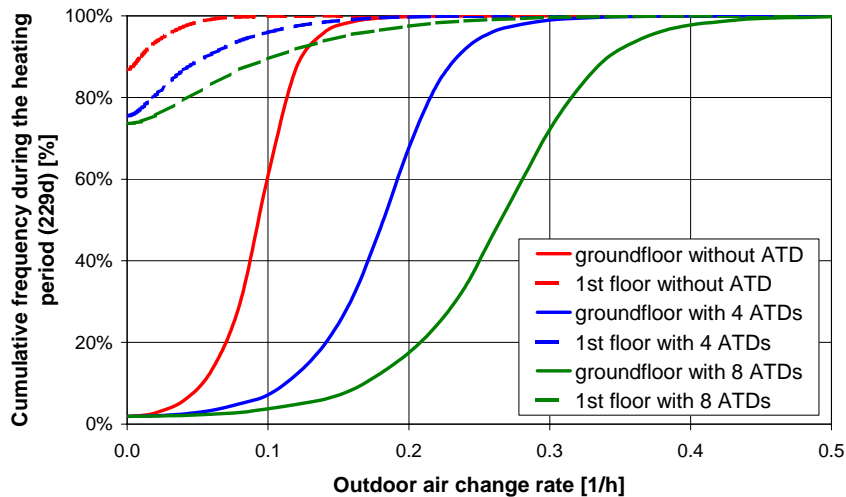


Figure 4.9: Cumulative frequency of the outdoor air change during the heating period caused by the natural ventilation (wind and thermal effects) for different floors and different number of ATDs. (1 ATD: 10 m³/h at 1 Pa)

Figure 4.10 shows the cumulative frequency of the outdoor air change rate when the exhaust system is in use. The design air change rate is $n = 0.4 \text{ h}^{-1}$. With the same number of ATDs installed in the lower and upper floor, the average difference in air change between the two storeys is in the range of $\Delta n = 0.3 \text{ h}^{-1}$. This can be reduced to about $\Delta n = 0.02 \text{ h}^{-1}$ if the number of ATDs in the ground floor is halved and in the 1st floor is doubled.

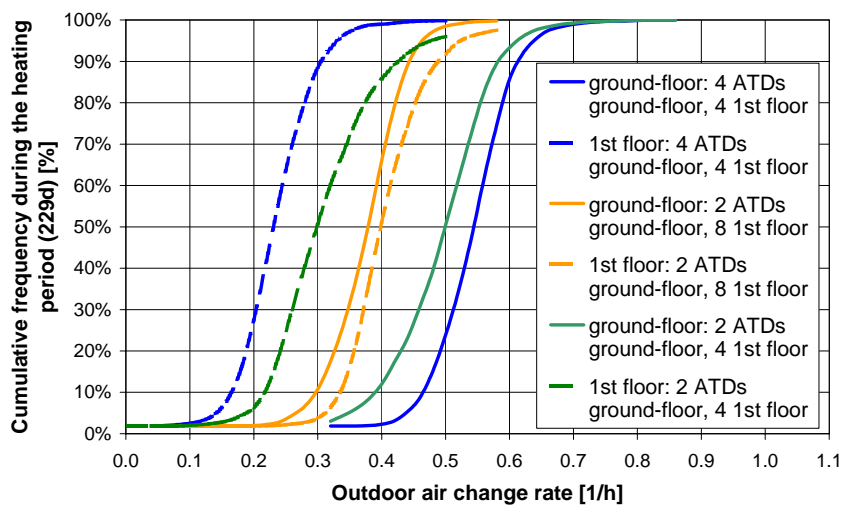


Figure 4.10: Cumulative frequency of the outdoor air change during the heating period caused by the natural ventilation as well as the exhaust ventilation system (design air change rate is $n = 0.4 \text{ h}^{-1}$) for the ground floor (continuous line) and first floor (dashed line) and different distributions of the ATDs.

5. Pressure difference across façades, exhaust grids and fan

5.1. Generic results of COMIS simulation for system 2

The impact of different parameters on the pressure differences across facades, exhaust grids and exhaust fan of a single family house with the hybrid ventilation system 2 has been investigated by simulation with the COMIS code [Feustel 2001]. The ventilation system consists of self regulating supply grids in the façades and an exhaust system with self regulating grids in the kitchen, bathroom and toilet, low pressure ducting and a fan. The system is demand controlled, that means, the supply grids in the different rooms are opened ore closed according to the number of persons present in the room. The volume flow is $7 \text{ dm}^3/\text{s}$ per person present, as long as the pressure difference is at least 1 Pa. The exhaust grids and the fan are controlled in order to maintain a balance or in some cases, a certain imbalance between the air flowing through the supply and the exhaust grids.

The impact of the following parameters on the pressure differences has been investigated:

- 1) building leakage
- 2) imbalance between supply and exhaust air flow
- 3) self regulating supply grids
- 4) resistance of the exhaust system

5.1.1. Building

The building modelled for the evaluation of system2 is a single family house with a floor plan as shown in figure 5.1. The air flow network of the building is also shown the same figure. The green links indicate the self regulating façade grids modeled with a test data component of COMIS.

The room temperatures have been estimated according to the results of a calculation with a thermal model (VA114) of the building.

5.1.2. System

Exhaust system:

The air flow model of the exhaust system is shown in figure 5.2. The system consists of:

- Self regulating grids in kitchen, bathroom and toilet
(pressure difference $> 1 \text{ Pa} \rightarrow$ desired flow)
- Low pressure ducting system. The ducts are modeled with cracks: $q_v = C_{sD} \Delta p^n$
Dimensions: central duct and duct to kitchen: $D = 0.23 \text{ m}$
 duct to bathroom: $D = 0.13 \text{ m}$
 duct to toilet: $D = 0.10 \text{ m}$
- The fan switches on when the flows through the exhaust grids are insufficient. Desired flows will be reached at about 1 Pa across the exhaust grids.
- The total exhaust flow is in balance with the total supply flow.

Façade grids:

Self regulating grids in kitchen, living room, bathroom and bedrooms working at 1 Pa (green links in figure 5.1).

Demand controlled: $7 \text{ dm}^3/\text{s}$ per person present in the room.

5.1.3. Outdoor climate

The simulations have been made with the weather data of The Bilt (in the center of NL) from 26 April 1994 to 25 April 1965.

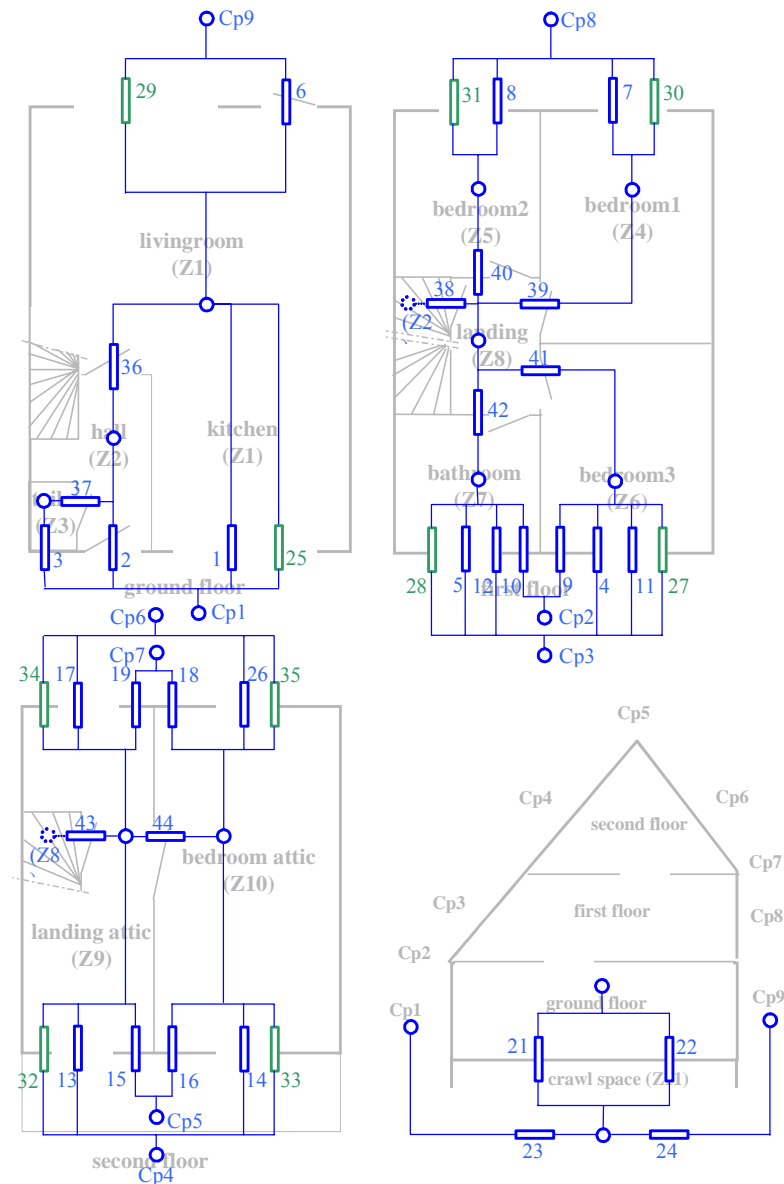


Figure 5.1: Air flow model of the building with system 2

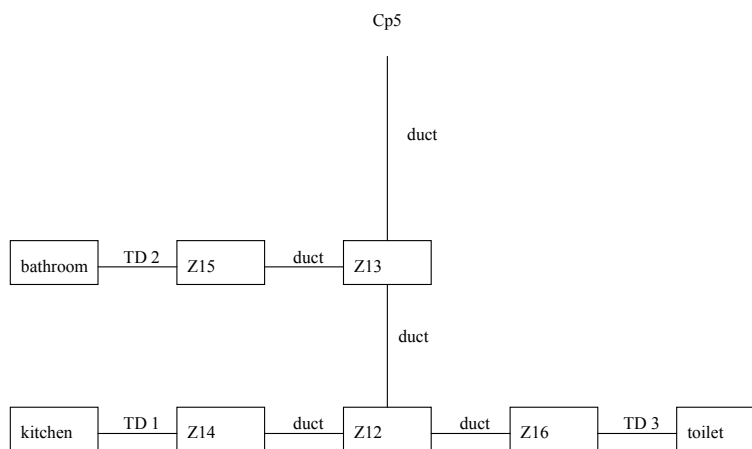


Figure 5.2: Air flow model of the exhaust system part

5.1.4. Presentation of results

Results are given in cumulative diagrams. In these diagrams the percentage of the time is shown when the pressure difference is lower as indicated.

Only situations in which the provisions are in use (opened) are considered. Therefore it has to be noted that the time percentages can not be compared for the different provisions, even if they are shown in the same diagram!

5.1.5. General characteristics of the cumulative diagrams

Façade grids

A positive pressure across a grid means a flow in the desired direction (outside to inside).

Fan

In the fan the flow is always in the desired direction (inside to outside) as the fan will bring up the missing pressure difference if the natural force is not sufficient. A positive pressure across the fan means the natural forces are sufficient and the fan is switched off. A negative pressure across the fan indicates that the fan is in use.

Exhaust grids:

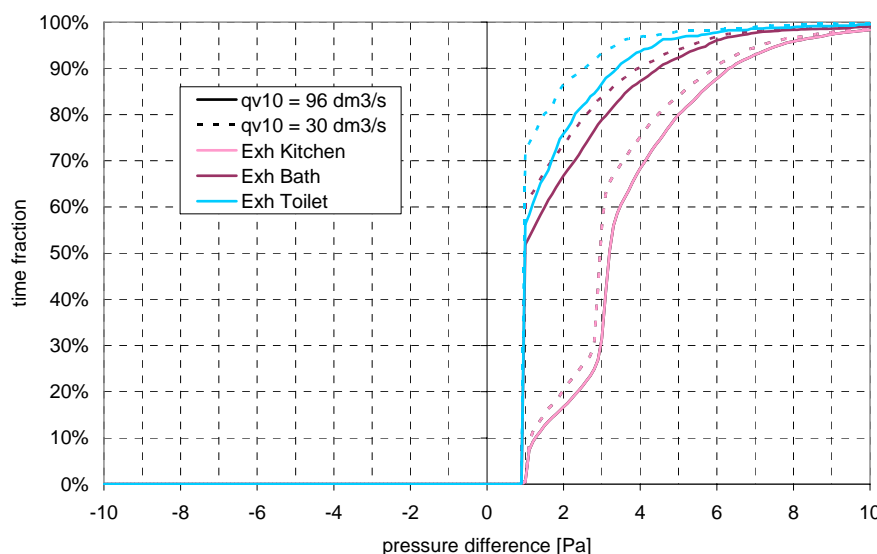
The exhaust grids work a certain percentage of the time (their time in use) on about 1 Pa. This concerns at least to all the situations in which the fan is in use. As stated the fan is on when the flows are insufficient and the exhaust grids will reach their desired flow at about 1 Pa. The rest of the time the pressure over the exhaust grids becomes higher than 1 Pa. These are the situations in which the natural driving forces are high enough. The grids will control and prevent too high air flows. The fan is then switched off.

The figures concerning the exhaust grid in the kitchen show additionally a certain percentage of the time on a more or less constant pressure above 1 Pa. The thermal force in the kitchen is stronger than in the bathroom because of the higher stack. Therefore there is a certain amount of time when the fan is switched on to enhance the pressure difference across the exhaust grid in the bathroom to 1 Pa while the pressure for grid in the kitchen is already sufficient. The pressure difference over the exhaust grid in the kitchen will then be higher than 1 Pa but more or less constant.

5.1.6. Impact of the building leakage

Pressure differences for an overall building leakage of $q_{v,10} = 30 \text{ dm}^3/\text{s}$ and $q_{v,10} = 96 \text{ dm}^3/\text{s}$ has been compared.

Exhaust grids:



*Figure 5.3:
Impact of the building
leakage on the
pressure difference
across the exhaust
grids*

With the tighter façade, a higher pressure difference across the façade is necessary for the same volume flow (leakage + grids). As a result there is less of the total pressure difference left for the exhaust grids during the time fraction when the fan is switched off. The time fraction with the fan turned on, in order to maintain the 1 Pa minimum across the exhaust grids, is higher.

Fan:

With a building leakage of $q_{v,10} = 30 \text{ dm}^3/\text{s}$, the fan has to be turned on during 50% of the occupied time. The pressure differences the switched on fan has to deliver are up to 1 Pa higher as with a leakage of $q_{v,10} = 96 \text{ dm}^3/\text{s}$.

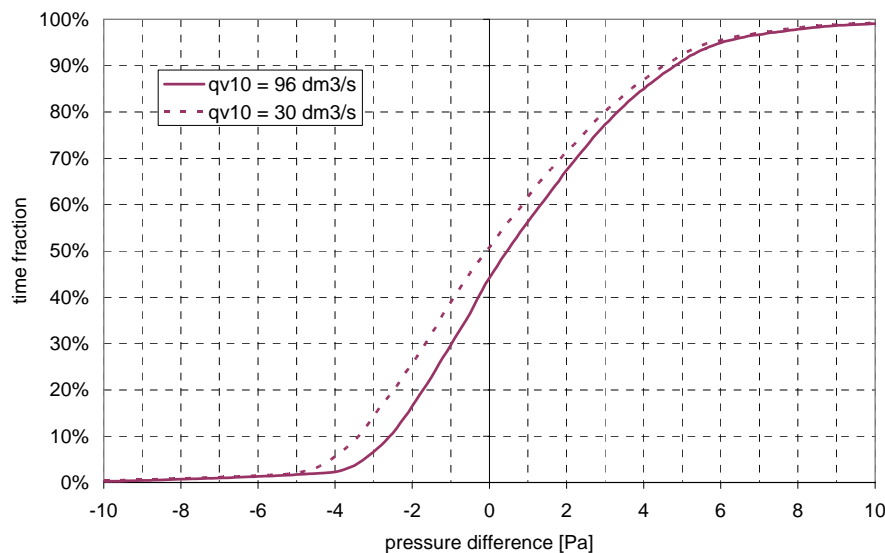


Figure 5.4:
Impact of the building
leakage on the
pressure difference
across the exhaust fan

Façade grids:

The pressure difference across the façade is about 0.5 to 1 Pa higher. But in the bedrooms and in the bath the pressure difference is still below 1 Pa during 80 to 100 % of the time. There might still not be enough supply air in these rooms during that time. In conclusion of that, the building should be as air tight as possible. The cases in the following chapters are therefore based on an air tightness of $q_{v,10} = 30 \text{ dm}^3/\text{s}$. In the bedroom 3 and in the bath there are still negative pressure differences (that means we have exfiltration) during about 10 % of the time.

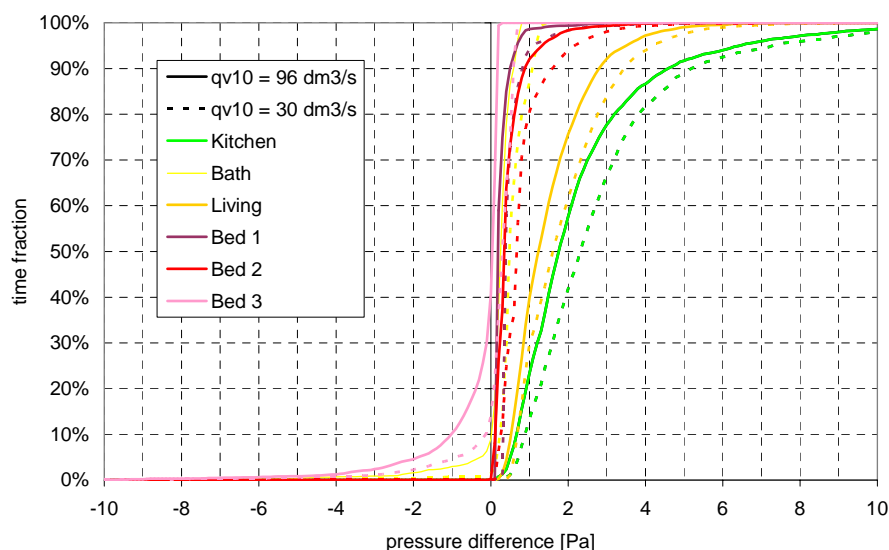


Figure 5.5:
Impact of the building
leakage on the
pressure difference
across the façade

5.1.7. Impact of imbalance

The ratio of the volume flow in the exhaust system to the volume flow through the supply grids is called imbalance ratio in the following. This ratio has been varied between 1.0 and 1.5 by increasing the exhaust volume flow. The supply volume flow has been kept constant. This imbalance will be compensated by infiltration.

Exhaust grids

The higher exhaust demand flow at the same 1 Pa minimum pressure difference leads to a bigger flow area in the exhaust grids. Therefore the pressure difference across the exhaust grids is decreasing with increasing imbalance. As a consequence, the time fraction with fan switched on to maintain the 1 Pa minimum is higher. The pressure difference across the exhaust grid in the toilet is exactly 1 Pa at almost 100% of the time fraction if the imbalance ratio has been increased up to 1.5. That means that the fan is switched on almost all the time when the ventilation provision in the toilet is in use.

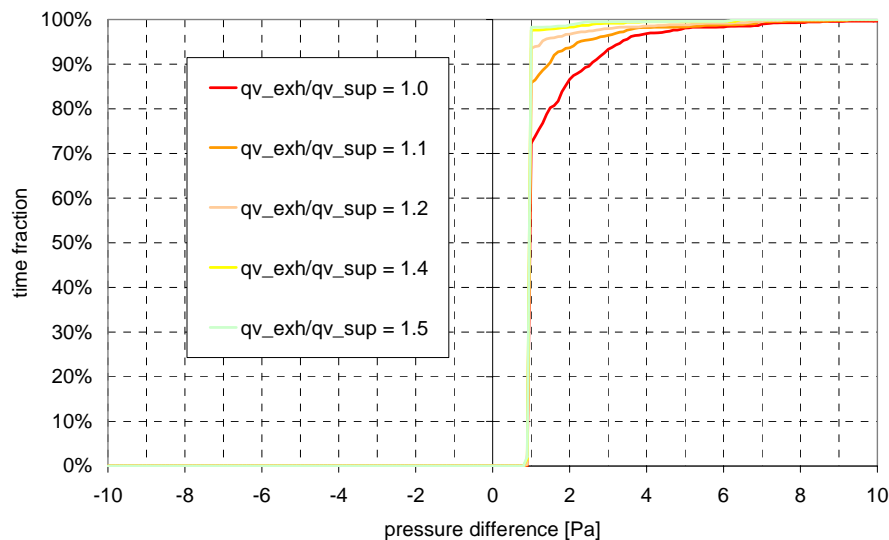


Figure 5.6:
Impact of the
imbalance on the
pressure difference
across the exhaust
grids

Exhaust fans

Without imbalance the fan is turned on 50% of the occupied time. This time fraction is increasing with the imbalance ratio up to 80% for the imbalance ratio of 1.5.

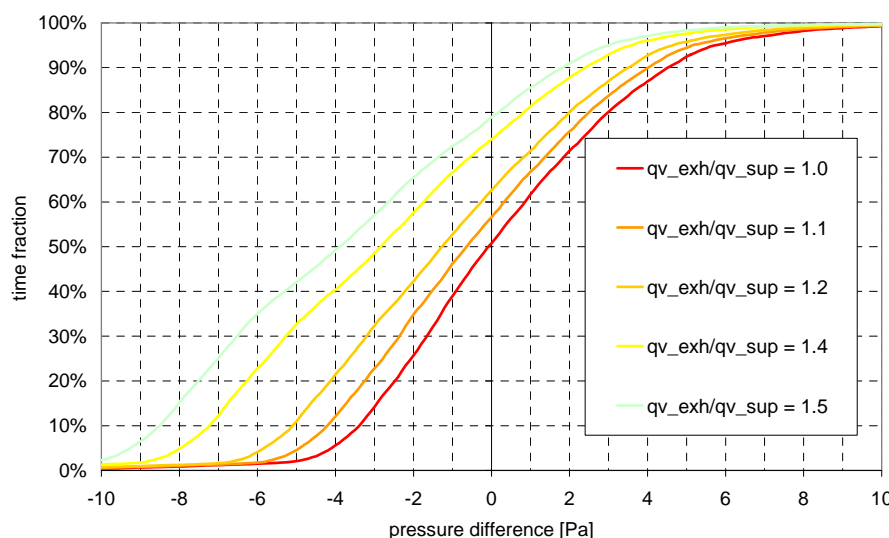


Figure 5.7:
Impact of the
imbalance on the
pressure difference
across the exhaust fan

Façade grids

The pressure across the façade is increasing about linearly with the square of the imbalance ratio.

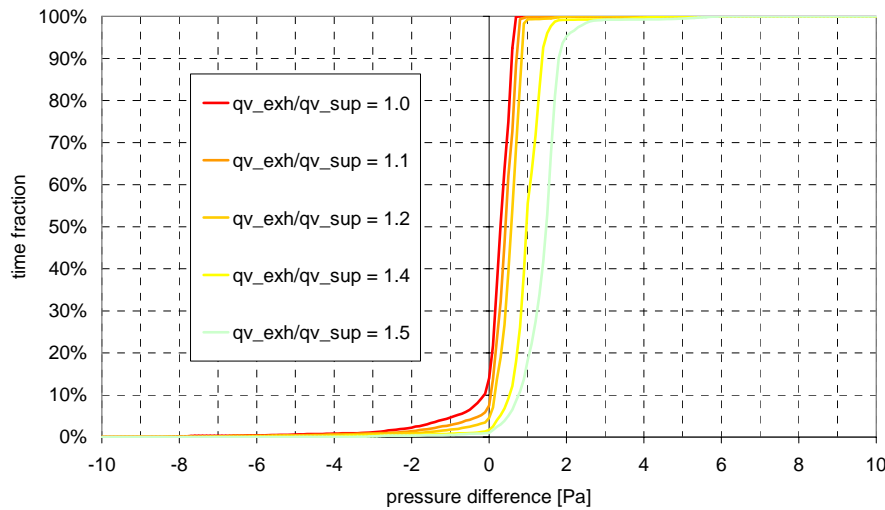


Figure 5.8:
Impact of the building
leakage on the
pressure difference
across the façade

5.1.8. Impact of the self regulating supply grids

Now, the impact of the self regulating supply grids has been studied. In the first case there are no supply grids at all and in the second case they have been replaced by conventional supply grids with crack characteristics (exponent = 0.65) which will not maintain a constant flow above 1 Pa like the self regulating grids. The supply grids are dimensioned for 7 dm³/s at 1 Pa per person. In both cases in the exhaust system still self regulating grids have been used.

Without supply grids

The supply air enters only through the building leakage, which is in this case $q_{v,10} = 96$ dm³/s.

Exhaust fan

Without supply grids the time fraction with the fan turned on increases from 45% to 65%.

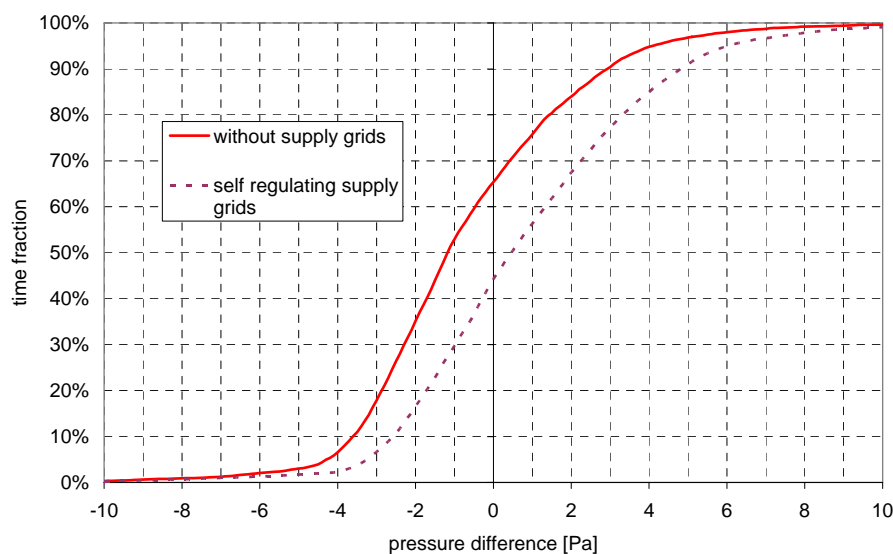


Figure 5.9:
Impact of self
regulating grid on the
pressure difference
across the exhaust fan

Façade

Without supply grids the pressures across the façades on the first floor are about 2 to 3 Pa and on the second floor about 1 to 2 Pa higher.

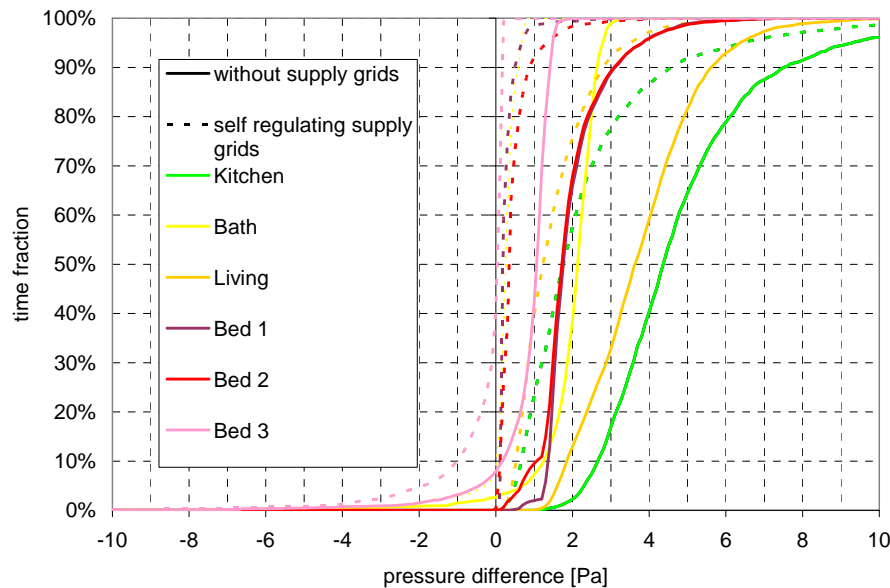


Figure 5.10:
Impact of self
regulating grid on the
pressure difference
across the façade

Conventional grids, demand controlled

The conventional grids have a crack characteristic with an exponent of 0.65. Such they cannot maintain a constant flow above 1 Pa like the self regulating grids. The supply grids are dimensioned for 7 dm³/s at 1 Pa per person. The openings are controlled according the number of present persons.

Exhaust grids

The pressure difference across the exhaust grid in the kitchen is about 0.5 to 1 Pa higher in the case where conventional supply grids are used instead of self regulating grids. In the bathroom the increasing is only minimal and in the toilet about 1 to 2 Pa.

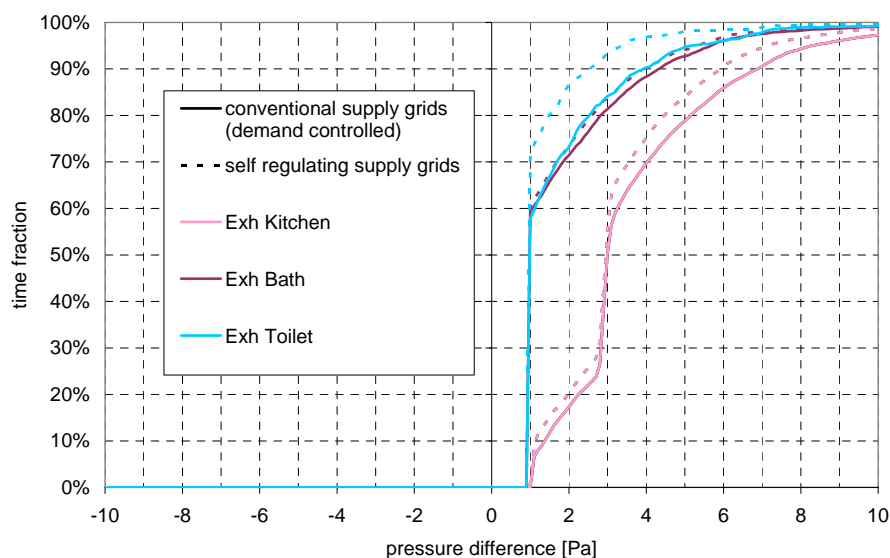


Figure 5.11:
Pressure difference
across exhaust grids
with conventional
demand controlled
supply grids

Façade grids

The pressure difference across those façades with high pressure differences is lower with conventional supply grids than with self regulating grids as the self regulating grids reduce the cross section with increasing pressure difference.

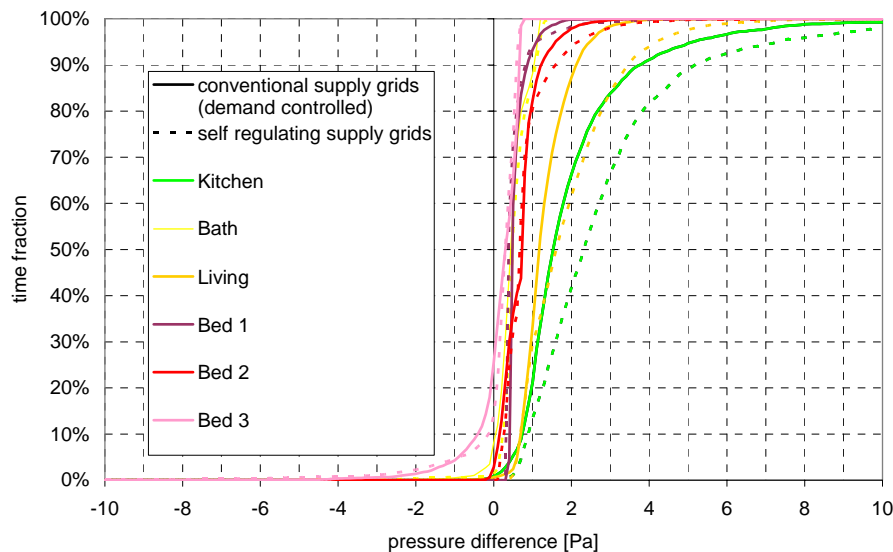


Figure 5.12:
Pressure difference
across conventional
demand controlled
supply grids

5.1.9. Impact of resistances of exhaust ducts

The exhaust ducts has been modeled with the crack equation: $q_v = C_{sD} \Delta p^n$. Compared with the reference case all C_{sD} values have been halved (higher resistance) in one case and doubled (lower resistance) in a second case.

Exhaust grids

During the time when the natural pressure difference is sufficient (fan is switched off) the pressure differences across the exhaust grids are lower with higher duct resistances because the ducts need a bigger fraction of the total pressure difference and there is less left for the exhaust grids.

During the time when the fan is on and more than one tree of the exhaust system is in use simultaneously, the pressure difference across the exhaust grid is higher with higher duct resistances, because the differences of the pressure drops of the different trees, which have to be equalized by the exhaust grids, are bigger.

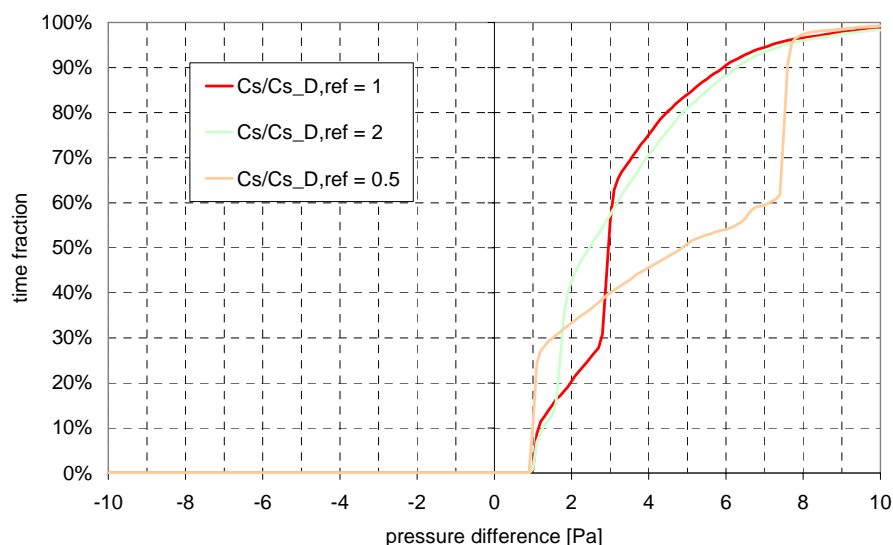


Figure 5.13:
Impact of resistances
of exhaust ducts on the
pressure difference
across the exhaust grid
in the kitchen

Exhaust fan

Compared with the reference case the exhaust fan has to be turned on during 70% of the time instead of 50% if the duct resistances have the twice of the reference values. The pressure difference which the fan has to deliver is then up to 6 Pa higher as in the reference case. The time fraction with turned on fan reduces from 50% to 40% and the pressure difference is about 1 to 1.5 Pa lower if the duct resistances are halved.

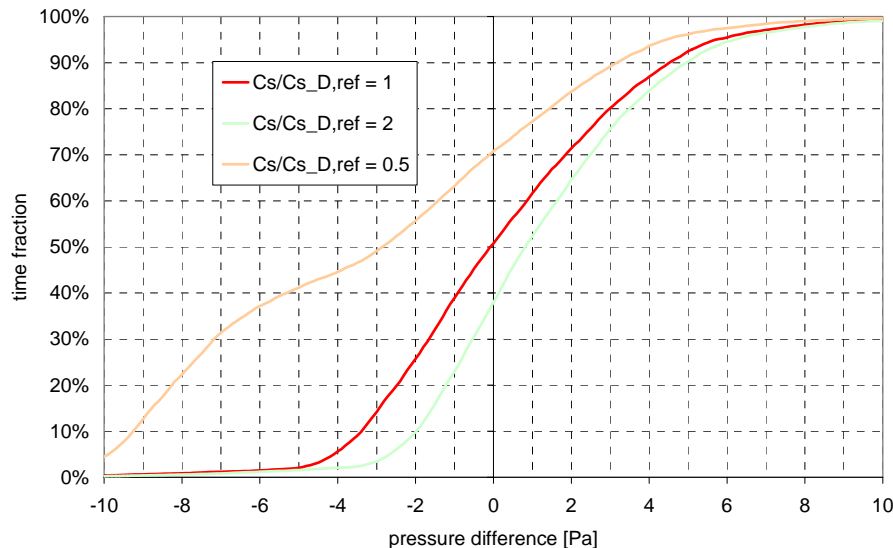


Figure 5.14:
Impact of resistances
of exhaust ducts on the
pressure difference
across the exhaust fan

Façade grids

There is no impact of the resistance of the exhaust ducts on the pressure differences across the supply grids.

5.1.10. Conclusions

It has been shown that the air tightness of the building is one of the most important factors. Even with an air tightness of $q_{v,10} = 30 \text{ dm}^3/\text{s}$, the intended distribution of the supply air can not be guaranteed for all the time. Especially on façades with negative C_p -values for all the wind directions, there will be a considerable fraction of time with too small or even negative pressure differences. A certain amount of imbalance can be a remedy for this, but only if the building is not too leaky. Therefore air tightness has the higher priority as imbalance. The disadvantage of both, increasing air tightness and increasing imbalance is: the time fraction when the fan is in use increases as well.

If there are no supply grids in the façade, the building has to be enough leaky, but then there is no possibility to control the distribution of the supply air. With conventional (non self regulating) but demand controlled supply grids, the pressure difference across the façades with high pressure differences is lower and higher across the self regulating exhaust grids. In this case, the pressure across the fan is about the same as with self regulating supply grids.

The resistance of the exhaust ducting system has a big influence on the pressure difference across the fan. Doubling the duct resistances requires the fan to produce up to 6 Pa higher pressures than in the reference case; and the time fraction with fan turned on increases from 50% to 70%.

6. Effect of outdoor air transfer devices on room air flow and thermal comfort

6.1. Introduction

Outdoor air transfer devices, used in natural or exhaust ventilation mode, are prone to draft risk problems due to the fact that cold outdoor air can directly flow into the occupied zone.

A comprehensive study on the topic has also been published by [Reichel 1999]. Results from measurements as well as from CFD calculations are given.

The issue of draft risk from fresh air supply has also been comprehensively treated by Sawachi in the frame of the IEA ECBCS Annex 27 project [Sawachi et. al. 1996], [Sawachi and Hironao 1997]. Room contour maps of a thermal comfort evaluation index are given for several types of air transfer devices. From these results, also a simplified evaluation tool has been developed.

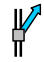





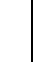



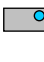

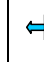




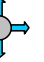
This chapter summarises results from laboratory measurements and CFD simulations, performed in the frame of a Swiss project on exhaust ventilation [Dorer and Pfeiffer 2002]. The results are also compared with analytical results.

6.2. Experimental investigations

6.2.1. Overview of the investigated outdoor air transfer devices

Experimental investigations considering thermal comfort have been performed with several commercially available outdoor air transfer devices (ATD). The products come from Scandinavia, Germany, France as well as Switzerland. For market neutrality reasons the products are described in the text by acronyms as e.g. F-SH-O, which means: installed in the window-frame, slot outlet in horizontal direction, jet direction upward. In table 6.1 the air jet characteristic of the investigated products are visualised in diagram form.

Table 6.1: Overview of the air jet characteristics of the investigated products

Name			F-SH-O	W-A-Q	W-A-H	W-R-OS	W-R-SOU	F-SH-OU	F-SH-H	W-R-R	F-A-O
schematic cross section											
schematic side view											
typical installation position	window frame wall or parapet	F W	F	W	W	W	W	F	F	W	F
aperture geometry in window/wall	slot horizontal rectangular round	SH A R	SH	A	A	R	R	SH	SH	R	A
jet direction	horizontal upward downward sideward radial displacement ventilation like	H O U S R Q	O		H	O S		O U	H	R	O

Many ATD are of simple construction, but they often include air filters, noise dampers and manually or automatically (according to air temperature or air humidity) controlled valves. One of the

investigated products (W-A-Q) includes a water supplied heat exchanger in order to heat or cool the incoming air.

6.2.2. Draft risk

Draft is perceived very locally on the body. Draft risk is one of the several criteria, with which thermal comfort is evaluated. A well-accepted method to calculate the predicted percentage of people dissatisfied concerning draft is equation (23), according to [CEN EN ISO 7730], [Olesen 2002]

$$DR = (34 - g_L) \cdot (v - 0.05)^{0.62} \cdot (0.37 \cdot v \cdot Tu + 3.14) \quad (23)$$

The draft risk, determined according to equation (23), gives the percentage of people dissatisfied (PPD) on the basis of an insulation value of the clothes of 0.75 clo and an activity level of 1.2 met. Therefore, equation (23) applies to summer conditions mainly. For winter conditions, a higher clo level may be assumed (1.0 clo). For a required PPD of e.g. 15%, a virtual higher percentage of dissatisfied (20 %) acc. to equation (23) corresponds to a PPD of 15 % in reality.

6.2.3. Occupied zone

Thermal comfort requirements must be met in principle in the occupied zone. This zone has to be defined according to the actual needs. Table 6.2 shows how the occupied zone is defined in [CEN EN 12792:2003]:

Table 6.2: Definition of the occupied zone as given in [CEN EN 12792:2003]

Element	Distance from the inner surface of the elements	
	Typical range [m]	Default value [m]
External windows, doors and radiators	0.50 to 1.50	1.00
External and internal walls	0.25 to 0.75	0.50
Floor (lower boundary)	0.00 to 0.20	0.10
Floor (upper boundary)	1.30 ^a to 2.00 ^b	1.80
^a mainly seated occupants ^b mainly standing occupants For external walls with windows or doors the element with the weaker requirement is taken as valid for the whole surface.		

6.2.4. Experiments in the room climate laboratory of EMPA

[CEN EN 13141-1:2004] defines test specifications to measure the air diffusion in the occupied zone. The room climate laboratory (see figure 6.1) of the Energy System and Building Equipment Laboratory at EMPA has been used to investigate the thermal comfort in the near surrounding of the ATDs.

In this room climate laboratory the thermal situation of a real room can be properly simulated. For the measurements, the inside surface temperature was set to 19 °C for the outdoor wall and to 15 °C for the window. In the experiment the air was supplied with a temperature of 1 to 2 °C. The influence of lower air supply temperatures was determined by CFD calculations. Moreover, the airflow rate was adjusted according to a pressure drop of 10 Pa across the ATD, a rather high value in practice. The heat loss caused by these cold surfaces and the cold outdoor air supply was either covered by a floor heating system or a convective heating element placed under the window and the ATD.

The air flow was visualised using fog and then room climate parameters like air temperature, air velocity and turbulence intensity have been measured at several points in the room. With these parameters, the draft risk values were calculated.



Figure 6.1: Room climate laboratory at EMPA,
Test room dimensions: $6.2 \times 4.6 \times 3.0 \text{ m}^3$

6.2.5. Influence of the ATD geometry

In general, as supply from the ATD, two different air jet types may occur, either a free jet or a wall jet. Sometimes also a combination of both phenomena can be observed.

1. Free jet: This jet type will occur if the supply is horizontally or if a critical angle (67° to 40° , depending on the speed of the jet at the ATD) between air jet and wall will be exceeded. Because the jet air temperature is below the room air temperature the jet is deflected downwards. Although the centre velocity decreases faster than in a wall jet, the zone of discomfort caused by draft is quite big because of the jet penetration into the occupant zone. A typical representative of this type is the ATD F-SH-H, as shown in figure 6.2.

Supply F-SH-H

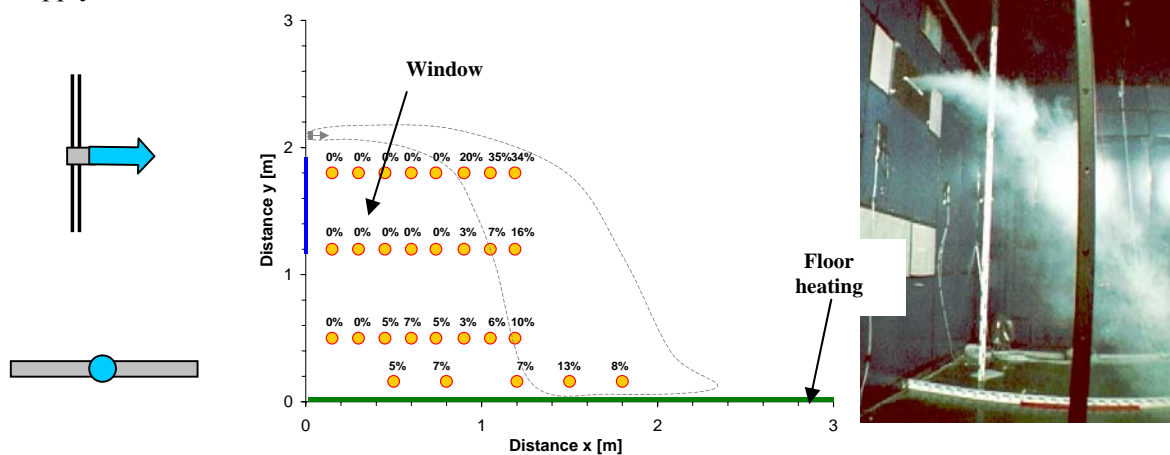


Figure 6.2: Because of the horizontal jet direction, the ATD F-SH-H causes a relatively big zone of discomfort in the occupant zone (left: airflow scheme, middle: measurements (draft-risk), right: airflow visualisation) - Floor heating

2. Wall jet: If an air jet is near to a parallel wall it will attach on it due to the Coanda-effect. Many ATD use this effect to generate horizontal or vertical jets (baffle principle). Although the stability of the jet in this case is very high, geometrical obstacles may cause a separation of the jet. The central velocity of this jet type does not decrease as fast as in the free jet. Because of the long mixing length outside the occupation zone, the discomfort zone is not very big. The ATD F-SH-OU shows the typical the behaviour of such a wall jet.

Supply F-SH-OU

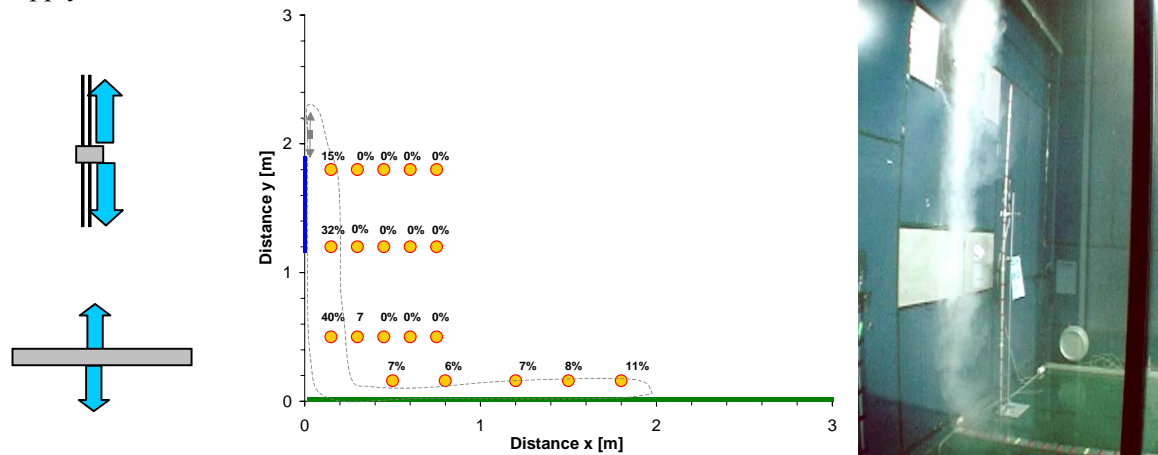


Figure 6.3: Because of the baffle principle, the ATD F-SH-OU causes a relatively small zone of discomfort in the occupant zone (left: airflow scheme, middle: Measurements (draft-risk), right: airflow visualisation) - Floor heating.

6.2.6. Influence of the installation position of the ATD

In general, two different installation positions are possible:

1. Installation above the window: The ATD is either installed in the wall or in the upper part of the window or window-frame.
2. Installation below the window: The ATD is either installed in the sill or in the lower part of the window or window-frame.

If the jet direction is horizontal, the installation position below the window shows better results concerning draft risk than the position above the window. This is because the discomfort zone in the first case is smaller and often penetrates less into the occupant zone (see also [Reichel 1999]). However, our measurements show that this does not fully apply if the ATD make use of the wall jet principle. Because of the higher fall, the air velocity near the floor is slightly higher if the ATD is installed above the window. Although the velocity is higher, the draft risk is lower compared with the installation below the window because of the longer mixing length (compare figure 6.3 and figure 6.4).

Supply F-SH-OU

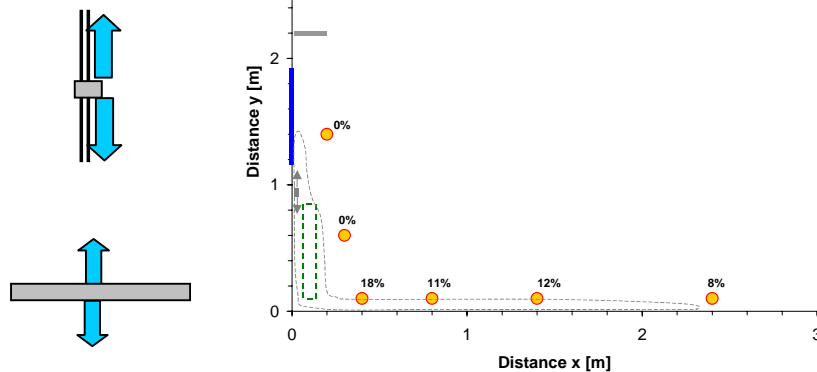


Figure 6.4: The penetration depth of the discomfort zone in the below position is less than in the above position, whereas the draft risk along the floor is remarkably high - Floor heating.

6.2.7. Influence of a convective heating element

The influence of a convective heat source, positioned under the ATD, was evaluated with measurements with several ATD types and with CFD calculations. A convective heat source placed under the ATD in general causes an intensive mixing of the inlet air with the preheated room air. Therefore such a configuration tends to show better thermal comfort in the occupant zone. If the air jet of the ATD is of high impulse in horizontal direction it may happen, that the jet is deflected directly into the occupant zone. This increases the penetration deep into the room the draft risk, however, is lower because of the mixing effect. A jet of low impulse will be entrained into the convective plume of the heat source.

Supply W-A-H

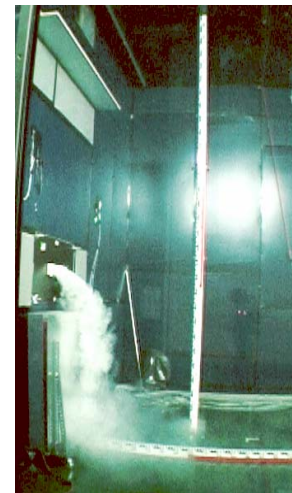
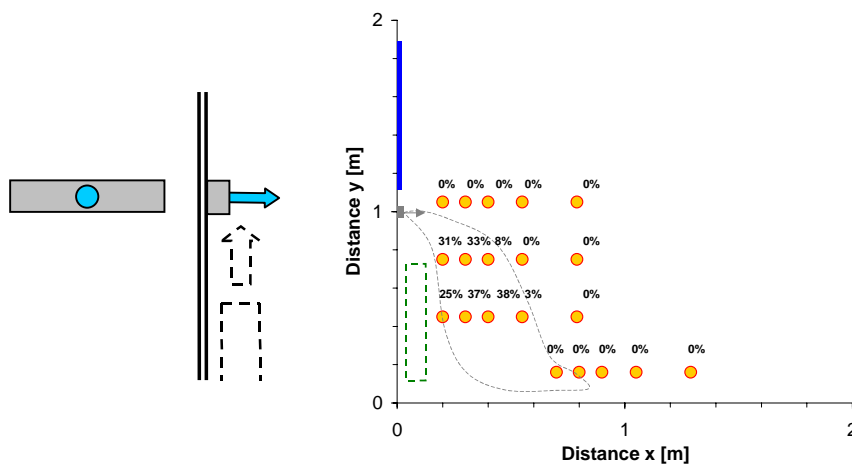


Figure 6.5: Convective heating element is switched off - Geometrical small discomfort zone near the outlet

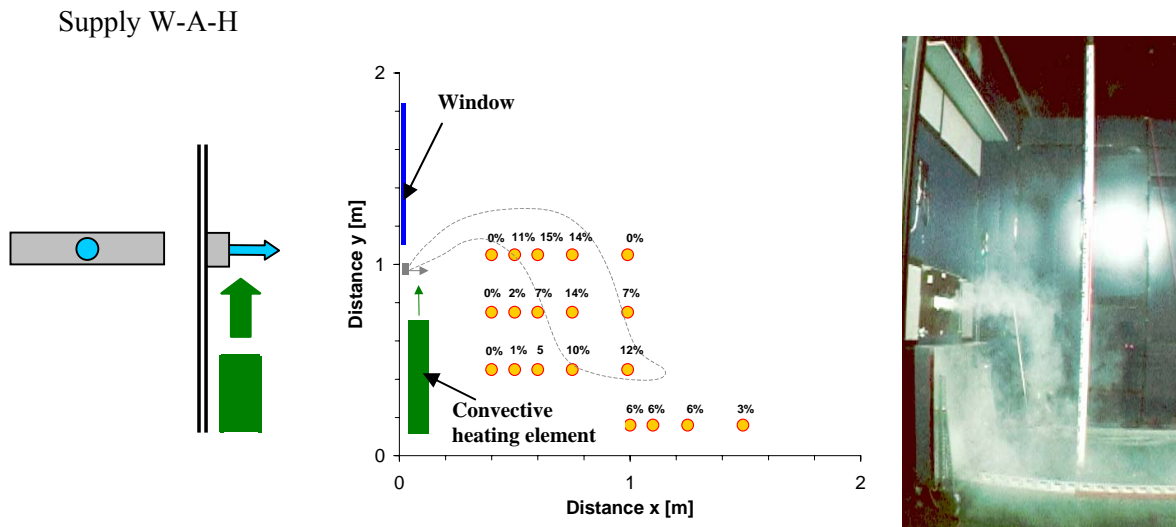


Figure 6.6: Convective heating element is switched on (145 W, ~ 100% convection), air jet is deflected upwards and is mixed with room air. The draft risk is generally smaller but the critical area is shifted more into the occupant zone.

6.2.8. Influence of obstacles

Protruding elements above the ATD such as window lintel or curtain rail boards may have a negative effect on the thermal comfort, especially if the jet direction is upwards (as shown in figure 6.8), or a convective heat source below the ATD deflects the jet upwards. In these cases the cold outdoor air penetrates deeper into the occupant zone which may lead to serious draft risk problems.



Figure 6.7: F-SH-O - Floor heating - Air inlet temperature 2 °C



Figure 6.8: F-SH-O - Convective heating element switched off - With curtain rail board - Air inlet temperature 2 °C

6.2.9. Influence of net curtains

The influence of net curtains was investigated only with fog visualisations. A narrow structured curtain (1 to 1.5 mm mesh) dams the supply air between wall and curtain. This results in a displacement ventilation effect between curtain and floor. The velocities are also quite low because the air is distributed over the whole length of the curtain (see figure 6.9). If a convective heating element

is installed under the ATD the convective airflow entrains the incoming air and distributes it over the upper third of the curtain (see figure 3.8). In this configuration the geometrical construction of the ATD has a minor influence on the airflow pattern.



Figure 6.9: F-SH-O - Convective heating element switched off and net curtain in front of the ATD - Air inlet temperature 2 °C



Figure 6.10: F-SH-O - Convective heating element switched on (190 W) and net curtain in front of the ATD - Air inlet temperature 2 °C

6.2.10. Influence of the air supply temperature

The measurements were carried with an air supply temperature of 1 to 2 °C. The influence of lower temperatures on the draft risk was investigated by means of CFD calculations [FLOVENT 3.1 1999], see chapter 6.4.

For air supply temperatures of –10 °C, these calculations show slightly higher air velocities in the down wash. Consecutively, the floor velocities are also increased. This leads to a 15 to 20 cm longer zone of high draft risk in the floor region (above 20 % dissatisfaction, see figure 6.11).

Also for other configurations the calculations showed that the differences in draft risk between a supply air temperature of 1 to 2 and of –10 °C are of minor significance.

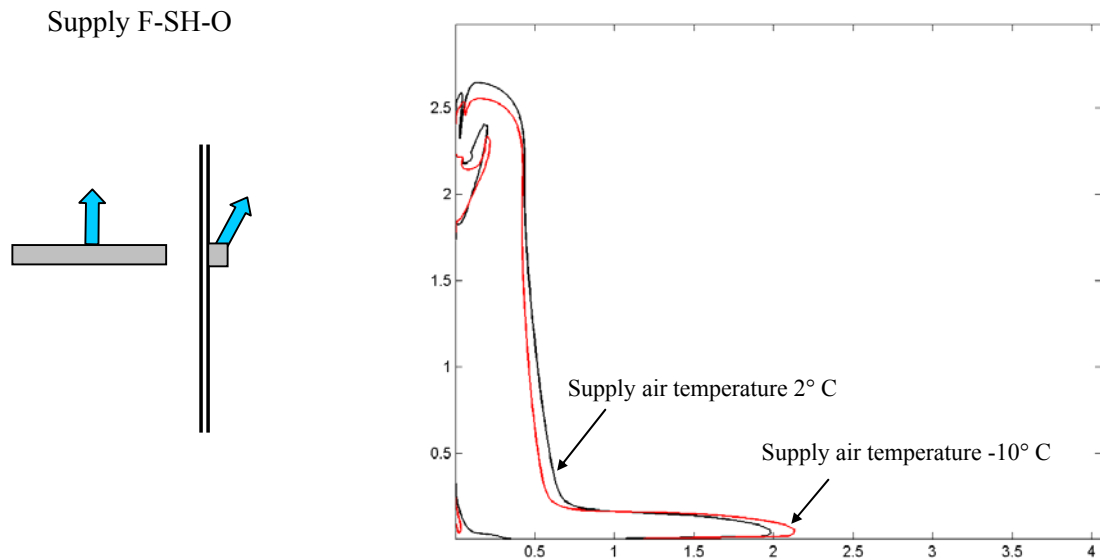


Figure 6.11: Comparison of the 20 % isoline of the draft risk in the axis of symmetry at a supply air temperature of 2° C (black) with an air supply temperature of -10°C (red) - Floor heating - CFD calculation.

6.2.11. Conclusions

Thermal comfort problem areas due to high draft risk are almost only expected near the wall (0.2 to 0.5 m depending on the ATD-type). Close to the floor, draft risk is expected at a high of approx. 0.1 m and within the first 1 to 2 meters from the ATD, depending on the flow rate and the ATD-type. All critical zones are on the boundary of the occupant zone (depending on the definition). Therefore, under optimised circumstances, the draft risk in the occupant zone can be reduced to marginal levels.

A convective heating element placed under the ATD causes a higher mixing effect on the supply air and therefore tends to increase the thermal comfort. A possible deflection of the air jet into the occupant zone has a negative influence.

Obstacles above an ATD with upwards directed jet may cause a deflection of the air jet directly into the room. Moreover, a high jet impulse combined with a weak convective heat source also may deflect the jet into the occupant zone.

Mesh curtains cause a low impulse flow near the floor and therefore tend to improve the comfort. If a convective heat source is installed the air is distributed on the upper part of the curtain.

An ideal flow field with low draft risk is achieved with a high induction air jet, where the flow path before the air penetrates into the occupant zone is as long as possible (long mixing length).

6.3. Theory of air jets applied to the flow field of ATD

6.3.1. Archimedes-number [Recknagel 2001]

In real situations the supply air has a temperature difference and therefore a density difference which causes a gravity effect (buoyancy). For the air flow pattern and the air velocities the ratio of the gravity and the force of inertia of the jet are of high importance. Also the directions of the forces are significant.

Two different cases are possible:

1. Buoyancy and inertia forces are directed in the same direction:
Cold jet from the ceiling or warm jet from the floor
2. Buoyancy and inertia forces are directed in the opposite direction:
Warm jet from the ceiling or cold jet from the floor

The ratio of buoyancy to inertia forces is described by the Archimedes number Ar :

$$Ar = \frac{\text{gravity}}{\text{force of inertia}} = \frac{g \cdot |T_J - T_R| \cdot h_J}{T_R \cdot v_0^2} \quad (24)$$

6.3.2. Basic equations for the flat free jet [Recknagel 2001]

In a flat free jet the centre velocity decreases not as fast as in a round jet because in the flat jet a velocity gradient exists only in the vertical plane while in the round jet there is also a gradient in a horizontal plane. Therefore the throw length of a free jet of height h is bigger the one of a round jet of diameter d equal height h (see figure 6.12).

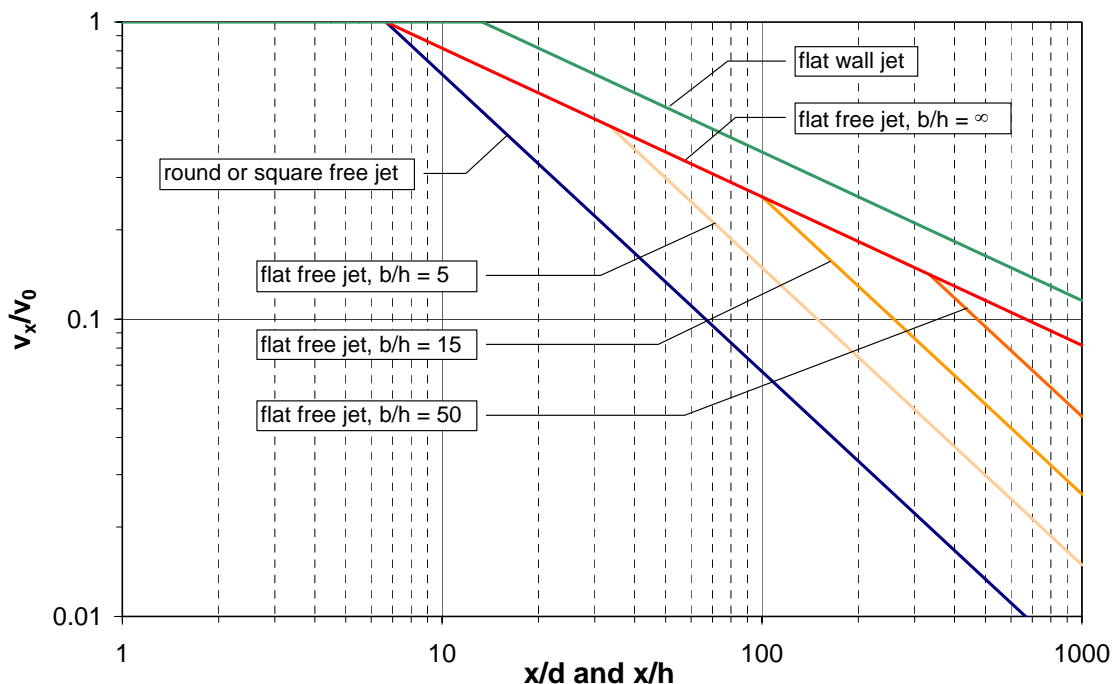


Figure 6.12: Decrease of the centre velocity for different air jet types

Downstream of the core-zone of the flat jet (see figure 6.12), the centre velocity decreases inverse proportionally to the square root of the distance x of the outlet. In the case of a non-isothermal jet the Archimedes number Ar as well as the mixing-number m have to be considered. Standard values for the mixing-number of different air supply openings are shown in *table 6.3*.

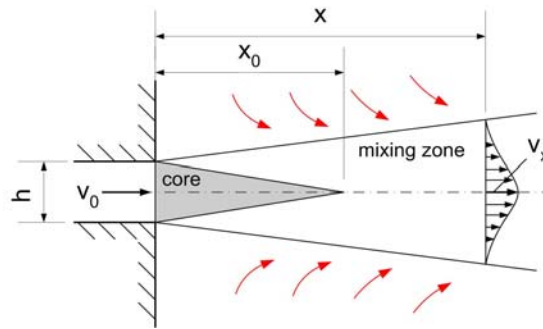


Figure 6.13: Diffusion of an isothermal flat free jet.

Core-length of a flat free jet:

$$x_0 = \frac{h}{m} \quad (25)$$

Centre velocity decrease of an non-isothermal flat free jet (positive sign if the jet effect is increased by buoyancy, negative sign if it is decreased):

$$\frac{v_x}{v_0} = \sqrt{\frac{x_0}{x}} \pm \sqrt{\frac{Ar}{m} \left(2.83 \cdot \sqrt{\frac{x}{x_0}} - 1 \right)} \quad (26)$$

Table 6.3: Standard values of mixing-number m for different air supply types [Recknagel 2001]

Type of supply ATD	Mixing number m
nozzle	0.14 – 0.17
Rectangular free ATD	0.17 – 0.2
slot with an aspect ration $s = 20 - 25$	0.2 – 0.25
hole grid with an area ration $r = 0.1 - 0.2$	0.22 – 0.28
bridge grid, straight	0.18 – 0.25

6.3.3. Coanda Effect

If an air supply opening is mounted in an internal wall in a short distance under the ceiling, the supply flow leaves the ATD as a free jet. However, the horizontal ceiling plate disturbs the secondary airflow, which is entrained by the jet. The mass deficiency on the upper side of the jet causes a lower pressure and consecutively, the jet attaches to the ceiling what is referred to as the Coanda Effect.

The Coanda Effect plays only a role, if no larger eddy between jet and boundary wall develops. Other parameters, which influence the origin of the Coanda Effect, are distance x , ceiling-wall or jet angle α , jet velocity v_0 , jet temperature ϑ_0 and geometry of the supply.

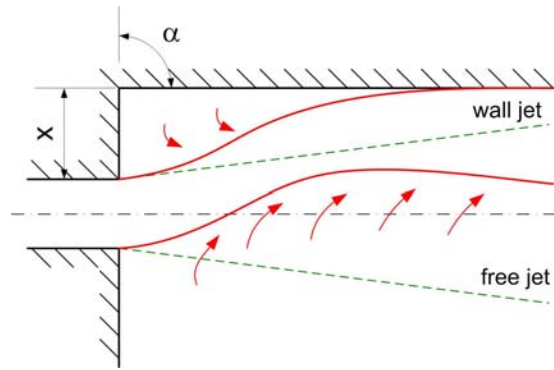


Figure 6.14: Influence of the Coanda Effect on flow field of a horizontal free jet.

6.3.4. Non-isothermal horizontal flat free jet [Recknagel 2001]

A temperature difference between the jet and the room air causes a rise or a fall of the jet. Equation (27) describes a theoretical model of the flow path of a flat free jet. The jet angle α can be considered in the calculation, but it has to be noticed that the Coanda Effect is not considered.

$$\frac{Y}{h} = \frac{X}{h} \cdot \tan \alpha \pm 0.4 \cdot \sqrt{m} \cdot Ar \cdot \left(\frac{X}{h \cdot \cos \alpha} \right)^{2.5} \quad (27)$$

(Sign positive if the jet is warmer than the room air, negative if it is colder than the room air.)

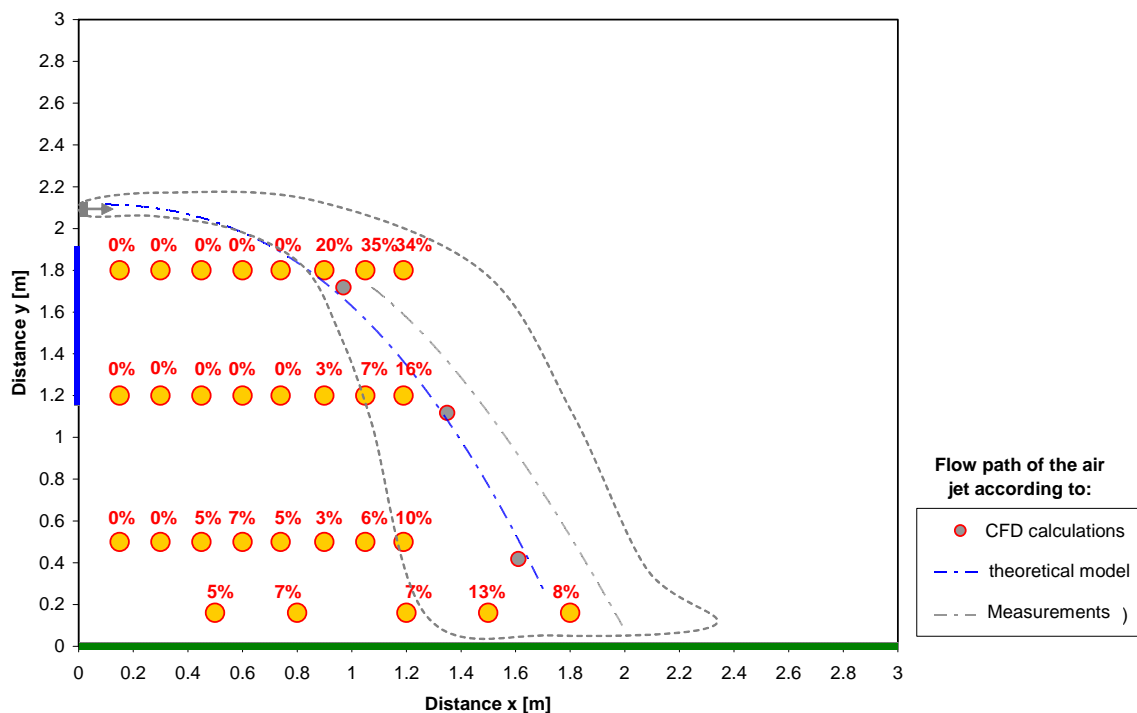


Figure 6.15: Example of a non-isothermal horizontal flat free jet in the axis of symmetry, comparison of measurements and theoretical model according to equation (27) (ATD type F-SH-H).

6.3.5. Theory of displacement ventilation according to [Heiselberg 2001]

Under non-isothermal conditions, an air jet from an ATD can be treated as a 3-dimensional thermal jet which mostly reaches the floor very near the wall (0.2 – 1 m). The air current at the floor is spread radially and stratified similar to the air distribution from a displacement supply unit. Measurements

have shown that the mixing-effect of this floor jet is very weak because of the large temperature gradient. Additionally, it was found that in cases of high Archimedes numbers the height of the cold air layer is constant. According to several investigations [Nielsen 1992] the maximal velocity v_x of a radially spread floor jet with constant boundary layer thickness and without induction of room air decreases inversely proportionally to the distance of the supply ATD:

$$v_x = \dot{V}_0 \cdot K \cdot \frac{1}{x + x_0} \quad (28)$$

The variable K differs in function of the supply type and the Archimedes number. Typical values for displacement ventilation are in the range of 4 to 12 m^{-1} , and for natural window ventilation between 6 and 20 m^{-1} , depending on the window type. This characteristic value can also be calculated for the ATD. CFD calculations were used to calculate K values. Measurements have shown that the velocity decrease is approximately reciprocally proportional to the distance (figure 6.16).

$$v_x \approx \frac{1}{x + x_0} \quad (29)$$

It can be concluded from measurements and comparisons, that the velocity near the floor in function of the volume flow rate, temperature difference and distance from the wall can approximately calculated as follows:

$$v_x \approx \dot{V}_0^{0.2} \cdot \Delta T^{0.4} \cdot \frac{1}{x + x_0} \quad (30)$$

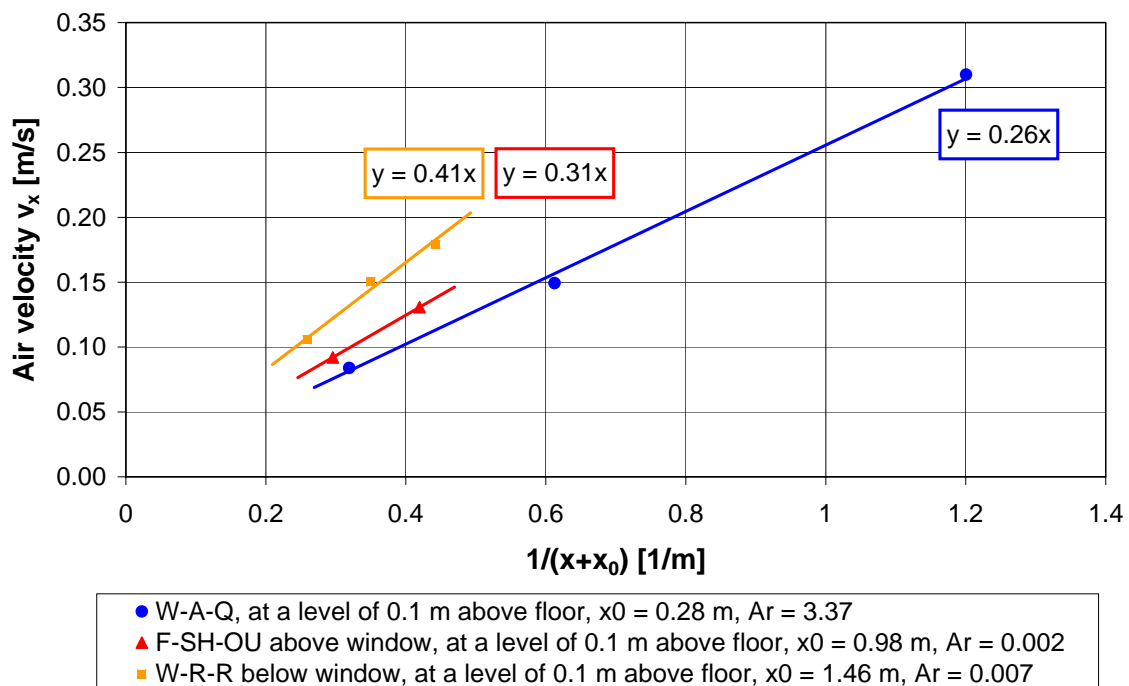


Figure 6.16: The air velocity decrease law also agrees with the measurements on a height of 10 cm above floor level.

6.3.6. Displacement flow characteristic values of ATD

Based on CFD calculations the velocity decrease of the floor current of four different ATD was investigated. According to these calculations, maximum velocities were reached on a height of 2 to 3

cm above floor level. In a certain distance from the ATD, the air velocity decrease characteristic corresponds with the equation (28). In order to evaluate both free parameters of equation (28), it was transformed into a linear function. After that, a linear regression of the CFD results was made.

The slope of the functions in figure 6.17 can be compared directly with the negative fictive origin of the jet. If the origin of the jet is in front of the ATD, the distance x_0 is negative. As figure 6.17 shows, the jet origin is in many cases behind the ATD and therefore positive. The ATD type F-SH-H has obviously a negative origin because it concerns a horizontal free jet. A completely different ATD type W-R-OS spread the air not only vertically above the supply but also to both wall sides which causes a better distribution of the air and lower velocities on the jet centre line. Because of this jet behaviour the fictive origin of the jet is behind the ATD. These examples show, that the geometry of the ATD has an influence on the fictive origin and therefore on the floor velocities. The intercept of the graph with the y-axis corresponds directly to the variable K .

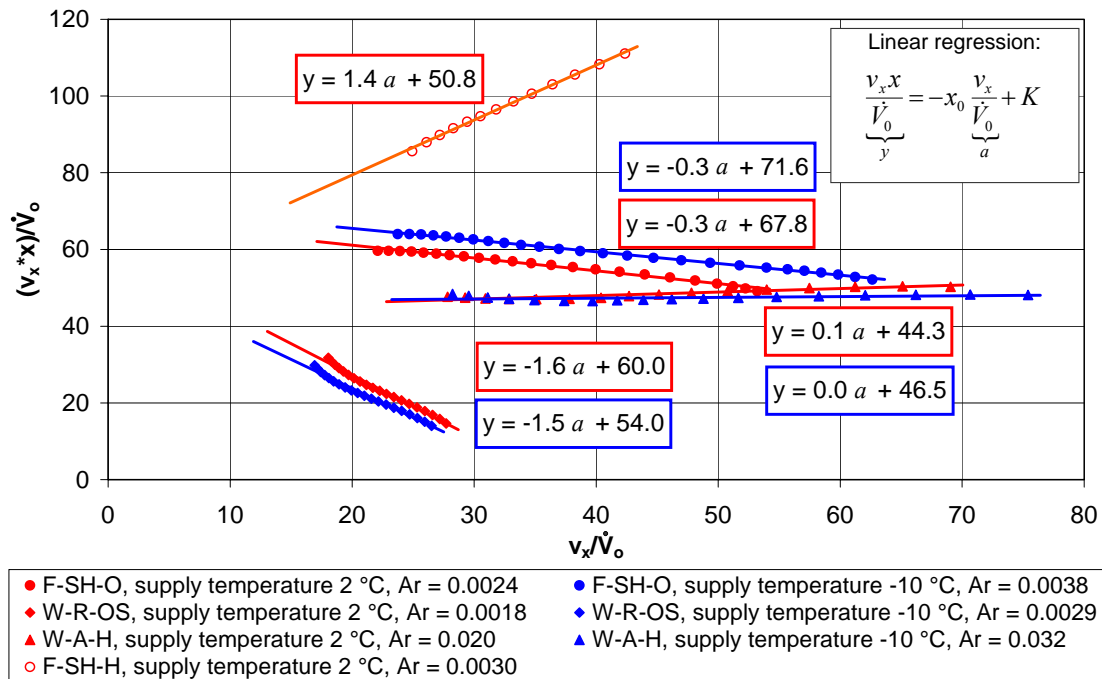


Figure 6.17: Linear regression curve fit of the velocity decrease on floor level with increasing distance from the ATD (extracted from CFD calculations).

Figure 6.18 gives an overview of the determined K values in function of the Archimedes number. Compared with natural window ventilation or displacement ventilation these values are significantly higher.

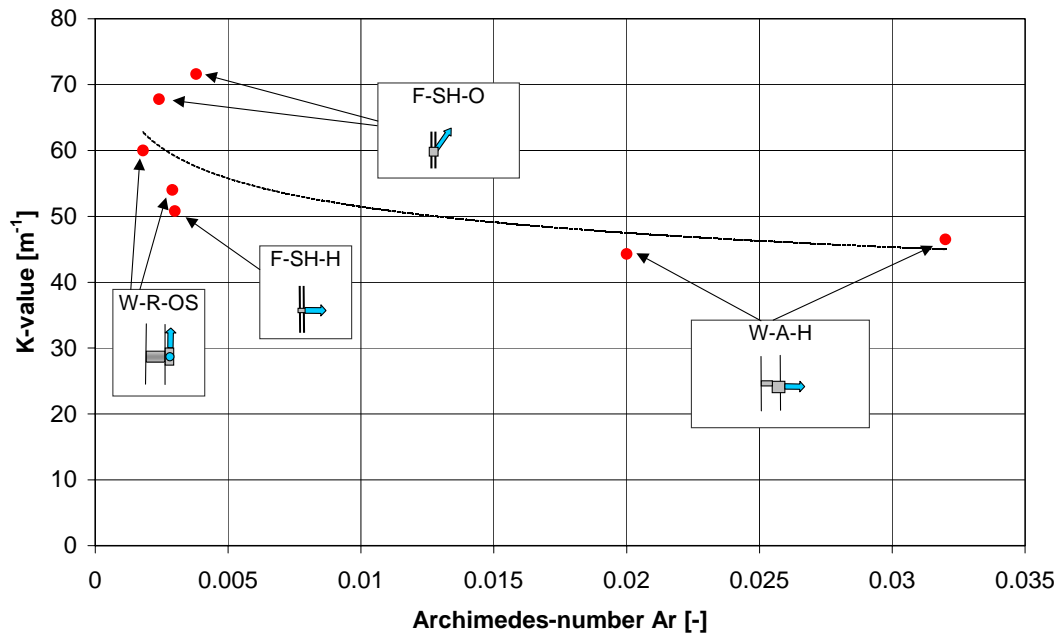


Figure 6.18: K values of different ATD types evaluated from CFD-calculation in function of the Archimedes number.

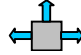
6.4. Comfort evaluation using CFD

6.4.1. Boundary conditions for the CFD calculations

The CFD calculations were carried out with FLOVENT 3.1 [FLOVENT 1999], a code specifically developed for room air flow simulation. In the CFD model, it was attempted to reproduce the same conditions like in the room climate laboratory. For that reason all boundary conditions from the laboratory were transferred to the CFD calculations.

Table 6.4 shows the boundary conditions used in the CFD calculations. Because the room air movement is primary driven by the cold air jet from the ATD, the accurate modelling of the near surrounding is very important (geometry of the ALD, jet angles, grid, etc.), especially if we are interested in the thermal comfort in the occupant zone near the ATD. Therefore many parameters in table 6.4 characterise the air jet. Nevertheless characteristic jet values like turbulent kinetic energy and turbulent dissipation rate are missing in the table 6.4. Investigations have shown that the effect of these parameters on the room air movement and thermal comfort are of minor importance. This is confirmed by the sensitivity study on air inlet parameters documented in [Schälin 1994].

Table 6.4: Boundary conditions for the CFD calculations

ATD type	unit	W-R-OS 		
case		1	2	3
task		comparison of CFD and measurements of draft risk	evaluate the effect of a lower supply air temperature	evaluate the effect of a convective heating element
arrangement of the ATD	-	above window	above window	above window
number of slots i on one symmetry half	pieces	2	2	2
supply air flow rate slot 1 to i	m ³ /h	3 (up) / 12 (side)	3 (up) / 12 (side)	3 (up) / 12 (side)
open cross section area of the slots	%	81 (up) / 65 (side)	81 (up) / 65 (side)	81 (up) / 65 (side)
length of the slots	mm	65 (up) / 130 (side)	65 (up) / 130 (side)	65 (up) / 130 (side)
width of the slots	mm	25	25	25
jet angle to x axis slot segment 1 to i	°	90 (up) / 90 (side)	90 (up) / 90 (side)	90 (up) / 90 (side)
jet angle to y axis slot segment 1 to i	°	0 (up) / 90 (side)	0 (up) / 90 (side)	0 (up) / 90 (side)
jet angle to z axis slot segment 1 to i	°	90 (up) / 0 (side)	90 (up) / 0 (side)	90 (up) / 0 (side)
air supply temperature	°C	2.1	-10	-10
window surface temperature	°C	15	15	15
outdoor wall surface temperature	°C	19	19	19
interior wall surface temperature	°C	22	22	21.5
floor surface temperature	°C	24	24	21.5
Heat source	-	floor heating	floor heating	conv. element under ATD
power of the convective heating element	W	-	-	150

6.4.2. Geometry and simplifications

The room geometry (figure 2.3) and the set up of the ventilation components correspond with the measurement conditions used in the room climate laboratory. In order to save calculation time only one half (axis of symmetry) and only a room 4.07 m deep (instead of 6.2 m) was simulated. Moreover, the extract opening, which has a minor influence on the room air flow pattern, was not placed at exactly the same position. The influence of all these simplifications on the air flow pattern in the near surrounding of the ATD can be neglected.

6.4.3. Heat sources

In the first two cases (table 6.4) the heat loss from the cold supply air and the cold surfaces is covered by a floor heating with constant surface temperature of 24 °C. In the third case the heat is supplied by a convective heating element of the same dimensions as in the experiment.

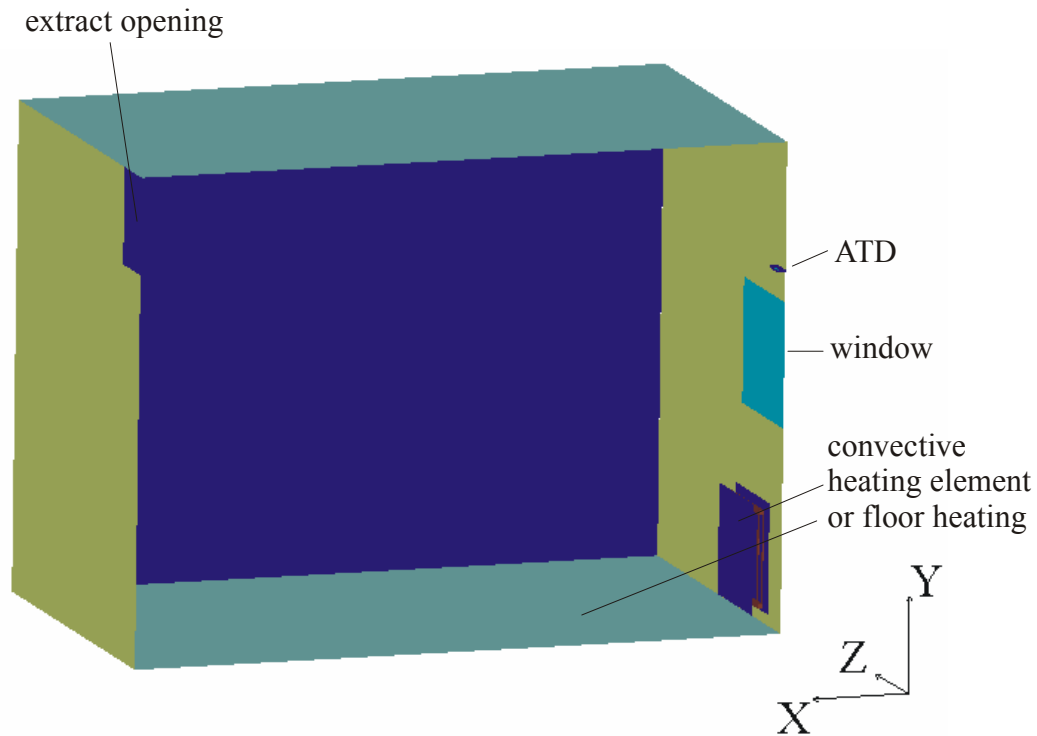


Figure 6.19: 3-dimensional room model for the CFD calculation

6.4.4. Calculation grid

The grid definition is one of the most important factors influencing the CFD results. Where complex physical phenomena (like eddies, boundary layer flow) are expected, the grid resolution has to be high enough to take into account these effects. On the other hand too many grid cells in the calculation space enormously increases the calculation time and lead to overestimation of certain physical effects. The CFD calculation program FLOVENT supports only an orthogonal calculation grid. In our specific calculation case the geometry of the ATD was very small compared to the calculation room. This may lead to a high number of grid cells and therefore long computing time. Fortunately since version 4.1 a local refinement feature has been implemented in FLOVENT. For the investigated ATD (W-R-OS) airflow case a local grid refinement around the ATD shown in the following figures saves up to 50% of total grid cells compared with no grid refinement.

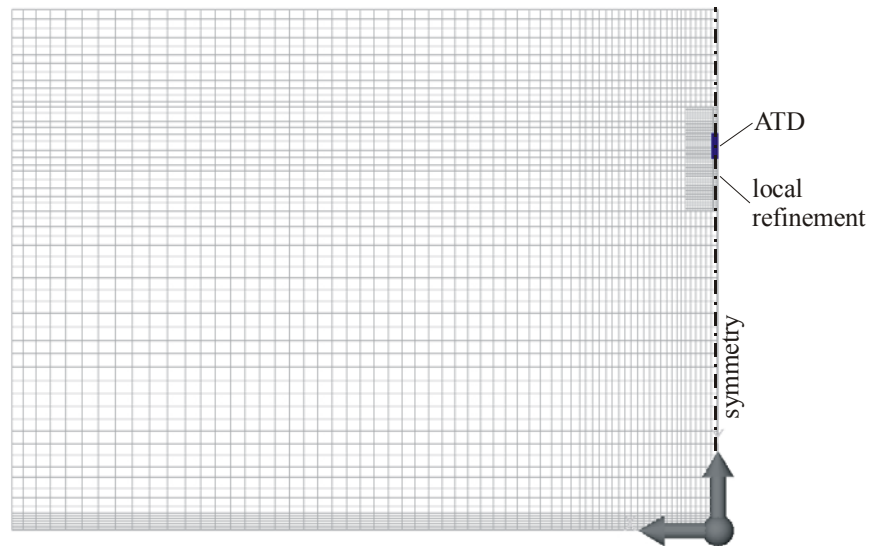


Figure 6.20: Orthogonal calculation grid in the x-y plain

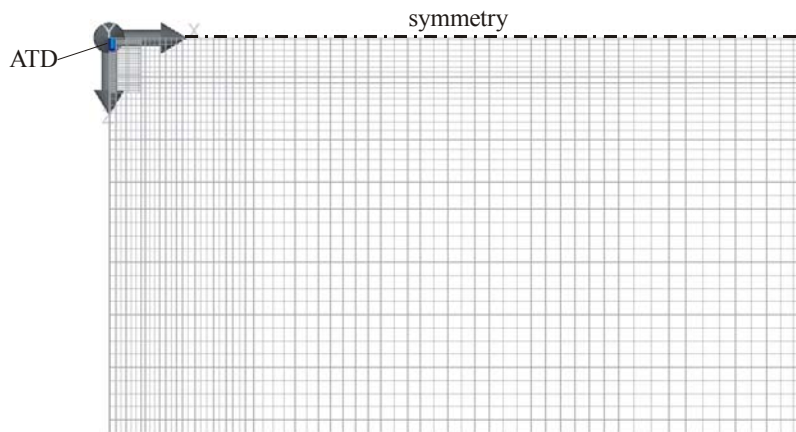


Figure 6.21: Orthogonal calculation grid in the x-z plain

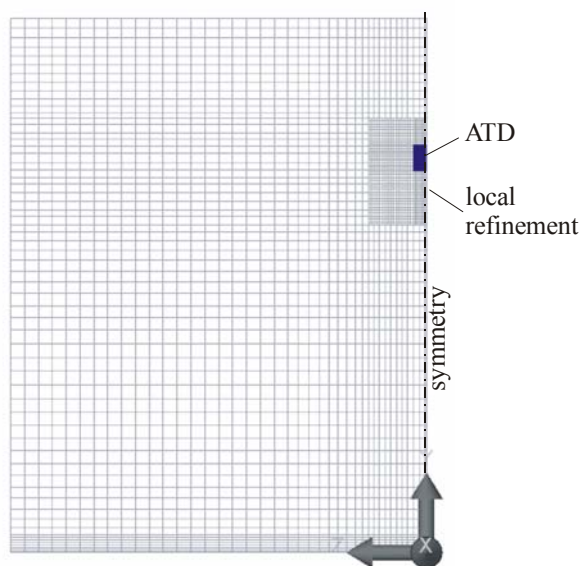


Figure 6.22: Orthogonal calculation grid in the y-z plain

6.4.5. Evaluation of draft risk and comparison with measurements W-R-OS (case 1)

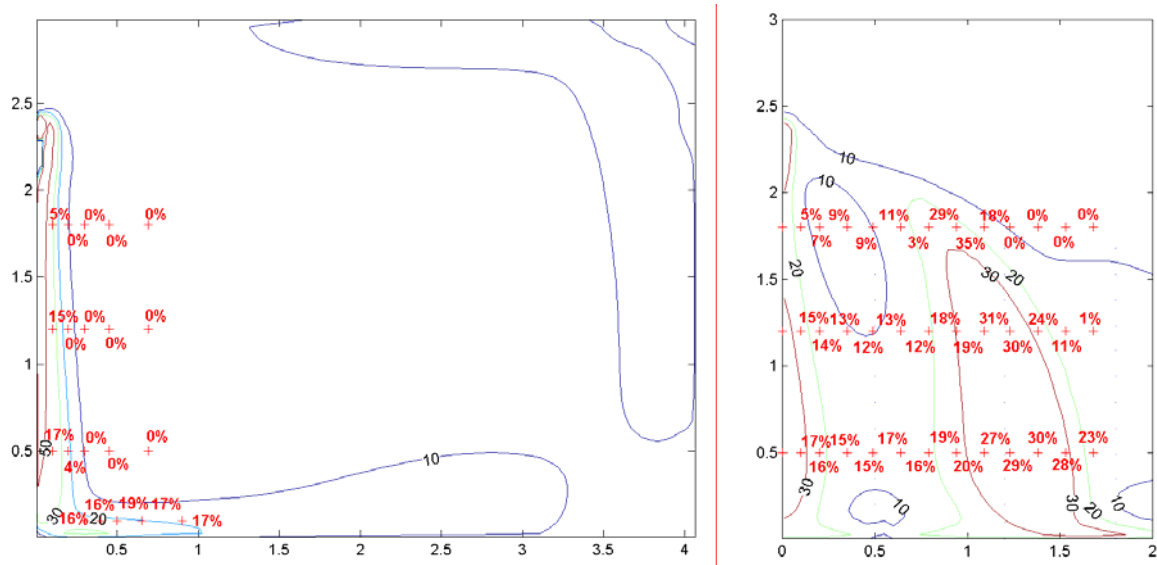


Figure 6.23: Comparison of CFD calculations of draft risk with measurements in the axis of symmetry (left) and near the outside wall $x = 0.1\text{ m}$ (right)

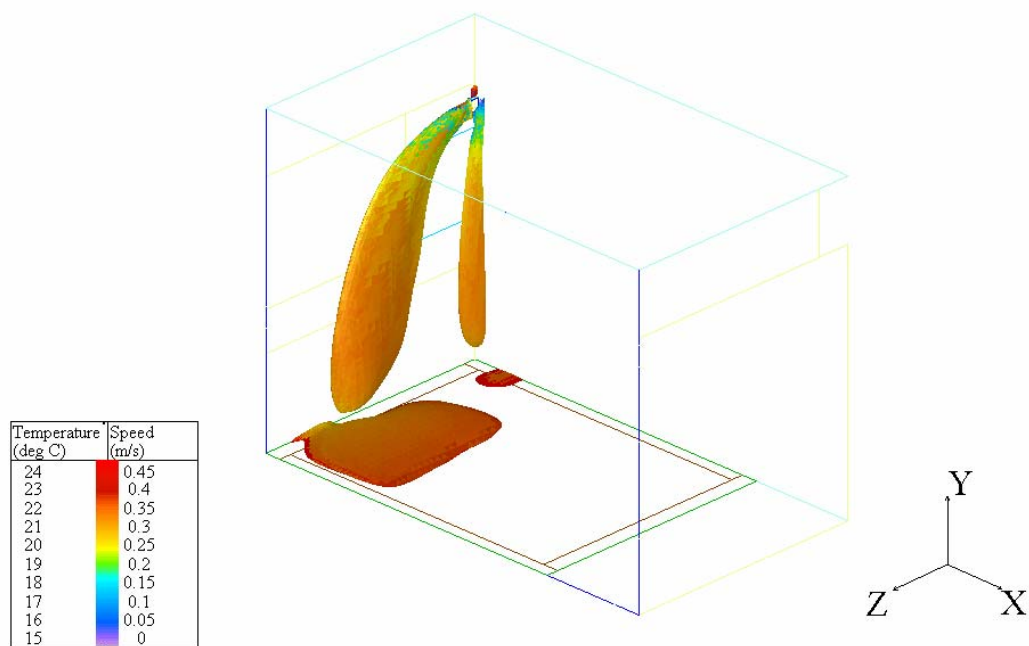


Figure 6.24: CFD calculation: Iso-velocity surfaces for a speed of 0.25 m/s , surface colour corresponds with the air temperature

6.4.6. Evaluation of draft risk at a supply temperature of $-10\text{ }^{\circ}\text{C}$ W-R-OS (case 2)

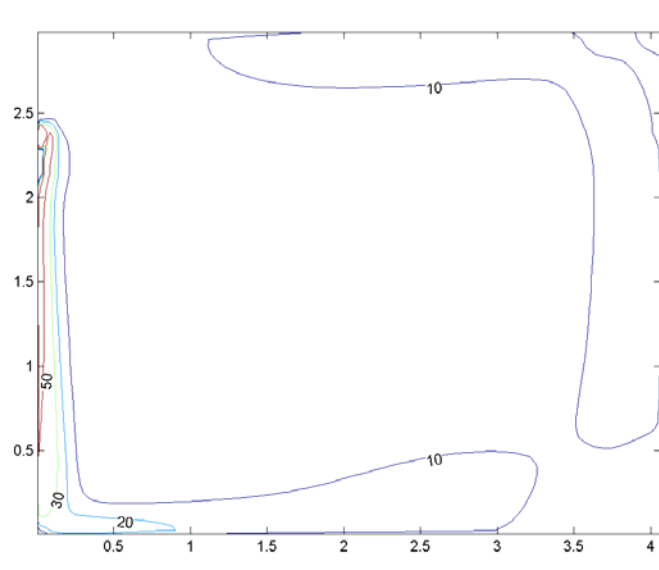


Figure 6.25: Calculated draft risk of CFD results, air supply temperature $-10\text{ }^{\circ}\text{C}$ in the axis of symmetry with floor heating

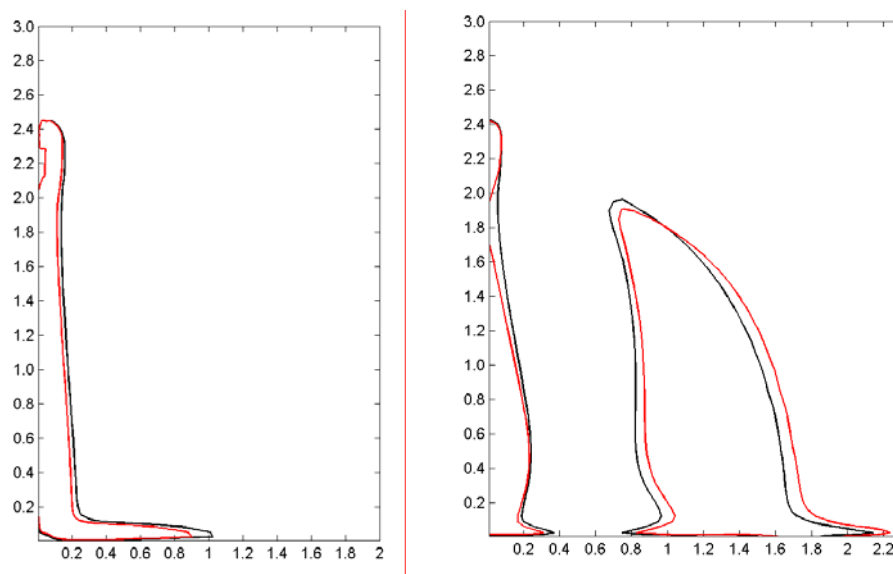


Figure 6.26: Comparison of the 20 % draft risk isoline at a supply temperature of $2\text{ }^{\circ}\text{C}$ (red) with a supply temperature of $-10\text{ }^{\circ}\text{C}$ (black) in the axis of symmetry (left) and near the outside wall $x = 0.1\text{ m}$ (right), with floor heating

6.4.7. Evaluation of draft risk at a supply temperature of $-10\text{ }^{\circ}\text{C}$ and convective heating element W-R-OS (case 3)

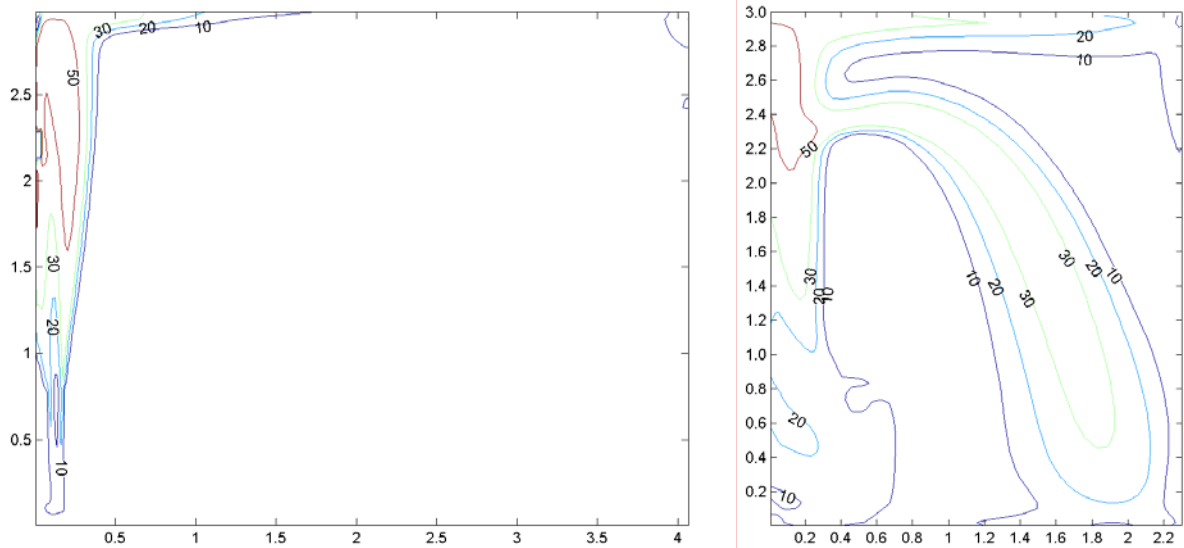


Figure 6.27: Calculated draft risk of CFD results, air supply temperature $-10\text{ }^{\circ}\text{C}$ in the axis of symmetry (left) and near the outside wall $x = 0.1\text{ m}$ (right) with convective heating element

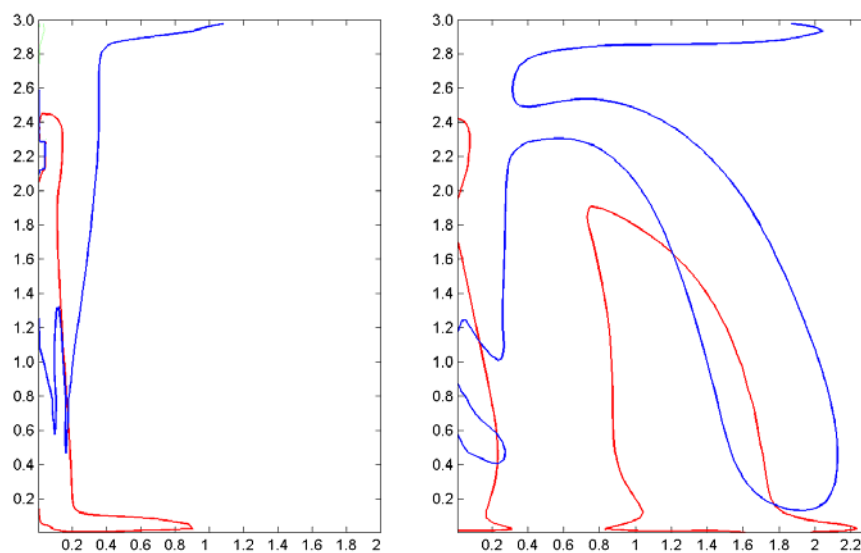


Figure 6.28: Comparison of the 20 % draft risk isoline with floor heating (red) and with convective heating element (blue) in the axis of symmetry (left) and near the outside wall $x = 0.1\text{ m}$ (right)

6.5. ATD with supply air preheating capability

6.5.1. Technical principle

This type of ATD is built in an outside wall and uses a water-air heat exchanger to heat the cold fresh air in wintertime. Either the heat exchanger is connected to the radiator or floor heating system or a separate circuit, which can be controlled separately and allows an air cooling in summertime. Because the supply air is preheated at a temperature of 10 to 15 °C this supply works with similar conditions like a displacement supply unit. The main advantage of these ATD is that the thermal comfort can be improved because of the higher supply temperatures compared with normal ATD.

One difficulty is that this ATD type has to cope with the freezing hazard of the heat exchanger in the case of power failures, for instances, when the supply of hot water fails. This problem can either be solved with an air valve, which close automatically if the air supply temperature falls below 5 °C or with a freezing damage protection called “ThermoGuard” like used in TK 35 (figure 6.30). Both ATD work without any electric power connection and control the supply temperature with an integrated thermostatic valve.

6.5.2. Water supply of the heat exchanger

Investigations in real buildings equipped with LuBo ATD have shown that if the heat exchanger is connected to a low temperature heating system (e.g. floor heating) thermal discomfort may occur during the transitional period. Furthermore, discomfort is also expected in the near surrounding of the supply unit. A separate water circuit would provide an autonomic control of the inlet temperature (separate heating curve) and would enable air cooling in the summer.

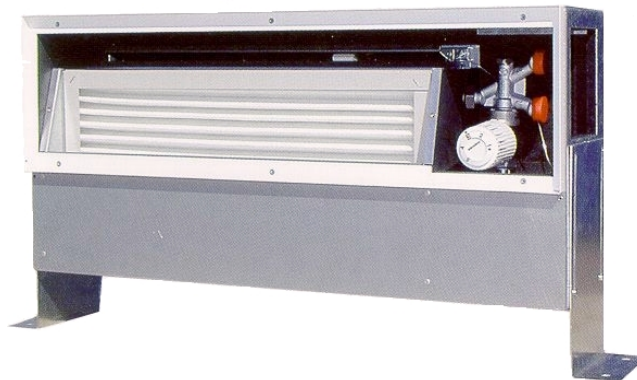


Figure 6.29: ATD with built in heat water-air heat exchanger: LuBo from Avenco AG, Switzerland

6.5.3. Generic results of simulation work for system 1

Supply air convector

Supply air convectors (SAC) TK 35 designed by L. Wetterstad (Sweden) (figure 6.30) are used for system 1. The draft risk of such a convector has been investigated by means of CFD modeling and compared with the draft risk of a supply air radiator (SAR) (figure 6.31).

The SAC is a stand alone device with heat exchanger and thermostat system so it's easy to control the temperature of the supply air. The plume from the supply air convector has a horizontal direction.

The SAR is an improved standard radiator (see fig. 1.1). The supply air comes through the wall to the radiator and warms up. The plume from supply air radiator has vertical direction. Temperature of the supply air depends on the thermal load of the radiator and can't be controlled exactly. The temperature is calculated assuming that 25% of the thermal load of the radiator goes to the incoming air.



Figure 6.30: Supply Air Convactor (SAC), from Sweden (source Thermopanel)

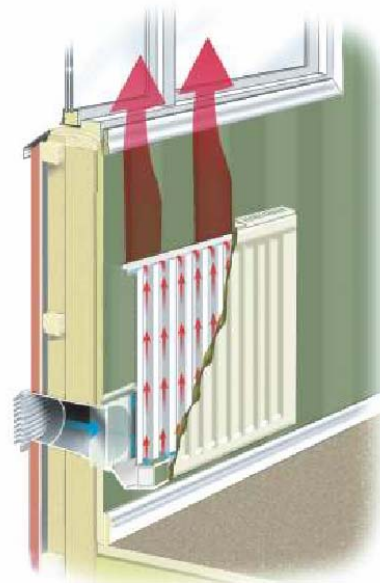


Figure 6.31: Supply Air Radiator (SAR) from Purmo, Sweden

Description of the room

As a sample room, the living room of a three-bedroom apartment was modelled. The floor area of this room is 29,4m². Bedrooms, bathroom, closet and WC were not considered in the model. The room contains kitchen line with kitchen range and cooker hood (pos. O5 in figure 6.32). The cooker hood was not considered in the model because of its irregular operation. The complete suction system is shown in figure 6.32. The main exhaust outlet, which was the only outlet in the model, is positioned at O4. Exhaust outlets in WC, closet and bathroom (pos. O1, O2, O3) were not considered.

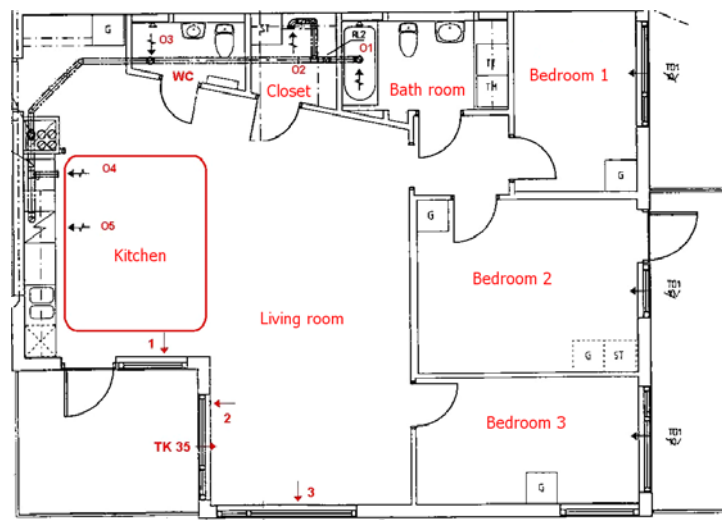


Figure 6.32: Floor plan of the apartment

The outdoor air enters the living room through a supply air convactor (SAC), (marked TK35 in the figure) or a supply air radiator (SAR) and by air leakage through the facade. Air leakage is assumed to occur in the joint between the exterior wall (pos. 1, 2, 3) and floor, the joint between the exterior wall and ceiling and the windows. The ATD is situated under the window (position TK35). The radiators are under the windows as well (position 1 and 3). Heat transfer through the exterior walls and

windows was taken into account by setting the proper thermal resistance. No heat exchange was considered between neighbouring rooms.

Results and their analysis

The results of the simulations are presented in a vertical plane RV1 and a horizontal plane RH1 (figure 6.33 and figure 6.34). The draft risk (DR) values according to equation (23) are evaluated for these planes.

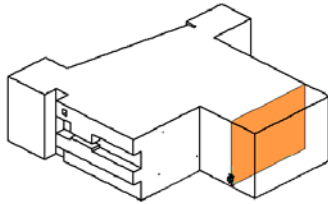


Figure 6.33: Vertical plane through supply air device RV1

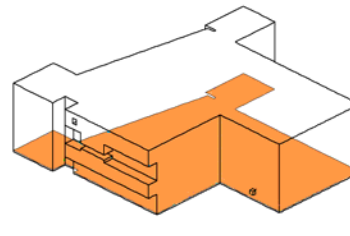


Figure 6.34: Horizontal plane 0,05m above the floor RH1

Results and their discussion

A total of 33 cases have been simulated, covering different air flow rates, air supply temperatures, outdoor and indoor temperatures.

Results for two cases are shown as examples in figure 6.35 and figure 6.36. The outdoor air temperature is -10°C in the first case and 0°C in the second case. The supply air temperatures are 18°C for the CAC and 0°C and 8°C respectively when the SAR is installed. These low supply temperatures have a significant influence on DR nearby the supply air radiator. Infiltration also affects the PPD distribution negatively.

The air leakage is assumed to occur in the joint between the exterior wall and the floor, the joint between the exterior wall and the ceiling and the windows, 1/3 evenly distributed at each location.

Simulations show that there are very high PPD values nearby the supply air radiator. The cold air that comes out from the SAR, turns down to the floor, so the PPD values exceed the recommended value of 10 % in this area (see figure 6.35 and figure 6.36 right).

In the case where the supply air convector is installed, there is a different distribution of the PPD in front of the device (see figure 6.35 and figure 6.36 left). As we can see, the highest PPD values are concentrated in the zones between floor and the distance 0.1m above the floor, under the ceiling and along the windows (these zones are due to infiltration through air leakage which brings in a very cold air at the temperature of -10°C).

When comparing the cases with SAR and SAC no significant differences can be observed in horizontal plane RH1. In all cases the required temperature of 22°C was achieved on the partition wall between the living room and bedroom 2.

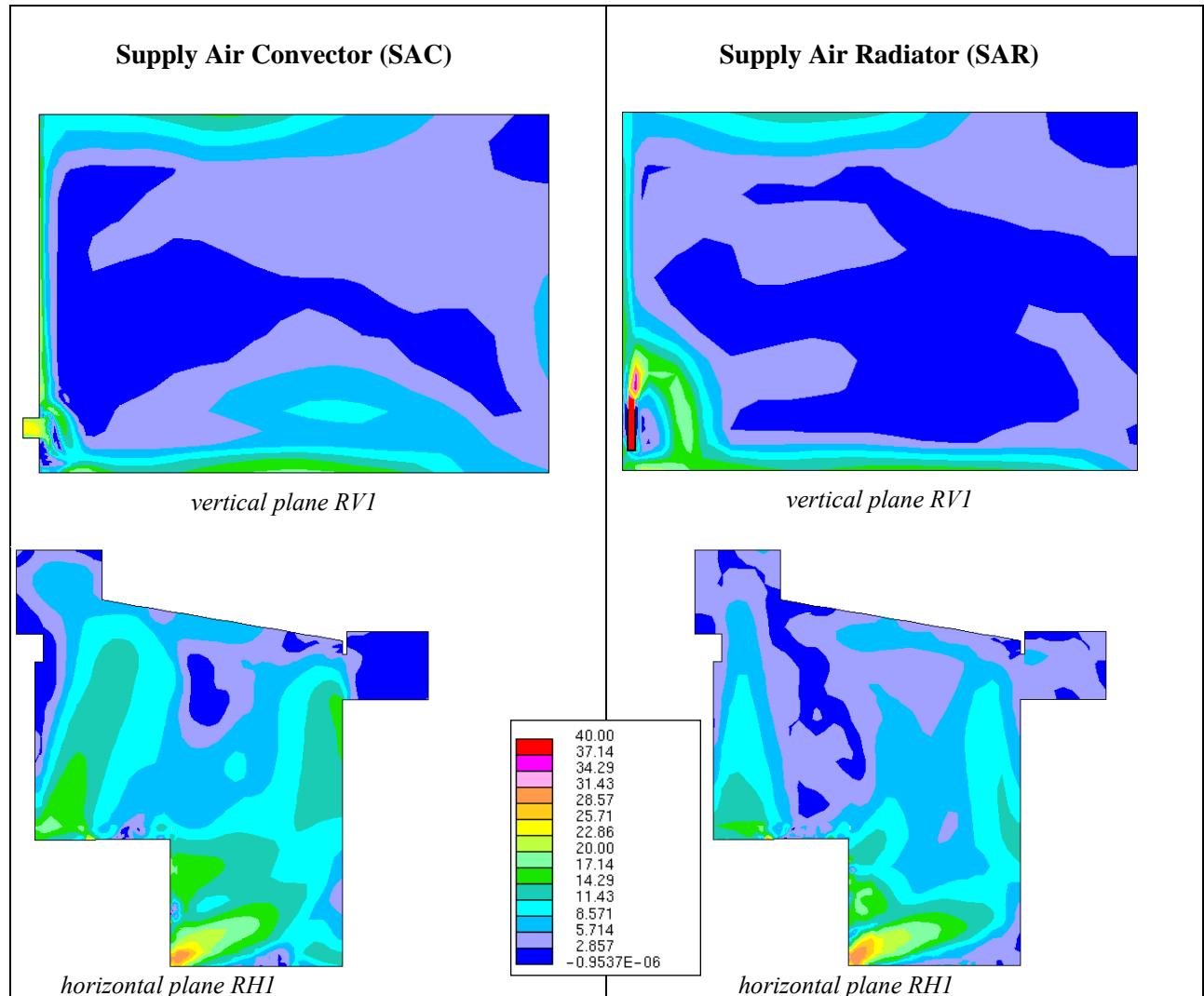


Figure 6.35: Comparison of draft risk values in vertical and horizontal plane
 With supply air convector (left), and supply air radiator (right)
 (outdoor air $T_e = -10^\circ\text{C}$; preheated air from convector $T_{SAC} = 18^\circ\text{C}$; from radiator $T_{SAR} = 0^\circ\text{C}$)

Conclusions

From all cases studied the following can be concluded for the SAC:

In the winter months with outdoor temperature below 0°C , the thermal comfort is strongly influenced by leakage air through slots between floor, external walls and ceiling. Maximum values of DR reach 35% in the area of living room and close to the kitchen line.

In general, the air leakage along the external walls substantially affects the thermal comfort. To reduce the discomfort caused by air leakage, the air supply convector has to work with maximum temperature and with maximum flow rate of preheated air.

In pre-, post and summer months, with outdoor temperatures above 0°C , values of DR are low and operation of the supply air convector is not expected with high temperature of supply air of 35°C .

In cases with supply air temperature of 18°C and supply air flow rate of 6.2l/s and 16.2l/s the no influence of the supply air from the convector on DR could be observed.

In cases with the lowest temperature of preheated air of 15°C and with the maximum supply air flow rate of 33.2l/s , the supply air stream tended to increase the values of DR.

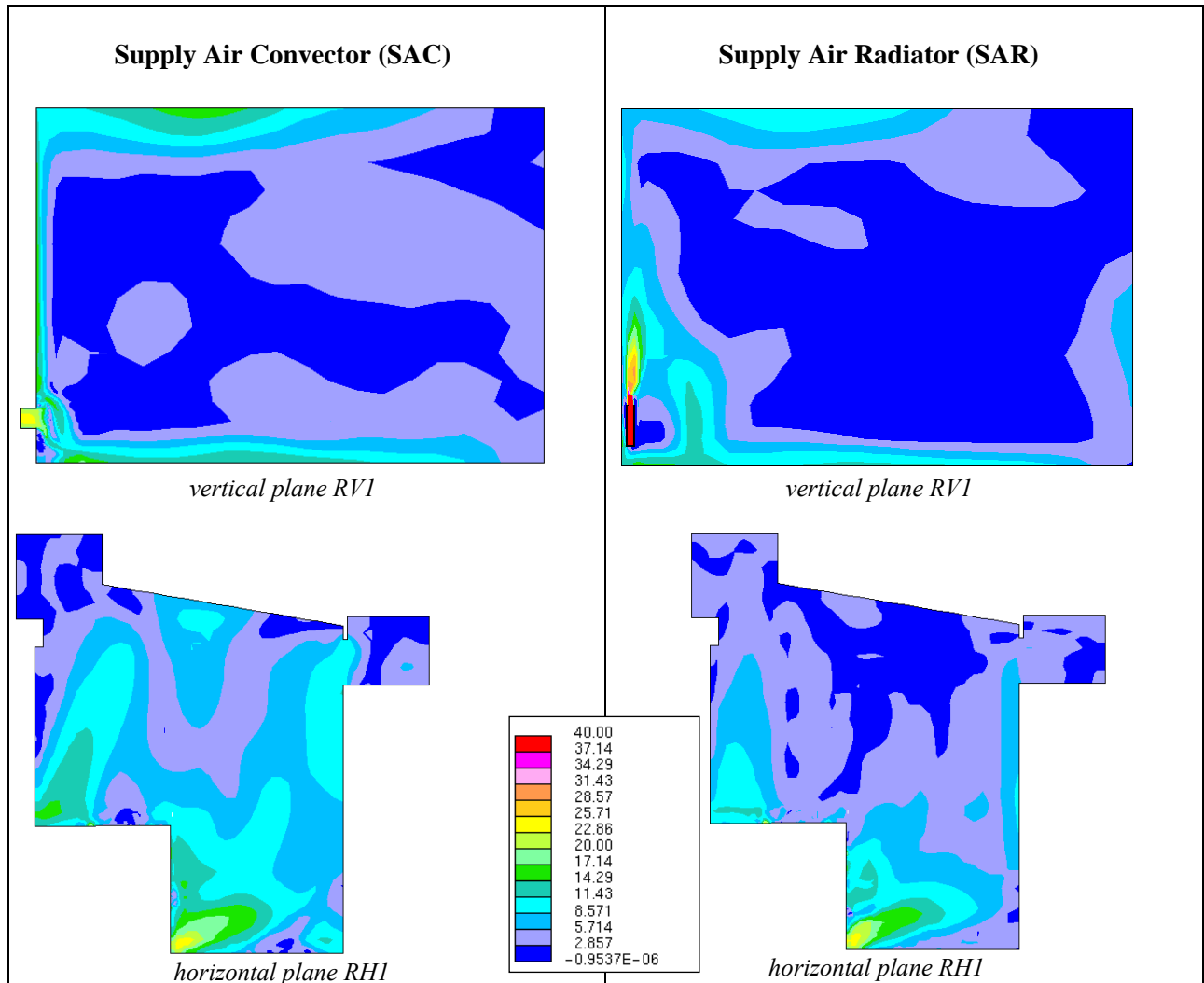


Figure 6.36 : Comparison of draft risk values in vertical and horizontal plane with supply air convector (left) and supply air radiator (right)
(outdoor air $T_e = 0^\circ\text{C}$; preheated air from convector $T_{SAC} = 18^\circ\text{C}$; from radiator $T_{SAR} = 8^\circ\text{C}$)

Comparing the two ATDs the following can be concluded:

The two air supply devices have quite a different impact in draught risk. The reasons are:

1. Air is supplied at different directions of from the device (SAC directs the air into the room in the direction perpendicular to the wall, SAR directs the air upwards by buoyancy force)
2. There supply air temperature of the two devices is quite different due to the different assumption about the preheating effects. In the case of SAC the air is preheated to $+18^\circ\text{C}$ in a controllable way, in case of SAR the air is preheated assuming that 25% of the radiator load is transferred to air.

PPD values of the draught risk in the horizontal plane RH1, i.e. in the plane 0.1m above the floor, are quite similar. Quite different values of PPD can be observed in the vertical plane RV1, i.e. in the plane drawn perpendicular to the supply device. There are higher PPD values in the case of SAR resulting from the fact that the cold air slightly rises after the radiator, but then sinks down, thus creating area of higher PPD in front of the external wall.

7. IAQ related factors

A good indoor air quality may be defined as air which is free of pollutants that cause irritations, discomfort or ill health to the occupants. Indoor air pollutants are derived from both outdoor and indoor sources. Clean outdoor air is essential for achieving good indoor air quality. In the following only the pollutants emitted inside the building are considered. Human metabolism, occupant activities and emissions from building materials are the major indoor pollutant sources.

Air contaminants can be classified as gaseous or particulates. Particles are solid or liquid and can be divided in several subclasses e.g. according to their size or according to their origin such as bioaerosols. Particle concentration is quantified as mass or number per volume unit of air (g/m^3 or number/m^3) and airborne microorganisms such as legionella or aspergillus mould are counted in colony forming units per cubic meter of air (cfu/m^3). The gaseous class covers chemical contaminants that exist as free molecules or atoms in air which are much smaller than particles and therefore may behave differently as a result. Gaseous concentration is measured in volume or mass of the contaminant per volume or mass unit of air (e.g. g/m^3 , kg/kg , ppm).

Perceived odour sensation depends very much on the individual. Therefore [Fanger 1988] defined a sedentary person in thermal comfort as a standard odour source (olf). The predicted percentage of dissatisfied persons (PPD) is depending on the ventilation rate per olf (figure 7.1). The total odour source of a room can be expressed as equivalent standard persons (i.e. in olfs) using this curve. Therefore the PPD and the ventilation rate of the room have to be measured. The sensory load of the room expressed in olfs is equal to the ratio of the measured ventilation rate and the ventilation rate indicated in figure 7.1 for the measured PPD level.

General information on air contaminants and odour can be found in [ASHRAE 2001].

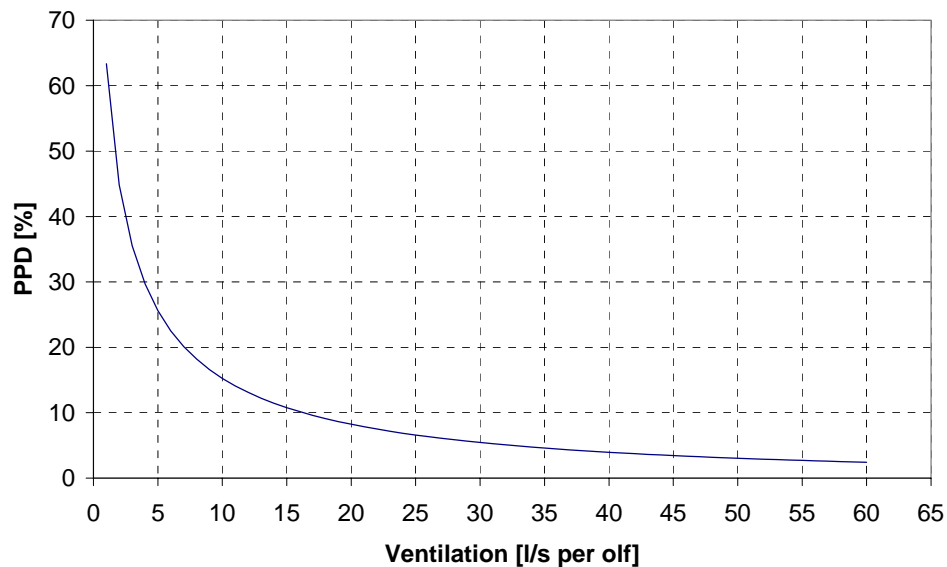


Figure 7.1: Percentage of dissatisfied persons as a function of ventilation rate per standard person (i.e., per olf)[CEN CR 1752]

7.1. Pollutant sources due to human metabolism

7.1.1. CO₂ production rates

The metabolic production rate of CO₂ q_{CO_2} for a human adult is dependant of the activity level. It can be calculated in l/h according to equation (31) using the metabolism M given in met or P given in W [Mansson 1995]:

$$q_{\text{CO}_2} = 17 \cdot M = 0.162 \cdot P \quad (31)$$

7.1.2. Water vapour release

The production rate of water vapour for a human adult is dependant of the activity level, clothing and the air temperature. Assuming a normal clothed man at light sedentary activity, still air, relative air humidity of 30 ... 70%, the following water vapour production rate follows [Recknagel 2001]:

Table 7.1: Water vapour production rates of a normal clothed man at light sedentary activity depending on the air temperature [Recknagel 2001]

air temperature (°C)	water vapour production rate (g/h)
18	33
20	38
22	47
24	58
26	70

7.1.3. Situation in dwellings

For the usual situation in a dwelling it is sufficient to distinguish between two typical activity levels (sleeping and awake). For children the metabolic rate at the same activity level is much lower than for adults. This is the case when sleeping. But awake the activity level of children is higher then the activity level of adults. Therefore the difference between adults and children is lower awake then asleep. The CO₂ and water vapour production rates given in table 7.2 can be used for dwellings [Millet 1998].

Table 7.2: Water vapour production rates of adults and children when awake and sleeping [Millet 1998]

		CO ₂ [l/(h*p)]	Water evaporation at 20°C [g/(h*p)]
Adult 15 years - ∞	awake	18	55
	sleeping	12	30
Children 13 and 10 years	awake	12	45
	sleeping	8	15
Child 2 years	awake	8	30
	sleeping	4	10

7.2. Internal pollutant sources

7.2.1. Water vapour release

Table 7.3: Water vapour production rates per person cooking and showering [Millet 1998]

Cooking g/h by person present at home			Shower (g by person)
breakfast	lunch	dinner	
50	150	300	300

Table 7.4: Typical moisture generation rates for household activities [CEN prEN14788]

Household activity	Moisture generation rate
Cooking (electric cooker)	2000 g/day
Cooking (gas cooker)	3000 g/day
Dishwashing (by hand)	400 g/day
Bathing/showering/washing	200 g/day per person
Washing clothes (by hand/open top machine)	500 g/day
Drying clothes indoors (natural drying or by unvented tumble dryer)	1500 g/day per person

7.2.2. Smoking

Tobacco smoke is an important source of many different pollutants. Besides organic components such as formaldehyde, nicotine or acrolein also inorganic compounds e.g. CO, CO₂ or NO_x are released. The distinction between particles and gaseous substances is often not quite clear because of the very fine aerosols. The composition of tobacco smoke is considerably influenced by the tobacco type, filter, firing temperature and pull velocity. Therefore very different values can be found in literature.

CO ₂	0.65 mg/s	[Huang J. 2004]
CO ₂	143 mg/cig	[Witthauer 1993]
NO _x	0.065 mg/cig	[Witthauer 1993]
CO	0.11 mg/s	[Huang J. 2004]
VOC	10 mg/cig	[Haghighat F. 1993] (Ref. No. 6864 in [ORME 2002])

7.2.3. Gas cooking

Gas cooking generates particulate and gaseous pollutant emissions. The main pollutant is CO₂. But the more important to pay attention on are the toxic pollutants CO and NO₂. Laboratory experiments in an environmental chamber give the following emission rates [Girman 1982]:

Table 7.5: pollutant emission rates for gas cooking in µg/kJ [Girman 1982]
(Ref. No. 1803 in [ORME 2002])

Pollutant	Oven		Top burners	
	Mean ± S.D.	Range	Mean ± S.D.	Range
<i>Gases</i>				
CO	226±17	214-238	200±34	172-249
CO ₂	42'700±2'300	38'380-46'360	45'320±1,700	43'900-47'600
NO _x	6.17±0.67	4.98-7.03	9.0±1.3	6.9-10.5
NO	6.61	-	9.7	-
NO ₂	1.14	-	14.8	-
SO ₂	0.11±0.02	0.08-0.13	0.16±0.02	0.14-0.18
HCHO	2.73±0.41	2.36-3.39	1.7±1.1	0.9-2.5
O ₂	-	-	78'200±7'300	73'000-83'300
<i>Particles (<2.5 mm)</i>				
Carbon	<0.02	-	0.22±0.01	0.21-0.23
Sulphur	<0.001	-	0.009±0.008	0.001-0.017
Mass	<0.05	-	0.41±0.19	0.24-0.62
Mass (<0.5 mm)	0.015±0.001	0.014-0.015	0.50±0.36	0.21-1.03

7.2.4. Material related sources

The database SOPHIE (Sources of Pollution for a Health and Comfortable Indoor Environment) is a common activity of participants of the three EU projects AIRLESS, MATHIS and “Database for Indoor Air Pollution Sources in buildings” sponsored by the JOULE Programme. SOPHIE is a tool with which emission data and toxicological information of building materials and HVAC components can be retrieved. [Bluyssen 2000]

In [Orme 2002] the pollutant data from 211 references can be retrieved in form of EXCEL sheets. Most of these tables give pollutant concentrations from building material sources measured in rooms or test chambers. Some of the data are given as emission factors in $\text{mg}/\text{m}^2/\text{h}$ or $\mu\text{g}/\text{m}^2/\text{h}$ (e.g. table 7.6). As all the hundreds of references show a very wide spread of the measured data, the requirements for standards or labelling programs might be more useful. (e.g. table 7.7 and Table 7.8)

[FiSIAQ 2001] defines three pollutant emission classes for building materials. The requirements of each class covers health and comfort (odour) related emission components. Emission class M1 corresponds to the best quality and emission class M3 includes materials with the highest emission rates. The pollutant emission rates of a material must be below the thresholds given in table 7.7 to fulfil the requirements of class M1 and M2. The class M3 includes materials with emission rates above the values given for class M2.

Table 7.6: Range of TVOC and formaldehyde emission rates for common materials (in $\mu\text{g}/\text{m}^2/\text{h}$) [Anon 1996] (Ref. No. 10414 in [ORME 2002])

Material	TVOC emissions		Formaldehyde emissions	
	Max	Min	Max	Min
Carpet	652	<1	48	<1
Carpet undercushion	856	<1	12	<1
Sheet vinyl flooring	9408	948		
Medium density fibreboard	835	37	1000	42
Composite wood (structural lumber)	290	67	85	4
Composite wood (structural panel)	386	55	655	3
Composite wood (cabinetry, coated)	1378	459	177	6
Gypsum board	25	<1	250	60
Foam insulation	68	<1	<1	<1
Glass fibre insulation	150	<1	105	<1
Latex paint	308	9		

Table 7.7: Emission classification of building materials [FiSIAQ 2001]

class	total volatile compounds (TVOC) [$\text{mg}/\text{m}^2/\text{h}$]	formaldehyde H_2CO [$\text{mg}/\text{m}^2/\text{h}$]	ammonia NH_3 [$\text{mg}/\text{m}^2/\text{h}$]	carcinogenic compounds [$\text{mg}/\text{m}^2/\text{h}$]
M1	0.2	0.05	0.03	0.005
M2	0.4	0.125	0.06	0.005

Table 7.8: Emission requirements in Canadian labelling programs [Anon 1996], (Ref. No. 10414 in [ORME 2002])

Program	Material	Pollutant	Limit	Description
Canadian Carpet Association (CCI)	carpets	TVOC	500 µg/m ² h	emission rate
		4-PC	100 µg/m ² h	
		Styrene	400 µg/m ² h	
		Formaldehyde	50 µg/m ² h	
Canadian Particleboard Association (CPA)	Particleboard flooring	Formaldehyde	0.2 ppm	concentration in test chamber
	other particleboard		0.3 ppm	
Environmental Choice (EcoLogo)	water-borne paints	VOC	250 g/L	VOC context of product (excl. water)
	solvent-borne paints		380 g/L	
	water-borne wood finishes		300 g/L	
	water-borne wood stain		250 g/L	
	adhesives		20 g/L	
	caulks and sealants		20 g/L	
	particleboard	Formaldehyde	0.15 ppm	chamber conc
	fibreboard: MDF, hardboard	Formaldehyde	0.15 ppm	chamber conc
	carpets	TVOC, 4-PC, styrene, formaldehyde	CCI standards as maximum	emission rate
	undercushion	TVOC, 4-PC, styrene, formaldehyde	CCI standards as maximum	emission rate
	resilient flooring	TVOC	1000 µg/m ² h	emission rate
	prefin.hardwood flooring	TVOC	500 µg/m ² h	emission rate
	office panels and partitions	TVOC	500 µg/m ² h	emission rate

7.2.5. Ground related sources

Radon is a naturally occurring radioactive noble gas. It is a member of the decay chain of uranium-238. As uranium is in varying concentration almost omnipresent in the earth's crust also radon can be found practically everywhere in the ground. As it is the first and only gaseous element in the decay chain it can easily leave the place of production (soil, rock and building material) and enter the indoor air. Radon is even in high concentrations invisible, odourless, non-toxic and not flammable. It decays with a half-life of 3.82 days in radioactive products.

Depending on the location the radon concentration in the air from ground causes a radioactivity of some 10'000 Bq/m³. Recommended reference levels in indoor air vary in the different countries from 150 up to 800 Bq/m³.

Investigations have shown that even in buildings with the same type of construction and located next to each other, totally different radon concentrations can be measured. The spread of radon in the ground and the infiltration process into the building is very complex. Therefore, up to now, it is not possible to predict the radon concentration in the indoor air, knowing the composition of the ground and the type of the building construction. Only measurements can deliver reliable information. A profound review of the radon problem is given in [Bohicchio 1995].

7.3. Occupant presence and activity schedules

7.3.1. Stochastic occupancy model

Occupancy has a high degree of randomness. As a result the indoor air quality output parameters will show as well a random character with a certain probability distribution dependent on the probability distribution of the occupancy. This can be evaluated with the Monte-Carlo technique [Rubinstein 1981]. Therefore a stochastic model for the occupancy is necessary.

The proposed stochastic occupancy model is based on the probability of presence of the occupant. Daily profiles of the probability of presence are given in [Månson 1995] for different occupant types. If only the probability of presence per hour of the day without any auto-correlation is taken into account, then the resulting occupancy pattern fluctuates more heavily than it does in reality. The probability of change (that means the probability of entering or leaving the dwelling) is a function of the probability of presence. This function is depending on the auto-correlation of the presence (see figure 7.2). A reduction factor for this probability of change has been introduced. If this reduction factor is 1 then no auto-correlation is taken into account. With a decreasing reduction factor down to zero the auto-correlation will be increased up to 1, and the fluctuation rate will be reduced without to influence the average probability of presence of the period. But the reduction factor will cause a distortion of the daily profile. That means a change in the probability of presence will undergo a delay. This has the advantage that an abrupt change in the profile will be smoothed out. Thus the profiles can be defined as rectangular profiles by just two values: one for the day time and one for the night time. As a result, the smoothed out profiles will look quite similar to the realistic ones given in [Månson 1995] (see figure 7.3).

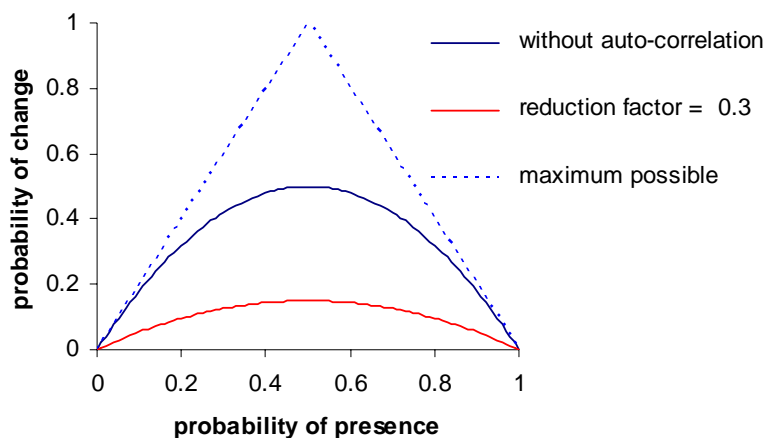


Figure 7.2:
Probability of change vs.
probability of presence for the
situations:
maximum possible probability
of change; no auto-correlation
is taken into account; reduced
probability of change with a
reduction factor of 0.3 (auto-
correlation is about 0.7)

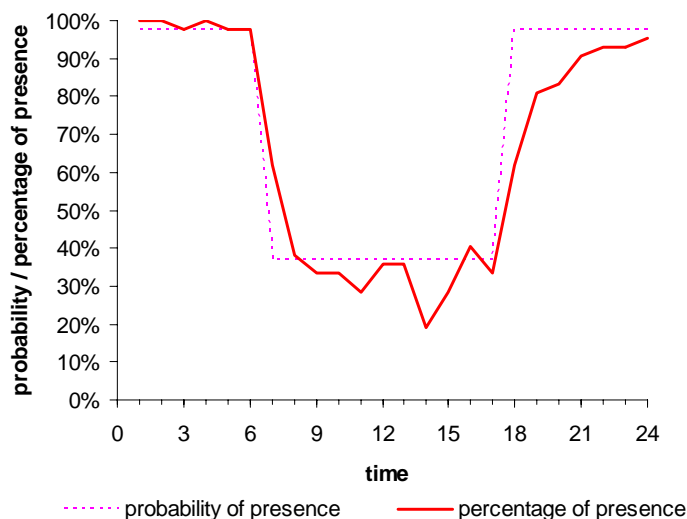


Figure 7.3:
Example of a daily rectangle
probability profile of presence
and a possible resulting profile
of the average percentage of
presence during a period of 42
days

The probability of presence of the actual hour, taking into account the above described reduction factor, can be calculated according to equation (32):

$$p_p(t) = (1 - r) \cdot P(t-1) + r \cdot p_{pa} \quad (32)$$

where:

- $p_p(t)$ probability of presence for the actual hour
- p_{pa} average probability of presence for a certain period
- $P(t-1)$ presence of the last hour
($P = 1$ means occupant is present; $P = 0$ means occupant is not present)
- r reduction factor for the probability of change

This probability is used to decide whether the occupant is present or not:

IF $u \leq p_p(t)$ the occupant is present
ELSE the occupant is not present

where:

u uniform random number in the range [0,1]

If the occupant is present in the dwelling it must be decided in which room he is. This can be done with the distribution of the probabilities of presence in the different rooms.

IF $\sum_{i=1}^{n-1} p_i \leq u \leq \sum_{i=1}^n p_i$ then the occupant is present in room number n

where:

- p_i probability of presence in room number i (the sum for all rooms has to be 1)
- u uniform random number in the range [0,1]

The selection of the room according to the above equation can be graphically shown with the cumulative probability of presence distribution. Figure 7.4 shows as an example the selection of the room in which a person is present, if the probabilities of presence for this person are as follows:

$p_{\text{Kitchen}} = 0.22$; $p_{\text{Livingroom}} = 0.68$; $p_{\text{Bedroom 1}} = 0.1$

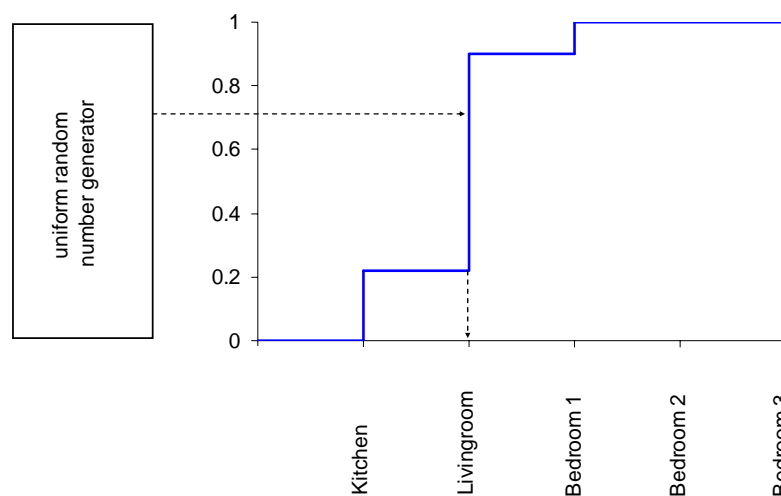


Figure 7.4: Selection of the room with the help of the cumulative presence probability distribution in the different rooms.

8. Application possibilities and limits of CFD

8.1. Modelling of air flows around buildings

8.1.1. General modelling guidelines from literature

Introduction

The purpose of this chapter is to extract information from literature in respect of the suitability of CFD for air flow around building modeling. The focus is such types of CFD codes which are used on the level of engineering offices and manufacturers as have participated in the RESHYVENT project. In this industry environment normally CFD codes are used which are specifically developed for room air flow simulation, and less for the determination of air flows around buildings.

Influence of dimensionality

[Oliveira et al. 2000] has demonstrated on a full-scale building that the widely used assumption of two-dimensional flow field in the mid-span leads to serious overestimation of the suction pressure over the roof and on the lee wall. Such differences in two- and three-dimensional modelling can be mainly related to the edge effects of the building, which causes strong eddies and swirling motions at the edges. Therefore, for the adequate calculation of flow fields around buildings, a three-dimensional calculation domain is needed if the building length is limited.

Computational domain size

The influence of the calculation domain size has been evaluated and documented by [Oliveira et al. 2000] and [Cowan et al. 1997]. Because of the higher blockage effect in two-dimensional calculations, a larger domain size is necessary. For two-dimensional calculations of a cubic building the upstream, downstream and cross-stream dimensions should not be less than $5H$, $15H$ and $\pm 4H$ (see figure 8.1). The domain height should at least be $10H$. For a three dimensional pitch roof building as shown in figure 8.1 the domain should have the minimal dimensions of $L_1/S = 3$ and $Y/H = 5$.

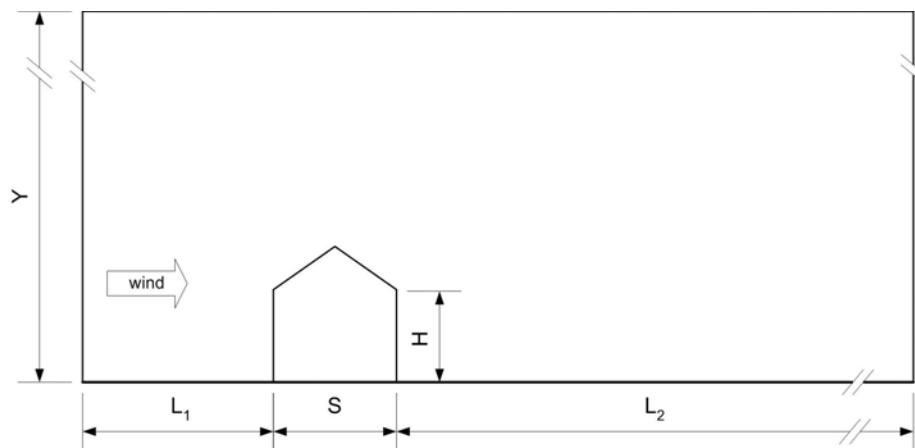


Figure 8.1: The computational domain size for CFD calculation must not fall below a certain minimal dimension because of the building blockage effect.

Calculation grid design

The design of the grid has significant influence on the simulation accuracy. A general approach is to maximise the mesh density in regions where high gradients in the flow variables could be expected. As mentioned by [Cowan et al. 1997] the mesh expansion ratios should not exceed about 1.2 as higher values can lead to calculation errors. Critical regions are those surrounding the sharp leading edges of the building. In order to resolve the shear layer adequately a special fine resolution ($1\% H$ or

less) is needed in regions where separation is expected. It has been shown that a coarser grid leads either to complete suppression of separation or much too early a reattachment. Therefore a local grid refinement would be a helpful CFD feature to reduce the computing time. Structured grid as used by FLOVENT may lead to problems by sloped surfaces. As mentioned by [Mikkelsen et al. 1995] the underestimation of C_p on the slope roof could be traced back to the grid refinement. In this case the slope roof has been modelled as a series of steps. To avoid numerical instabilities because of the diagonal grid cell flow, often unstructured or pseudo-unstructured grids are used successfully. As well as that, this grid arrangement allows an adequate simulation of sloped surfaces and also leads to a smaller amount of cells in the calculation domain. As shown in figure 8.2 [Oliveira et al. 2000] and [Jianming et al. 1997] made use of a pseudo-unstructured grid to analyse air flows around buildings.

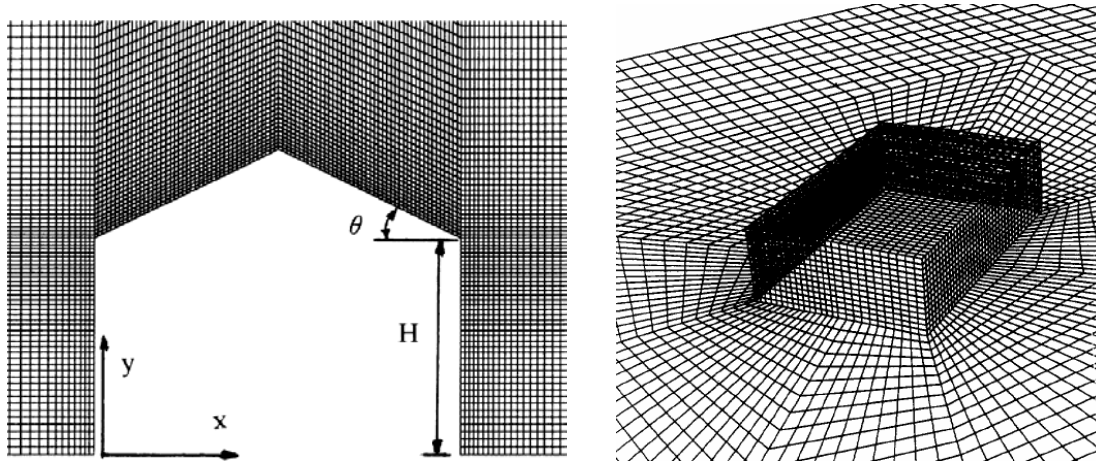


Figure 8.2: pseudo-unstructured grids are often used for the investigations of air flows around buildings. Left: Grid construct for calculation of pitch roof buildings. (Source: Reprinted from Publication Journal of Wind Engineering and Industrial Aerodynamics, Vol. 86, Oliveira P.J., Younis B.A., On the prediction of turbulent flows around full-scale buildings, p. 203-220, Fig. 1, Copyright (2000), with permission from Elsevier), Right: Grid construct for calculation of the roof corner vortex caused by a diagonal air flow. (Source: Reprinted from Publication Journal of Wind Engineering and Industrial Aerodynamics, Vol. 67&68, Jianming H., Song C.C.S., A numerical study of wind flow around the TTU building and the roof corner vortex, p. 547-558, Fig. 1, Copyright (1997), with permission from Elsevier)

Turbulence Model

Several references state that the standard k-ε turbulence model fails to model appropriately cases with high-streamwise strain rates [Cowan et al. 1997], [Yongsheng et al. 1997] and [Oliveira et al. 2000]. Such cases occur in wind flow over cubic shaped buildings, or bluff bodies in general, and lead to physically unrealistic high levels of turbulence energy upwind of the building leading edges. Therefore it is actually well known that the k-ε model method is little able to accurately predict the reverse flow after separation on roof surface and side walls [Murakami 1997], [Murakami et al. 1999]. It has been attempted to improve the k-ε model by modifying the term representing the production of the turbulence-energy dissipation in order to reduce the over-prediction of turbulent energy.

In some previous investigations other turbulence modelling methods have been used and compared with the standard k-ε model. [Yongsheng et al. 1997] described a two-layer modelling method, combining k-ε for fully turbulent regions and one-equation model in near wall regions. It has been found as an effective way to model the flow separation above roof surface and near the side walls.

[Oliveira et al. 2000] and [Meroney et al. 1999] used Reynolds stress turbulence model (RSM) in combination with pressure strain model of Speziale, Sarkar and Gatski (SSG) and compared the results with the standard k-ε model. Oliveira states that the k-ε model overestimates the roof suction for a roof pitch of 27° by about 15% in his specific case. Meroney also carried out calculations of the same

configuration with the k- ϵ RNG model (re-normalised group theory) [Lien et al. 1994], [Kim et al. 1978].

The figure 8.3 shows a comparison of the streamlines around the building calculated once with k- ϵ and once with RSM-SSG turbulence model. The presence of a region of flow reversal over the windward roof is confirmed from the plots of mean-flow streamlines. It can be gathered that the k- ϵ model does not capture the expected flow separation over the windward eaves as has been observed in experiments. Because the CFD software used for the following calculations (FLOVENT) contains only the standard k- ϵ model, building geometries prone to high separation flows must not be investigated.

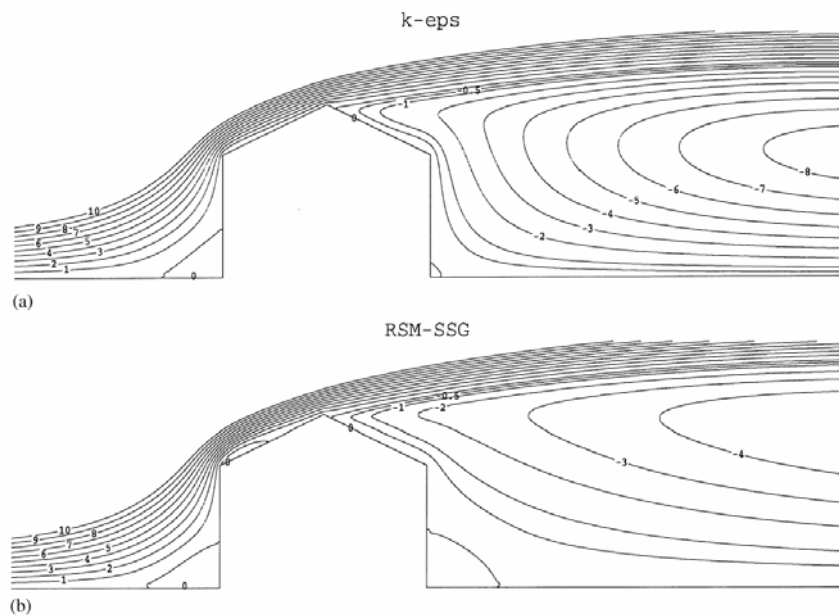


Figure 8.3: Streamlines around a building as an example for local separation:

(a) 2-D predictions with the k- ϵ model; (b) 2-D predictions with the RSM-SSG model.

(Source: Reprinted from Publication Journal of Wind Engineering and Industrial Aerodynamics, Vol. 86, Oliveira P.J., Younis B.A., On the prediction of turbulent flows around full-scale buildings, p. 203-220, Fig. 10, Copyright (2000), with permission from Elsevier)

8.1.2. Comparison and verification with literature

Creating CFD data on such complex flows normally needs a validation with experimental data (either wind tunnel or on site measurements). Nearly all investigations on flows around buildings have been compared with measurements of exactly the same building shape and boundary conditions. In our project unknown building shapes will be investigated, without having experimental data available. Firstly, two different very well known cases shall be calculated with FLOVENT and be compared to earlier works to evaluate the suitability of this CFD software for this kind of flow investigations. Furthermore, also some experience for how to size grid and calculation domain adequately shall be gathered. Secondly, qualitative comparisons of typical phenomena like reattachment length, corner vortex, etc. documented in several papers can be done.

8.1.3. Three dimensional air flow around a cubic building

To evaluate the suitability of the CFD program FLOVENT for calculation of wind flow around buildings initial investigations with the boundary conditions of [Mikkelsen et al. 1995] have been done. Mikkelsen have made comparisons between k- ϵ model and wind channel measurements of cubic buildings done by [Sakamoto et al. 1982] for different wind incident angles. Comparisons of the C_p -

value along the centre line as done by [Zhou et al. 1997] and can also be compared with our calculations.

Figure 8.9 to figure 8.12 show the calculated C_p -values and velocities on all surfaces for a normal directed wind flow. Not only the C_p -values have been compared but also the air velocities near the surfaces.

Simulation conditions

The pressure distribution and air velocities of the surface of the cube immersed in a turbulent boundary layer was calculated using the CFD software FLOVENT, matching as closely as possible the calculation conditions used by Mikkelsen. The size of the boundary domain was $0.6 \times 0.6 \times 0.6 \text{ m}^3$, corresponding the wind tunnel measurements. As well as that, the cube has a dimension of $0.05 \times 0.05 \times 0.05 \text{ m}^3$. The upstream boundary condition was a logarithmic wind velocity profile with a free-stream velocity of 25 m/s at the high of 54 mm. This profile was modelled by twelve different shaped air outlets with increasing air velocity boundary conditions in the upper direction. figure 8.4 shows the pre-set wind profile.

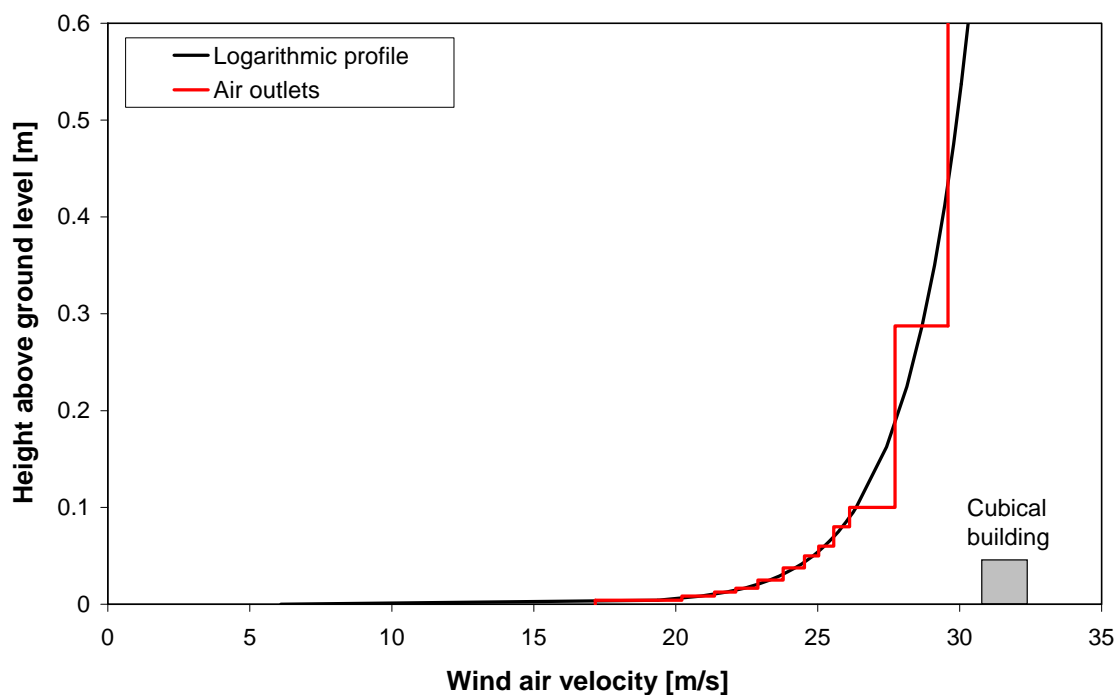


Figure 8.4: Wind air velocity profile used for the CFD calculation. The wind was modelled by using 12 air outlets.

The downstream boundary was an open face, the top and vertical sides of the domain had symmetry conditions. The bottom was a flat plate with a roughness parameter z_0 of $6.4 \cdot 10^{-4} \text{ mm}$. Because of the high gradient the smallest grid cells can be found near the building roof surface with a thickness of 1.17 mm. More detailed information about the mesh design can be found in table 8.1.

Table 8.1: Mesh design for two different incident of wind.

Mesh	NX	NY	NZ	NC	dx_{\min}	dy_{\min}	dz_{\min}
Wind angle 0°	89	70	80	498'400	0.0417	0.0233	0.0417
Wind angle 45°	95	76	84	606'480	0.0415	0.0233	0.0396

The following figures show the calculation domain and the chosen grid for the simulations.

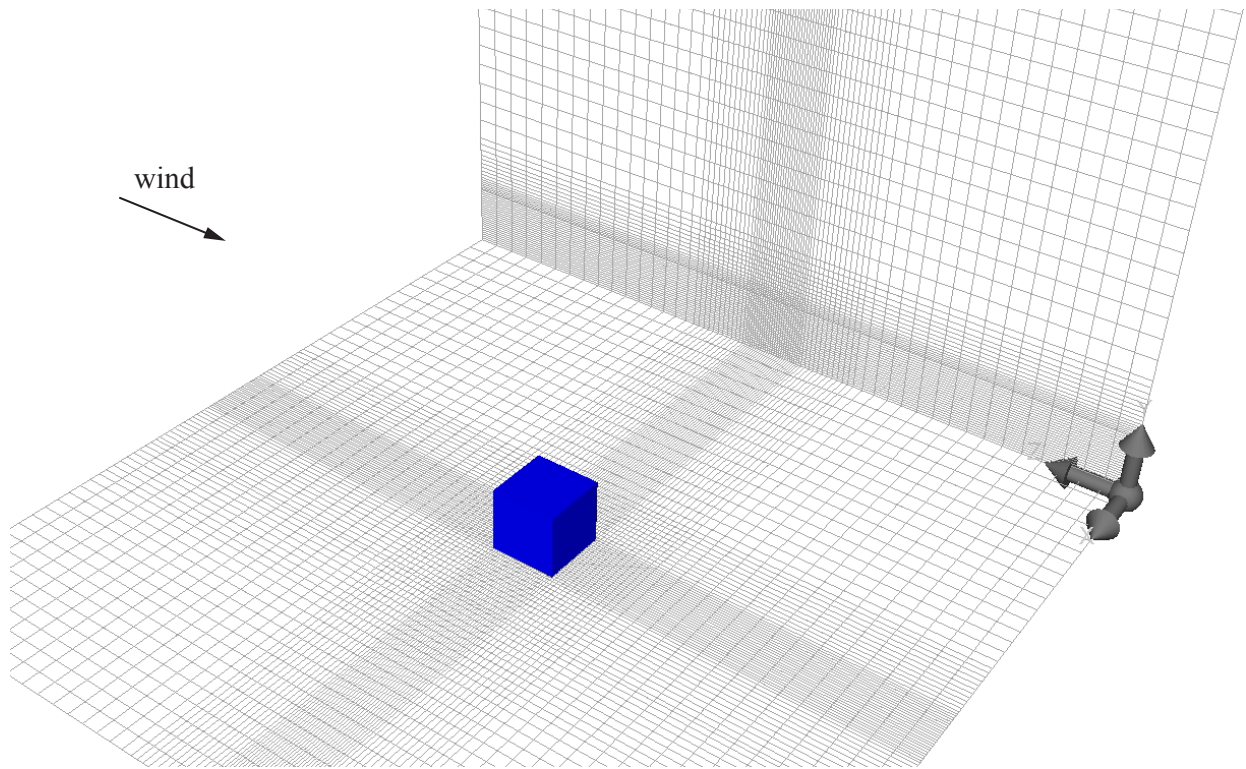


Figure 8.5: x-z and x-y grid used in the CFD calculation domain without using local grid refinement for the wind angle of 0°

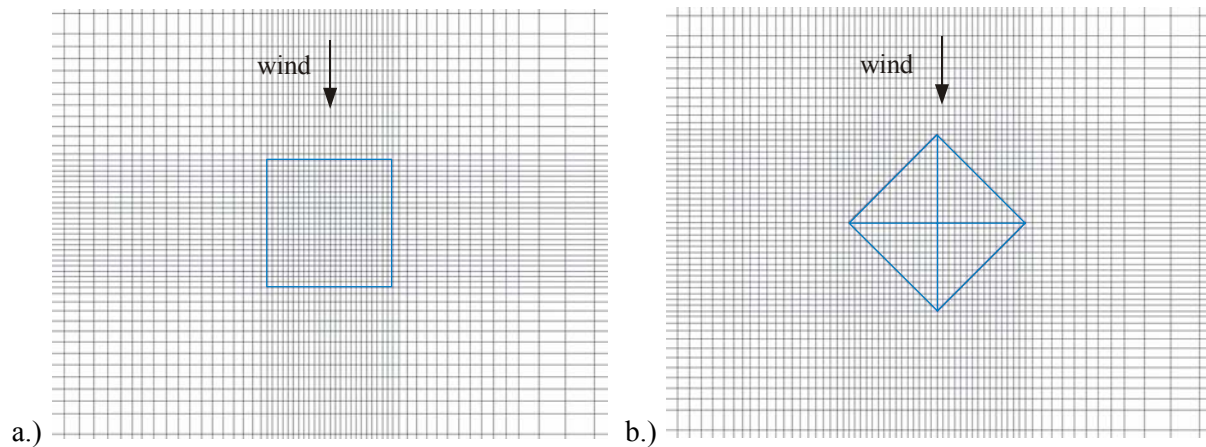


Figure 8.6: x-z grid of the CFD calculation domain. a.) wind incident angle of 0° , $89 \times 70 \times 90$ grid cells; b.) wind incident angle of 45° , $95 \times 76 \times 84$ grid cells

In the meantime new features have been implemented in the latest version of FLOVENT (version 4.2). The so called local grid refinement is one of them. This feature helps to reduce the number of grid cells in the cube surrounding as shown in Figure 8.7.

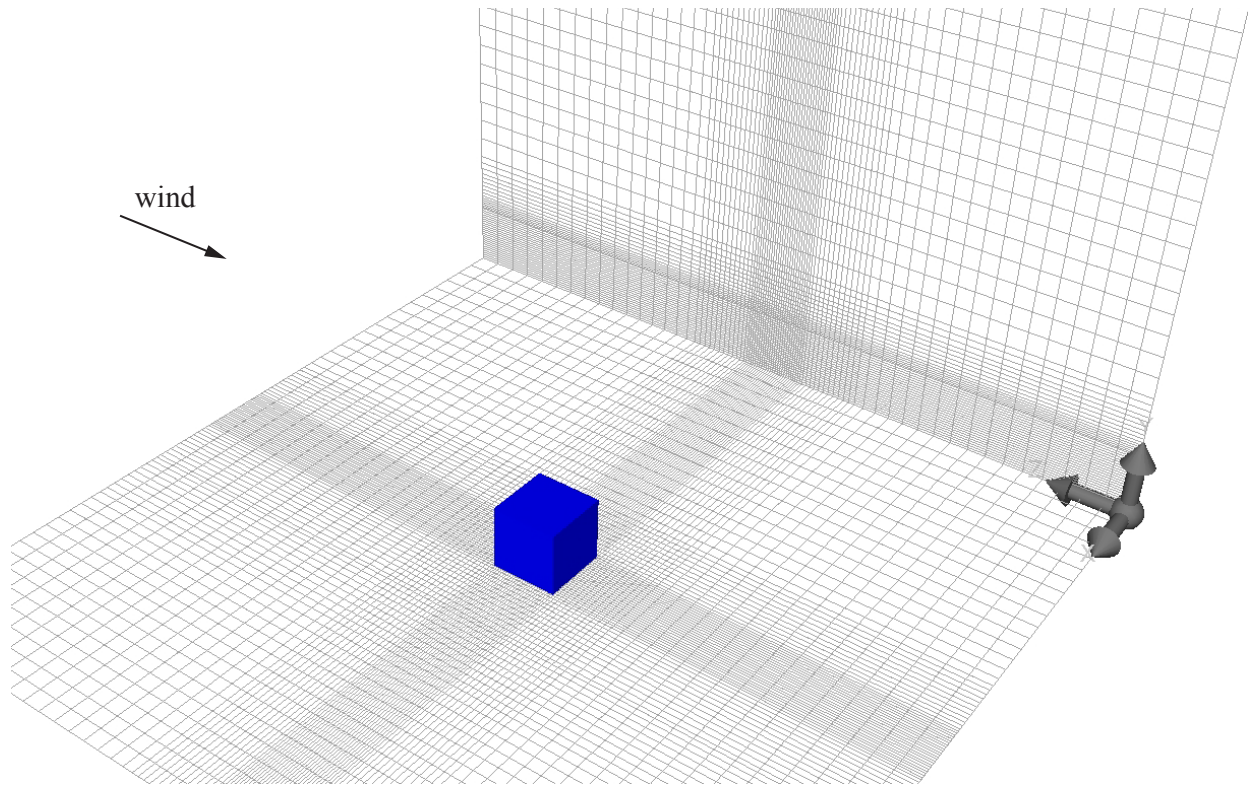


Figure 8.7: Alternative CFD case using the new feature of local grid refinement (provided in FLOVENT version 4.1 and later), only 110'000 instead of 498'400 grid cells are needed

The pressure distribution was calculated for wind angles of 0° and 45° and is presented as pressure coefficients in isobar plots and centre line diagrams. The C_p -value has been calculated according to equation (33) considering static pressure difference, air density and reference velocity at building roof height.

$$C_p = \frac{2(p_s - p_{s,r})}{\rho U_r^2} \quad (33)$$

Comparison for a wind direction of 0°

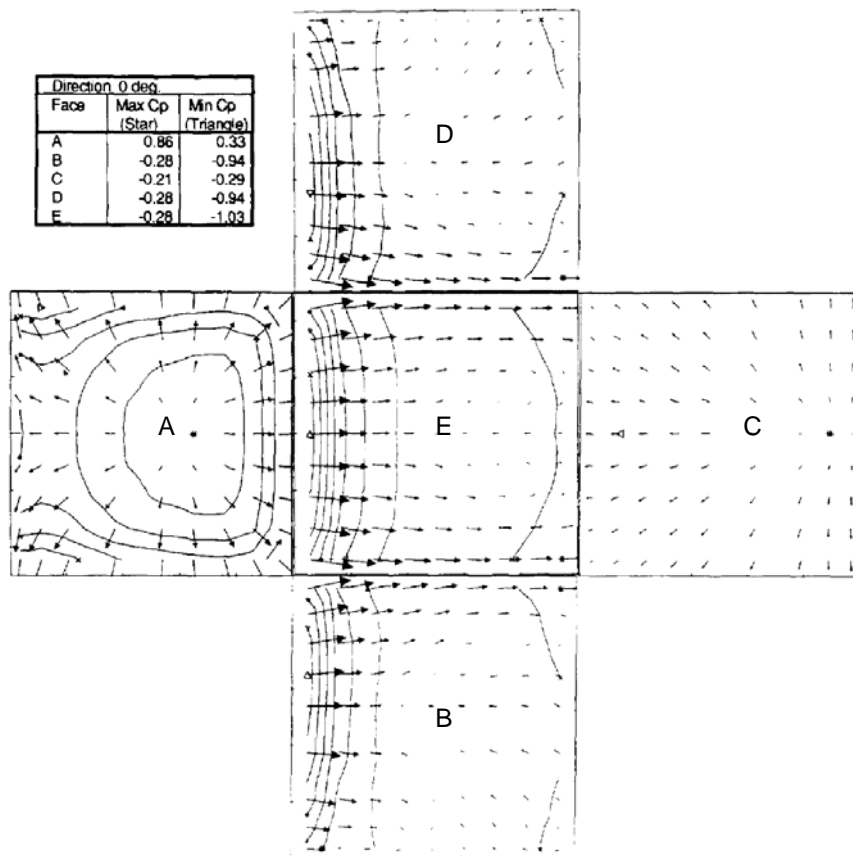


Figure 8.8: Calculated C_p -values shown as isobars and air velocities for an incident angle of 0°. (Source: Reprinted from Publication Journal of Wind Engineering and Industrial Aerodynamics, Vol. 57, Mikkelsen, A.C., Livesey F.M., Evaluation of the numerical k-e model Kameleon II for predicting wind pressures on building surfaces, p. 375-389, Fig. 2, Copyright (1995), with permission from Elsevier)

The following four figures show the computed results carried out with the CFD software FLOVENT. For the windward wall (surface A) a very good agreement with Mikkelsen can be found. As in these calculations the maximum C_p is in the lower third and has a value about 0.9. The isolines are slightly closer than in the earlier simulation, maybe because of the finer calculation grid. Also the leeward wall (surface C) agrees quite well with the example from literature.

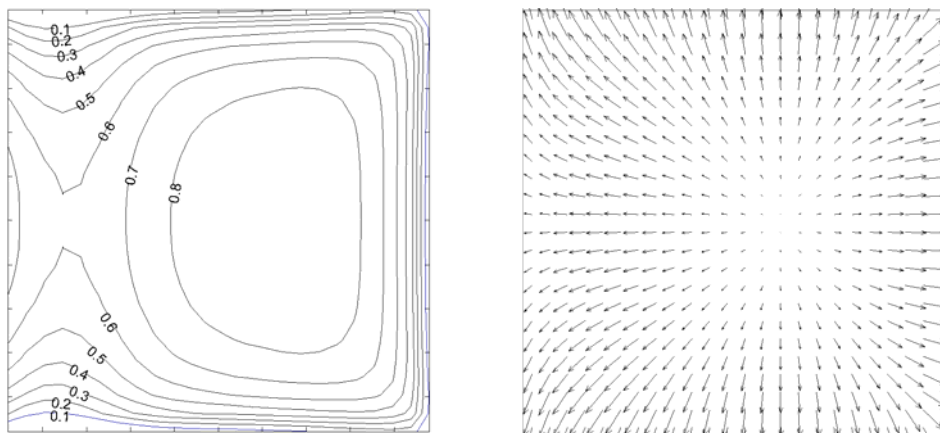


Figure 8.9: CFD calculations of surface A, using FLOVENT with k-e turbulence model
left: Calculated C_p -values shown as isobars. min. = -0.13; max. = 0.90
right: Air flow vectors near the surface

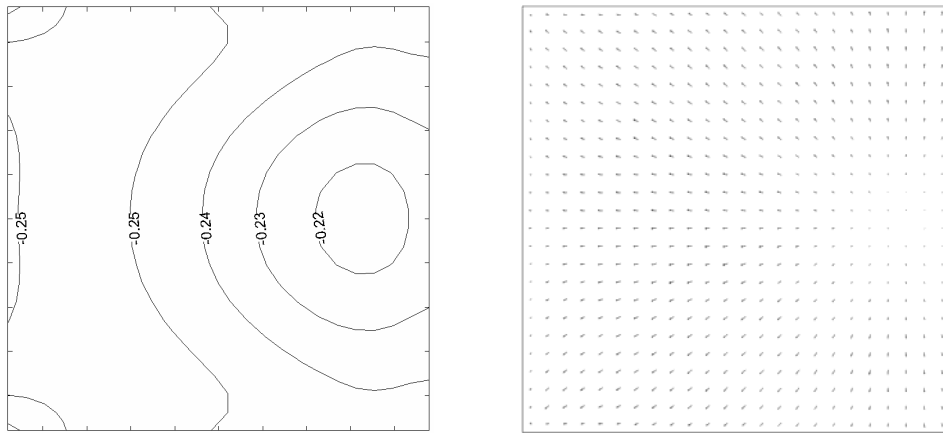


Figure 8.10: CFD calculations of wall C using FLOVENT with $k\text{-}e$ turbulence model
 left: Calculated C_p -values shown as isobars. min. = -0.26; max. = -0.20
 right: Air flow vectors near the surface

The maximal value of the side walls and the roof is very near earlier calculations. Although the distribution is quite similar, the minimum C_p -value is lower than in the calculation of Mikkelsen, perhaps because of the more detailed grid resolution. It has been found that the left and right side wall had exactly same C_p -values. Because of the $k\text{-}e$ model the C_p gradient at the building leading edges is higher than in reality. It can be mentioned, that such a strong backflow on the roof can not be detected in earlier calculations.

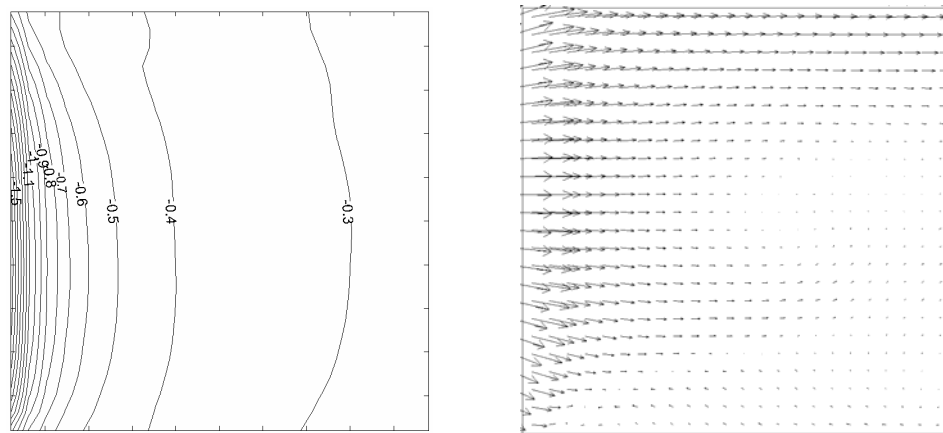


Figure 8.11: CFD calculations of surface B/D using FLOVENT with $k\text{-}e$ turbulence model
 left: Calculated C_p -values shown as isobars. min. = -1.87; max. = -0.24
 right: Air flow vectors near the surface

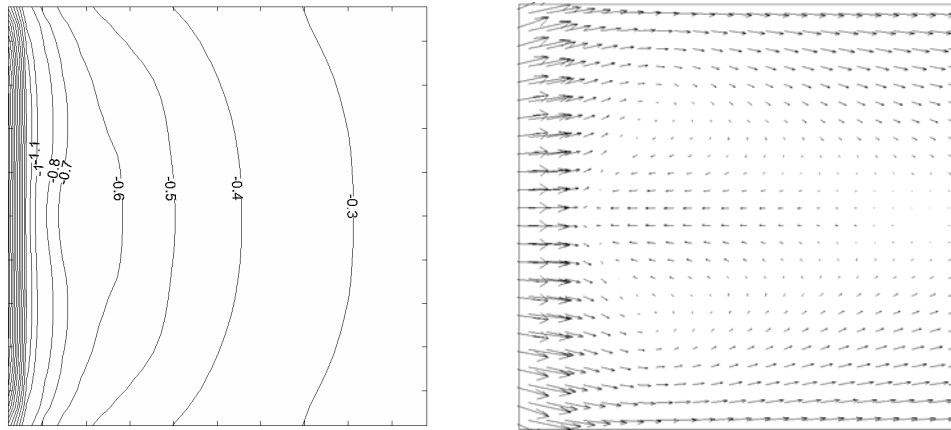


Figure 8.12: CFD calculations of surface E using FLOVENT with k - ϵ turbulence model
 left: Calculated C_p -values shown as isobars. min. = -2.27; max. = -0.25
 right: Air flow vectors near the surface

The C_p -values in the centre line can also be compared with earlier data from [Zhou et al. 1997]. Good agreement is observed, except for the too low C_p on the upper third of the windward wall and the effect of backflow on the roof.

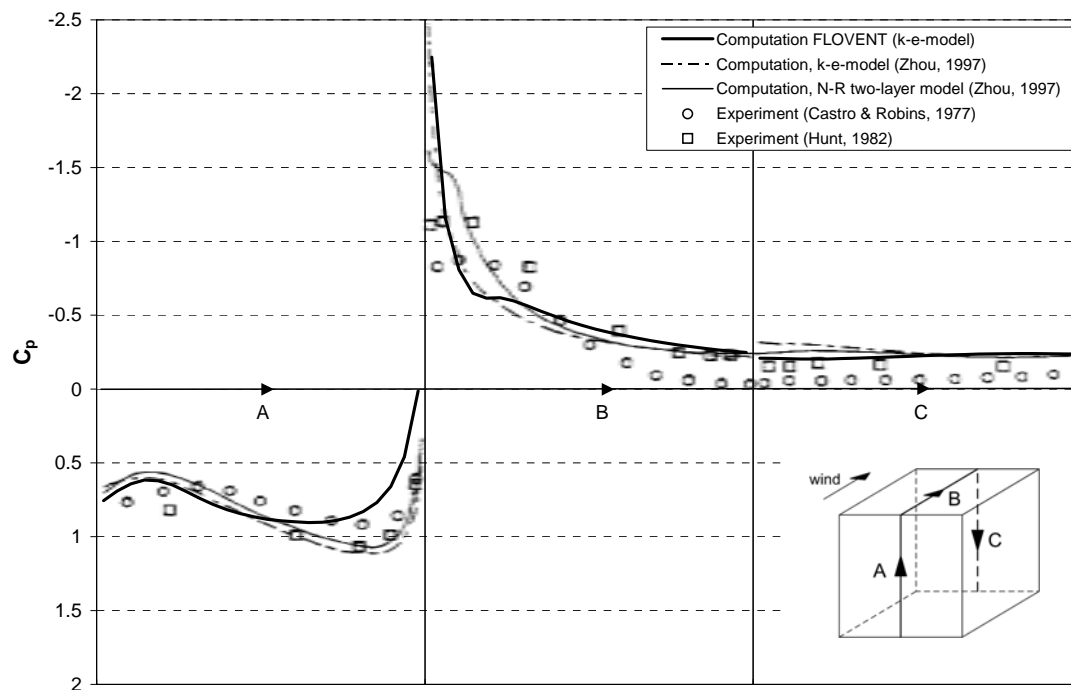


Figure 8.13: Comparison of the calculated C_p -values by FLOVENT for a wind direction of 0° with earlier computations and experiments. (Source: Reprinted from Publication Journal of Wind Engineering and Industrial Aerodynamics, Vol. 72, Zhou Y., Stathopoulos T., A new technique for the numerical simulation of wind flow around buildings, p. 137-147, Fig. 3, Copyright (1997), with permission from Elsevier)

Comparison for a wind direction of 45°

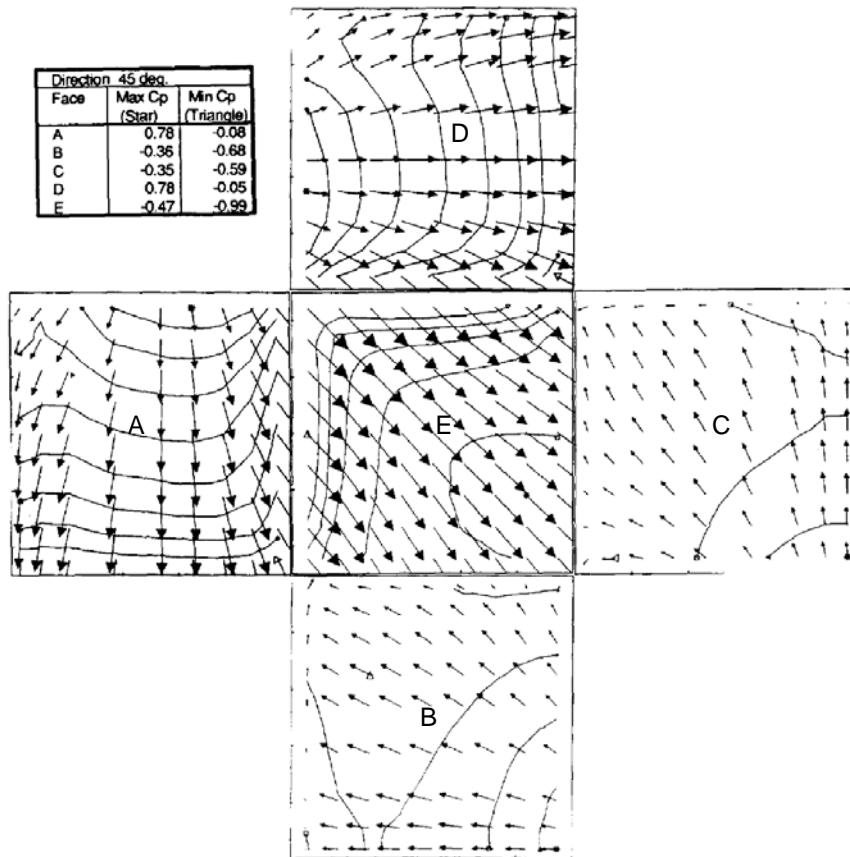


Figure 8.14: Calculated C_p -values shown as isobars and air velocities for an incident angle of 45°. (Source: Reprinted from Publication Journal of Wind Engineering and Industrial Aerodynamics, Vol. 57, Mikkelsen, A.C., Livesey F.M., Evaluation of the numerical k-e model Kameleon II for predicting wind pressures on building surfaces, p. 375-389, Fig. 5, Copyright (1995), with permission from Elsevier)

The simulation was done by keeping the wind direction and turning the cube by 45 degrees. Moreover, the same boundary condition like in the first case was chosen. Because of the orthogonal grind in FLOVENT the walls were modelled by stepped surfaces and therefore no vector plot of the air velocity could be created. Windward and leeward wall shows a sufficient agreement with the earlier simulations although the C_p -values especially at the leeward wall are slightly higher, maybe because of higher wall friction (stepped surface).

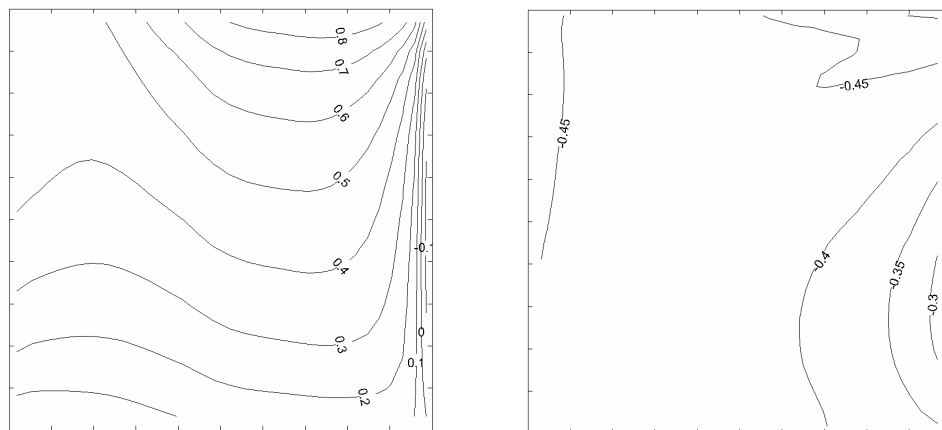


Figure 8.15: CFD calculations using FLOVENT with k-e turbulence model
 left: Calculated C_p -values of surface A/D shown as isobars. min. = -0.12; max. = 0.85
 right: Calculated C_p -values of surface B/C shown as isobars. min. = -0.51; max. = -0.29

For the roof an acceptable agreement of C_p -values was found. At some points the values are too low compared with Mikkelsen. Also the air velocity above roof is slightly different because the more distinctive outflow at the leeward walls. These flow phenomena can not be observed by the calculations of Mikkelsen.

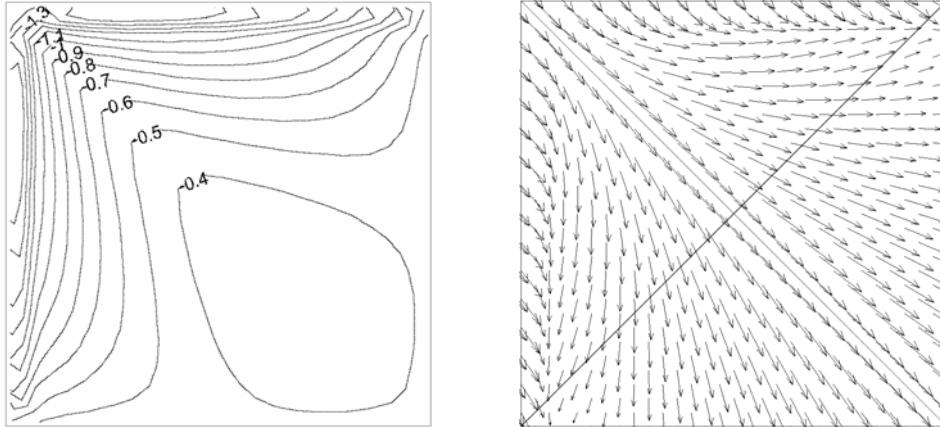


Figure 8.16: CFD calculations of surface E using FLOVENT with k - ϵ turbulence model
 left: Calculated C_p -values shown as isobars. min. = -1.64; max. = -0.32
 right: Air flow vectors near the surface

Comparison of C_p -values on walls and roofs in the centre line show a good agreement with earlier experiments and measurements. As already mentioned it can be seen in this diagram, that the C_p -values on the leeward wall (surface C) should be lower.

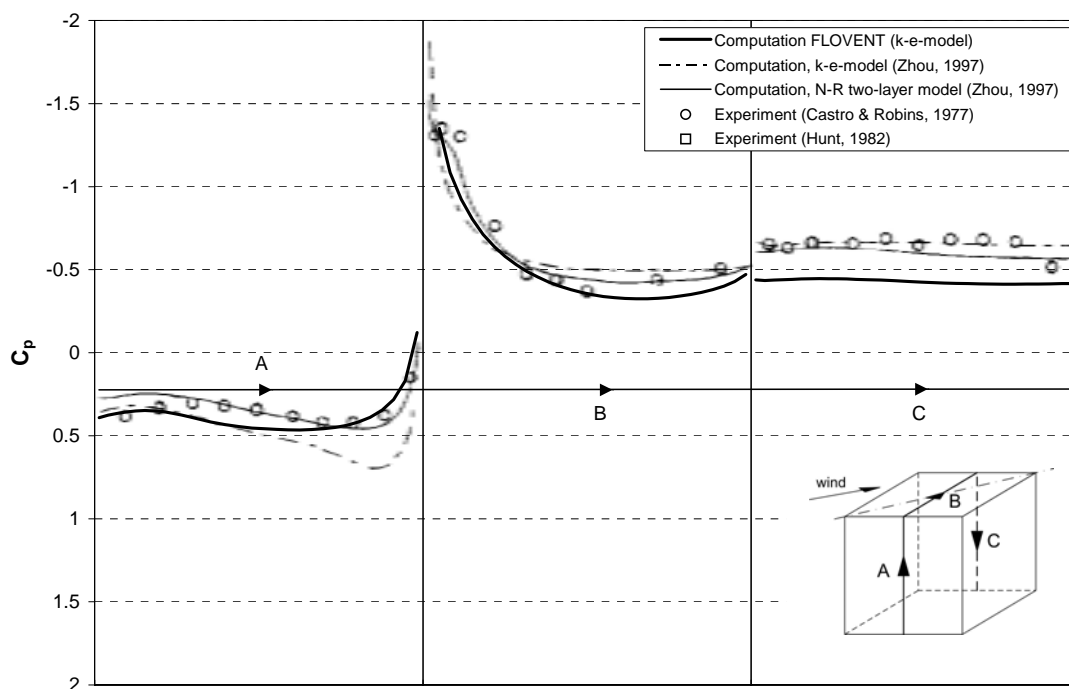


Figure 8.17: Comparison of the calculated C_p -values by FLOVENT for a wind direction of 0° with earlier computations and experiments. (Source: Reprinted from Publication Journal of Wind Engineering and Industrial Aerodynamics, Vol. 72, Zhou Y., Stathopoulos T., A new technique for the numerical simulation of wind flow around buildings, p. 137-147, Fig. 4, Copyright (1997), with permission from Elsevier)

Symmetric boundary conditions

In order to reduce the computing time the symmetry of geometry can be used to save grid cells. Depending on robustness of the air flow pattern it is not guaranteed that a correct and stable solution is found. In our case we have done calculations for the same situation with and without symmetrical boundary. It can be mentioned, that the results computed with symmetric boundaries are identical with full domain simulation.

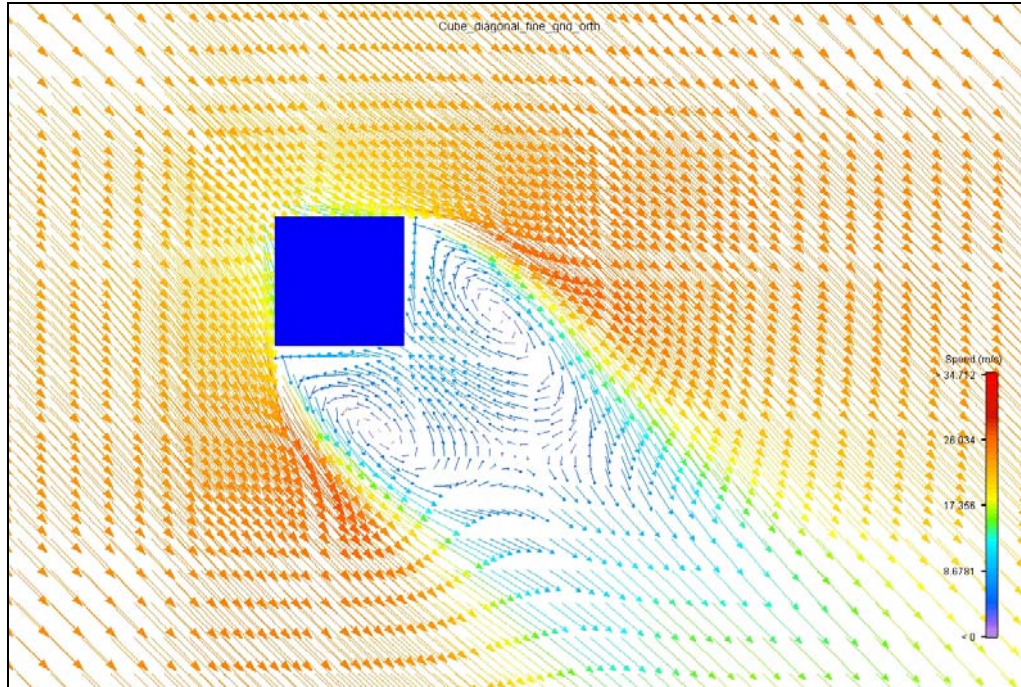


Figure 8.18: Full domain CFD simulation: Air velocity vectors on a y height of 2.5 cm

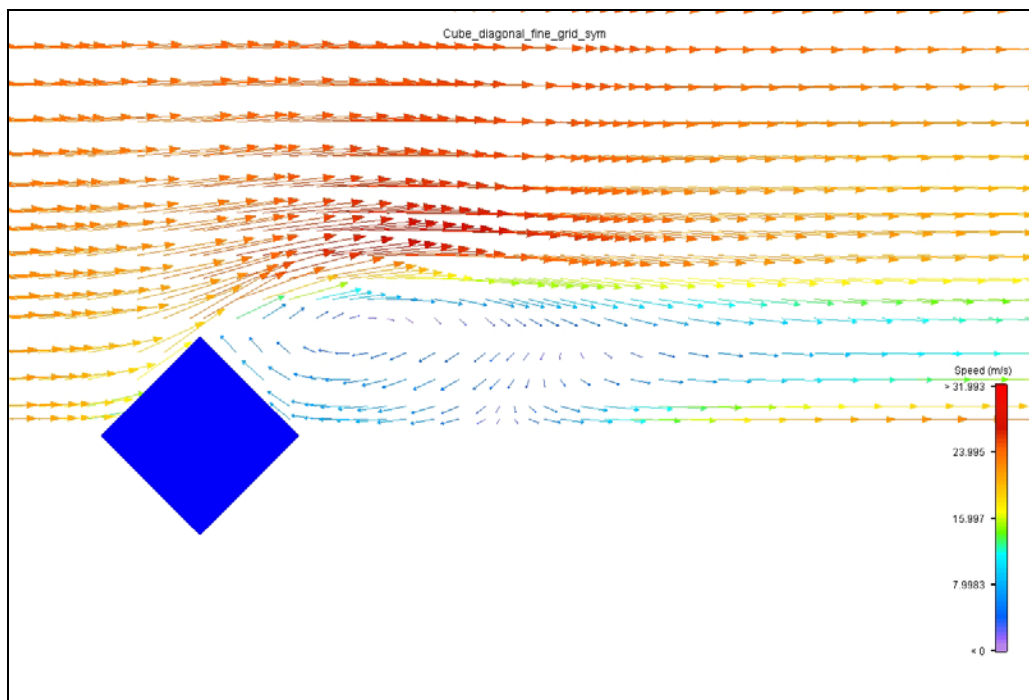


Figure 8.19: Symmetric domain CFD simulation: Air velocity vectors on a y height of 2.5 cm

8.1.4. Two and three dimensional air flow around a glass house with pitched roof

Simulation conditions

The pressure distribution in the centre line of the building surfaces was calculated using the CFD software FLOVENT, matching as closely as possible the calculation conditions used by [Oliveira et al., 2000]. According to the example a full-scale glasshouse with a length (L) of 22.6 m, a span (S) of 7 m and eaves at a height (H) of 4.15 m was defined. The pitch of the roof is 27° . Two and three dimensional calculations were carried out using the CFD software FLOVENT with k-e model. The calculation domain was chosen according to the limits set-up by Oliveira in order to get a domain independent solution. The defined domain size for two and three dimensional investigations can be seen in figure 8.20.

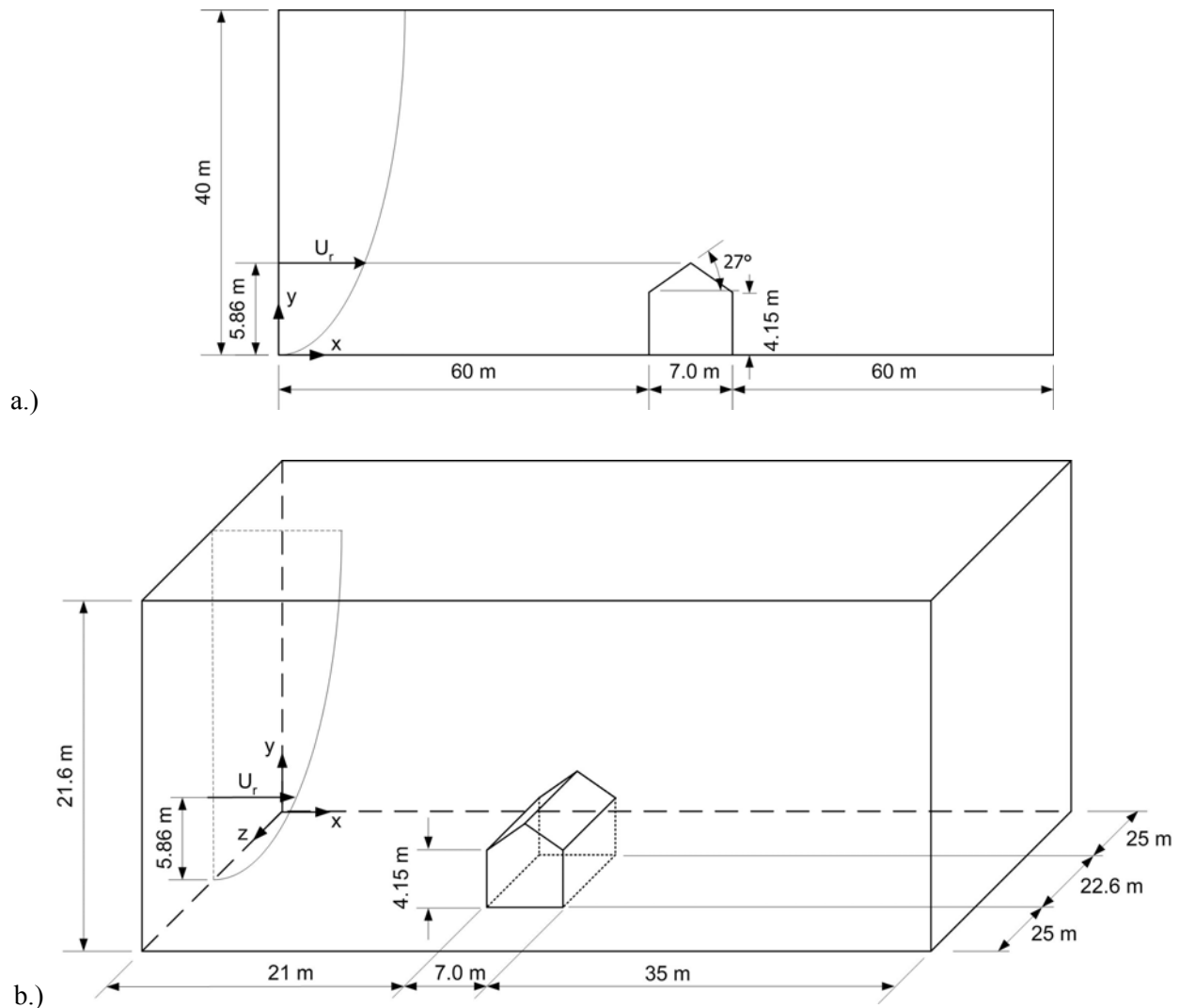


Figure 8.20: Size of the calculation domain.

a.) for two dimensional calculations; b.) for three dimensional calculations

The upstream boundary condition was a logarithmic wind velocity profile with a free-stream velocity of 9.02 m/s at ridge-height. A ground roughness parameter (z_0) of 10 mm was assumed in these simulations according to earlier experiments. This profile was modelled by twelve different shaped air outlets with increasing air velocity boundary conditions in higher regions. Figure 8.21 and figure 8.22 show the pre-set wind profile for two and three dimensional simulations.

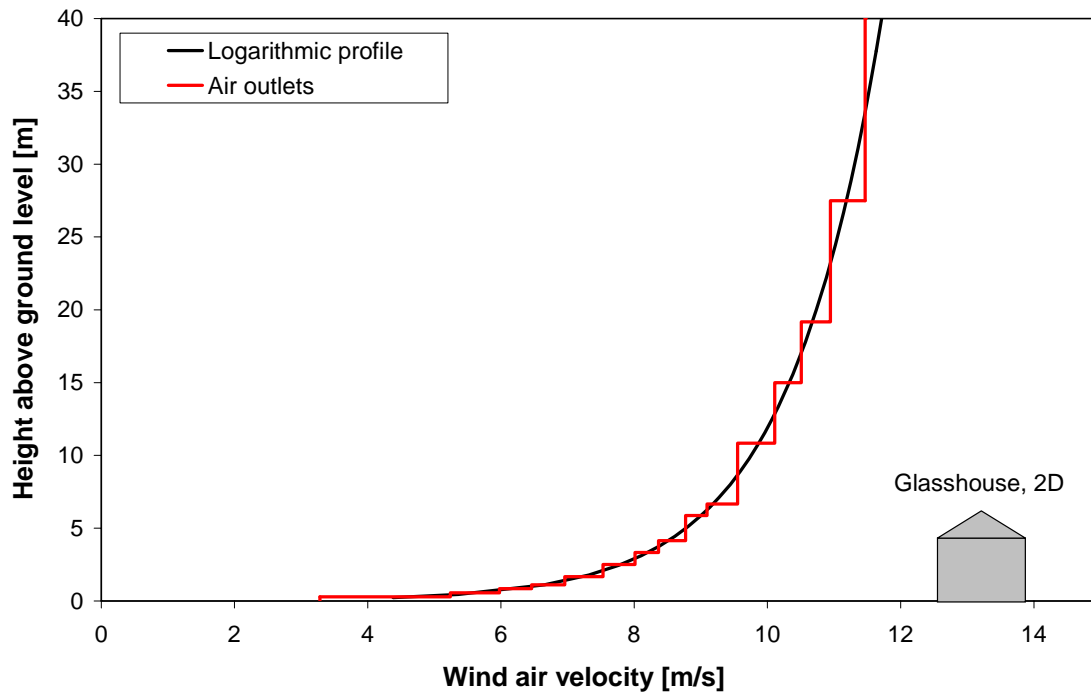


Figure 8.21: Wind air velocity profile used for the two dimensional CFD calculation. The wind was modelled by using 15 air outlets.

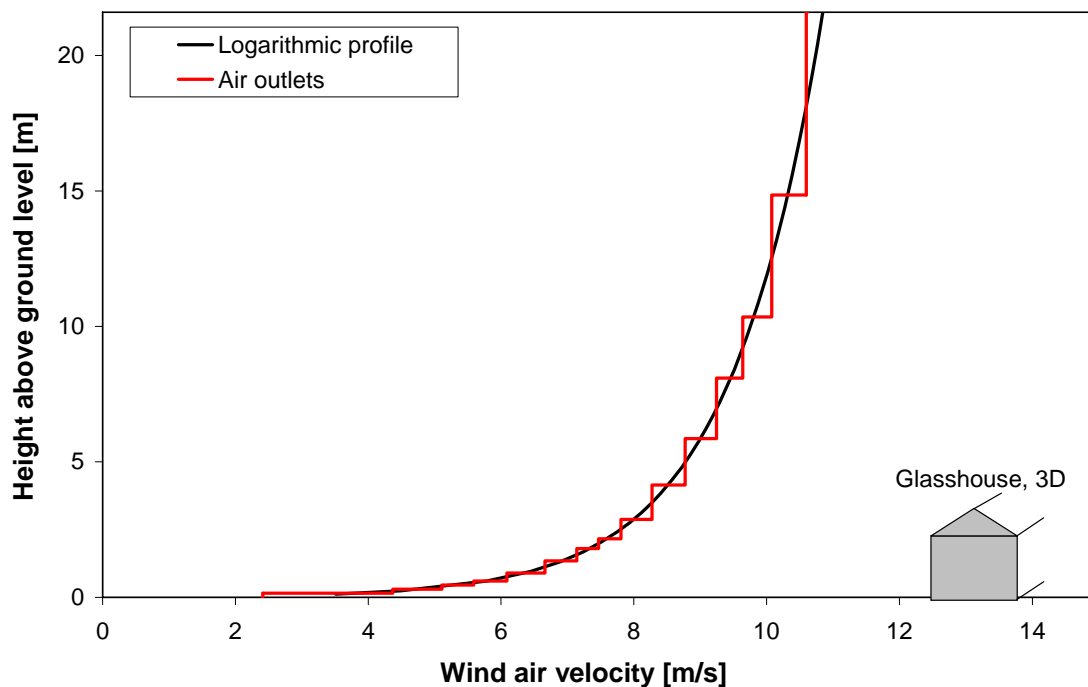


Figure 8.22: Wind air velocity profile used for the three dimensional CFD calculation. The wind was modelled by using 15 air outlets.

The downstream boundary was a open face, the top and vertical sides of the domain had symmetry conditions. Because of the high gradient, the smallest grid cells can be found near the cube surface. The table 8.2 shows a summary of the meshes used in computations. NX, NY and NZ there refer to the number of nodes in the x, y and z directions, respectively. NC refers to the total number of control volumes located within the flow domain and dx_{min} , dy_{min} and dz_{min} refers to the size (normalised with H) of the smallest grid spacing in the x, y and z directions respectively.

Table 8.2: Mesh design for two and three dimensional calculations.

Mesh	NX	NY	NZ	NC	dx_{min}	dy_{min}	dz_{min}
Medium grid 2D	232	166	-	38'512	0.0407	0.0223	-
Fine grid 2D	464	332	-	154'048	0.0177	0.0111	-
Medium grid 3D	168	128	114	2'451'456	0.0463	0.0181	0.0909

The following three figures show details of the calculation domain and the chosen grid for solving the flow problem.

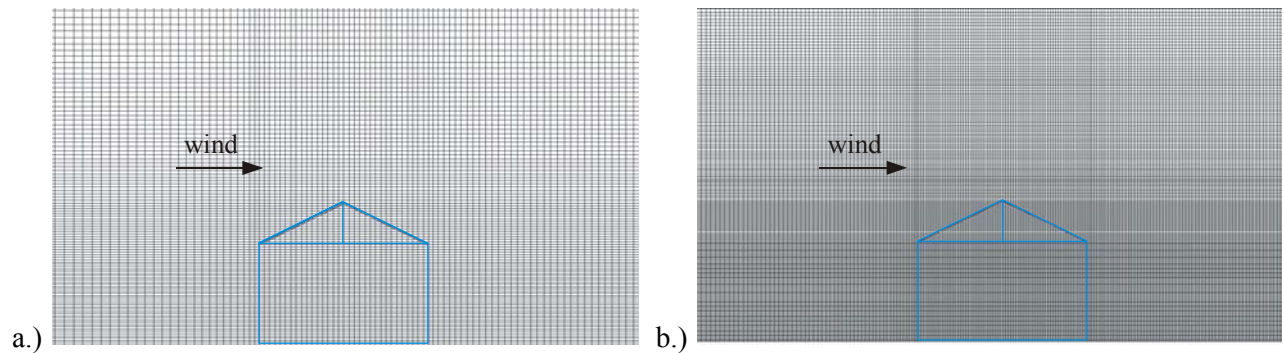


Figure 8.23: Grid design for two dimensional calculation of a full-scale pitched roof building
a.) case "medium grid"; b.) case "fine grid"

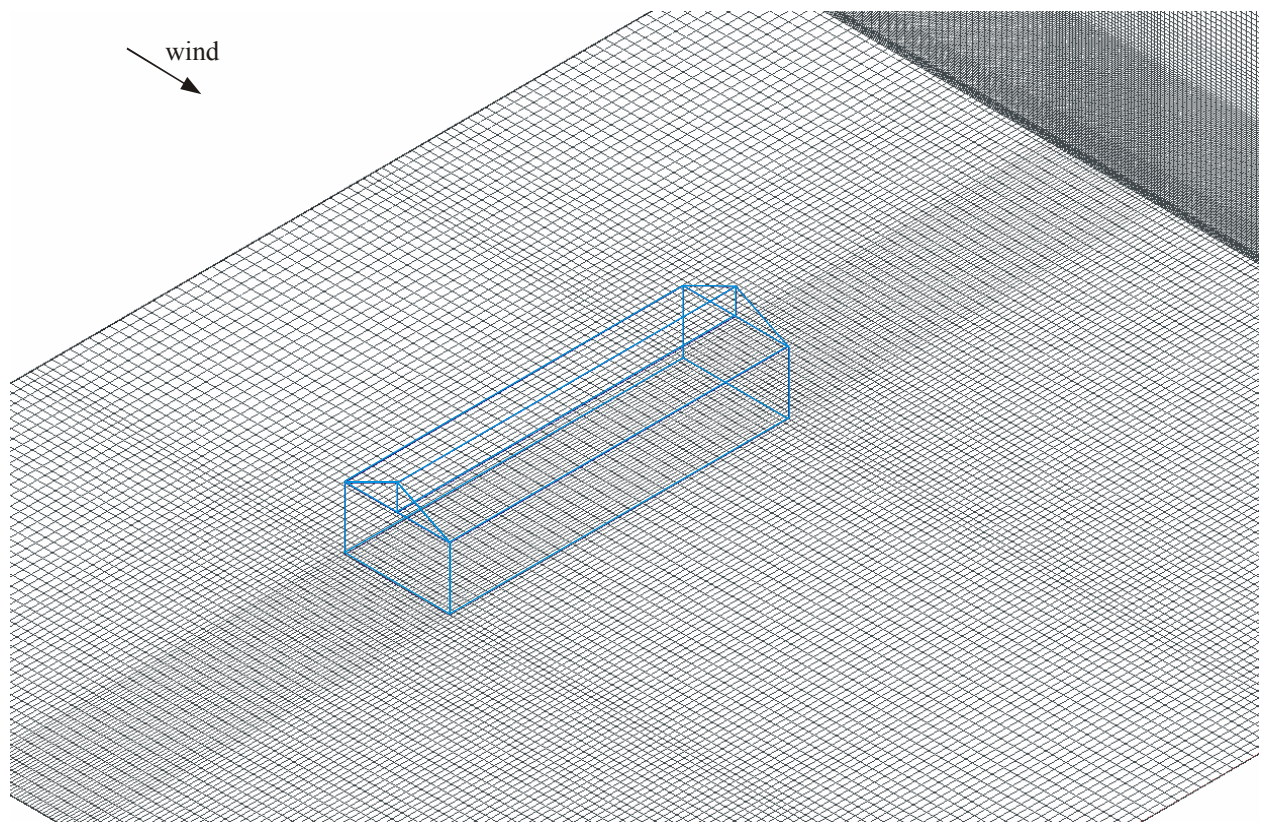


Figure 8.24: Grid design for three dimensional case "medium grid" of a full-scale pitched roof building

The pressure distribution was calculated and presented as pressure coefficients in centre line diagrams. The C_p -value has been calculated according to equation (33) considering static pressure difference, air density and reference velocity at ridge-height.

As can be seen from figure 8.25, there is a sufficient agreement between both calculated three dimensional cases. Near the eaves our C_p -values are slightly lower than the values from Oliveira. As well as that, the on site measurements are very close to our computation results in this region. In fact it can be mentioned that our results are as near as Oliveira's to the experiments from [Hoxey et al., 1991].

The two dimensional leads to small C_p -value near the building eaves because of the over-prediction of the suction pressure above the roof but agrees very well with earlier calculations. Furthermore, it can be gathered that a further grid refinement does not affect the computed results. Therefore the medium grid is close enough to predict C_p -values accurately.

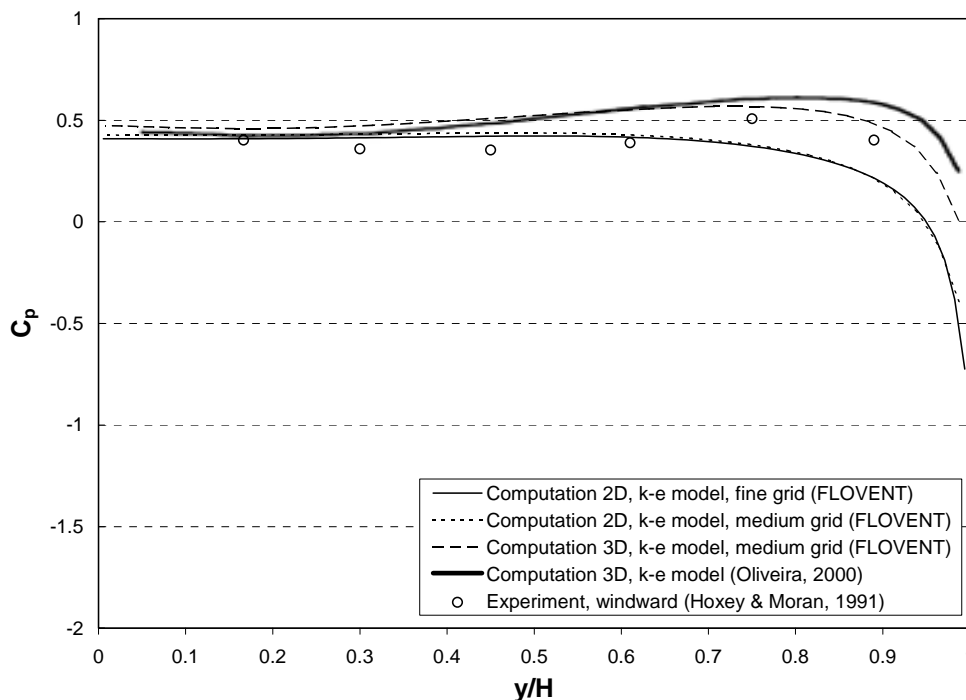


Figure 8.25: C_p -values in the centre line of the windward wall surface. Comparison between FLOVENT CFD calculations with k - ϵ turbulence model and earlier calculations from [Oliveira et al., 2000] and measurements by [Hoxey et al., 1991]

The best agreement can be found for the leeward wall. There our calculations match exactly the predictions of Oliveira. Because the blockage effect is higher in the two-dimensional case, higher air velocities above roof, and a longer reattachment zone behind the building are assumed. This leads to an over-prediction of the suction loads on the leeward wall. The closer grid in the two dimensional case does not cause any changes in the result.

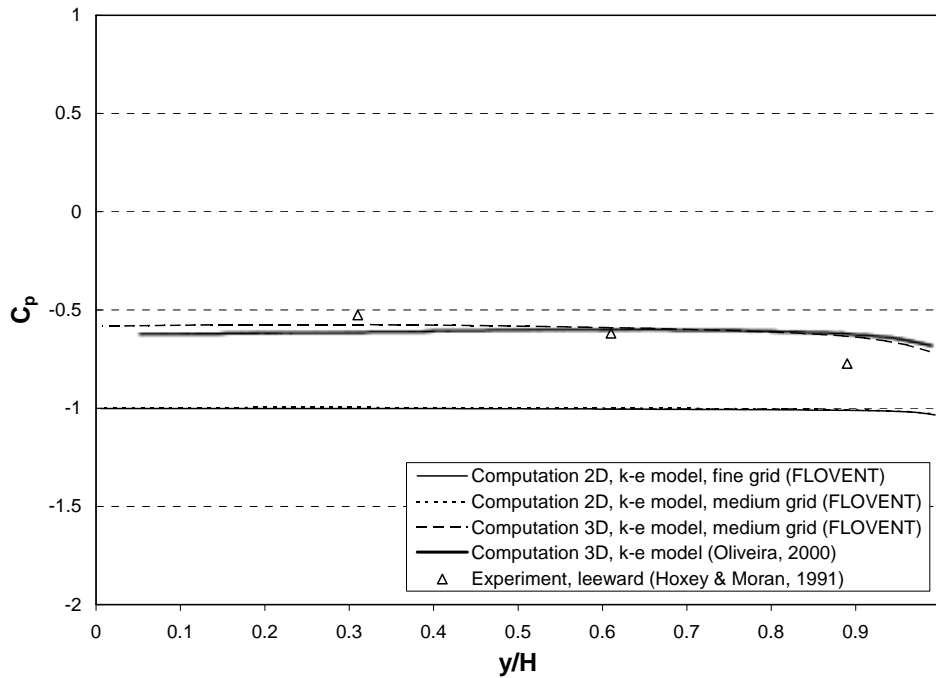


Figure 8.26: C_p -values in the centre line of the leeward wall surface. Comparison between FLOVENT CFD calculations with k - ϵ turbulence model and earlier calculations from [Oliveira et al., 2000] and measurements by [Hoxey et al., 1991]

Firstly, it can be mentioned, that our calculations correspond quite well with the experiments by Hoxey but also with earlier CFD results. The pressure drop on the ridge is not as distinct as in Oliveira's calculation, maybe because of the different grid design. The two dimensional cases show the typical under-prediction of the C_p -value because of the already mentioned higher air flow velocities.

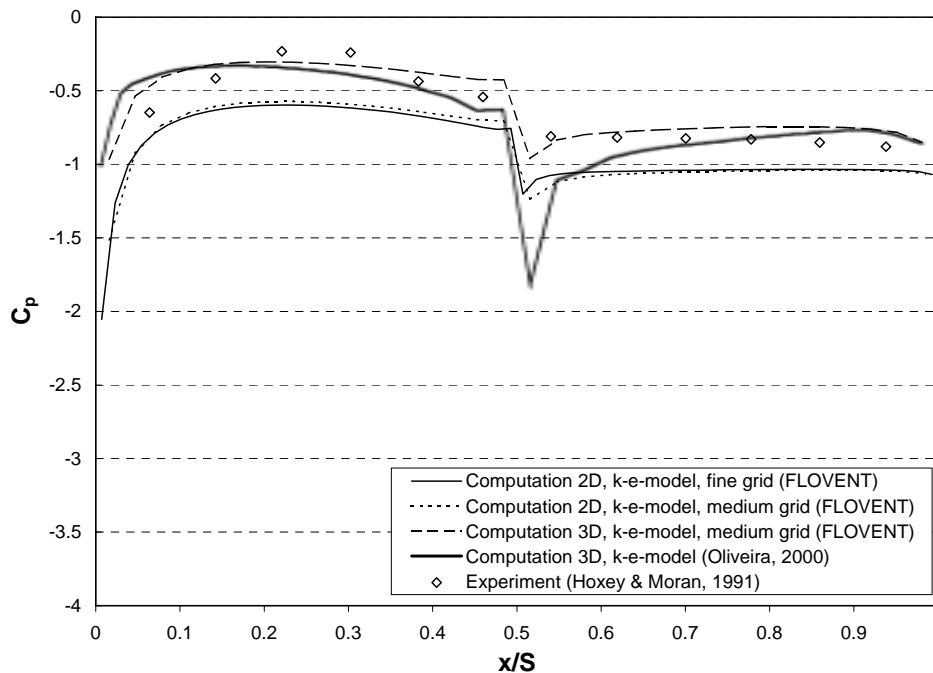


Figure 8.27: C_p -values in the centre line of the roof surface. Comparison between FLOVENT CFD calculations with k - ϵ turbulence model and earlier calculations from [Oliveira et al., 2000] and measurements by [Hoxey et al., 1991]

As can be seen from figure 8.28, the streamlines around the building are very similar in both cases. In reality a flow separation above the windward roof near the leading edge can be observed. But like already mentioned the weakness of the k-e model is found in overestimate the turbulent kinetic energy. This causes too high pressure values in regions of expected separation.

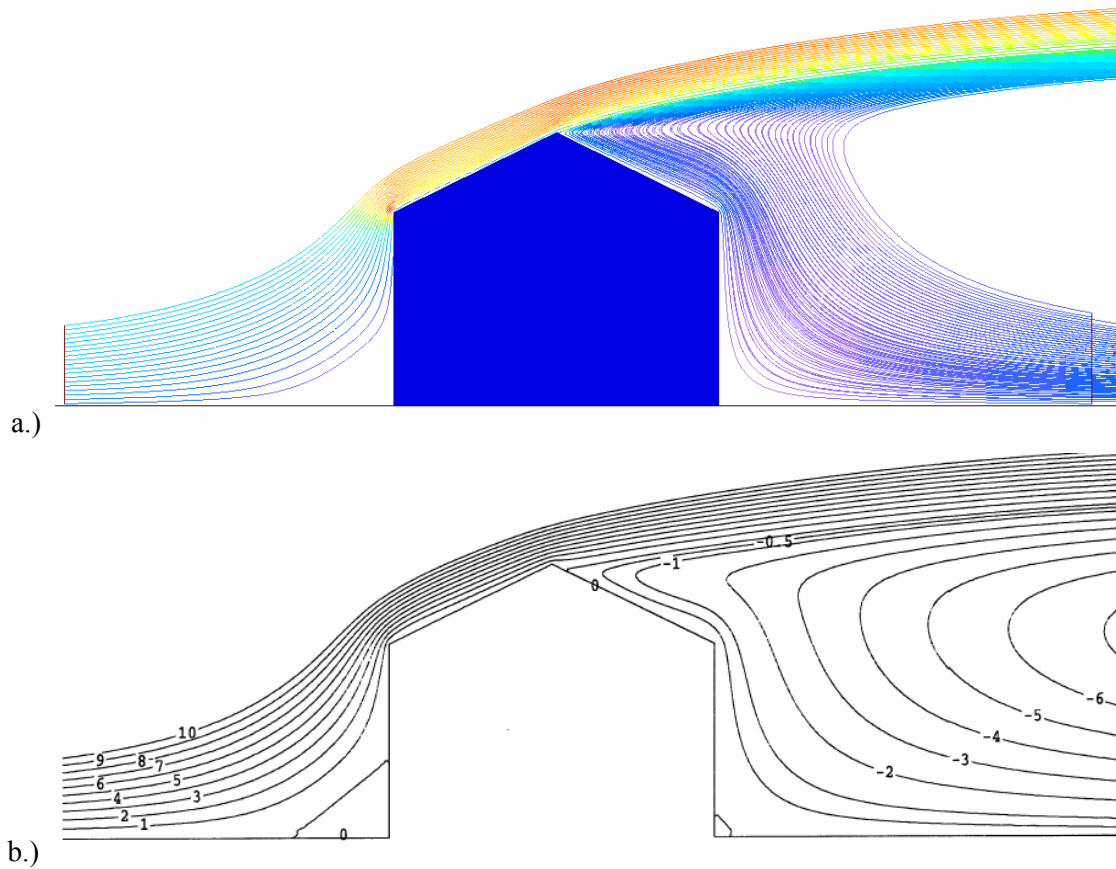


Figure 8.28: Comparison of the predicted streamlines around the building

a.) Computed results using FLOVENT with k-e turbulence model.

b.) Computed results from [Oliveira et al., 2000] with k-e turbulence model. (Source: Reprinted from Publication Journal of Wind Engineering and Industrial Aerodynamics, Vol. 86, Oliveira P.J., Younis B.A., On the prediction of turbulent flows around full-scale buildings, p. 203-220, Fig. 10a, Copyright (2000), with permission from Elsevier)

8.1.5. Typical flow phenomena

Reattachment length

The reattachment length of the vortex behind a building is a characteristic value of the flow field pattern. [Smith et al. 2001] show a diagram of a normalised reattachment length versus the Froude number, valid for a cubical building. Figure 8.29 shows measurements compared with CFD calculations of this length in function of the Froude number. The reattachment length remains constant at Froude numbers higher than 5.

The Froude number is a function of air velocity, characteristic length and gravity and can be calculated as follows:

$$Fr = \frac{v}{\sqrt{L \cdot g}} \quad (34)$$

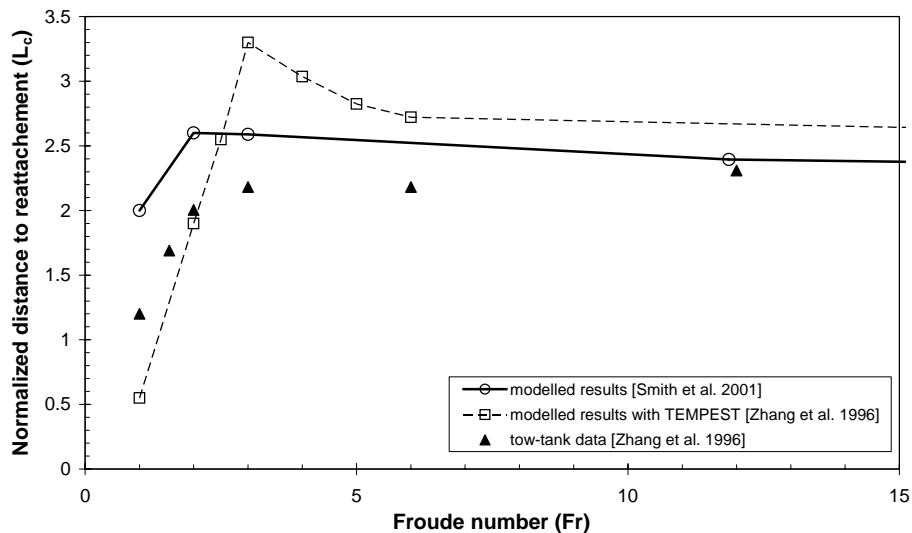


Figure 8.29: Normalised reattachment length (L_c) versus Froude number (Fr): Comparison of modelled results [Smith et al. 2001], [Zhang et al. 1996] with tow-tank data [Zhang et al. 1996]

[Baskaran et al. 1996] have done investigations on the influence of the grid arrangement on the recirculation length of cubic buildings. It has been found, that the reattachment length increases with increasing number of nodes behind the obstacle. As can be seen from figure 8.30 the normalised reattachment length in our simulation is about $L_c/S = 2.6$. This value corresponds very well with earlier simulations and experiments mentioned in figure 8.29.

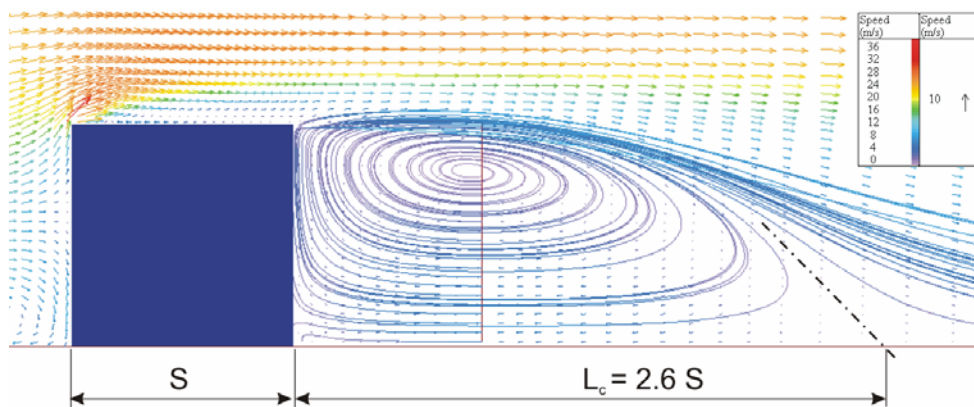


Figure 8.30: The reattachment length behind a building is a characteristic flow pattern. The figure shows the flow paths and velocities in the centreline of a cubic building 3-D for a Froude number of 35.4 modelled by FLOVENT with $k-\epsilon$ model.

Roof corner vortex

The roof corner vortex by a quartering wind flow of a rectangular building approach has been investigated in detail by [Jianming et al. 1997], using an advanced CFD method with large eddy simulation.

Flow patterns and C_p -values on roof and walls of a slope roof building have been investigated by [Oliveira et al. 2000] and by [Mikkelsen et al. 1995]. In both papers, only a normal wind flow direction is considered. In general, not many investigations have been found which deal with flows around slope roof buildings.

Experimental velocity measurements in front of a cubic building have been done by [Minson et al. 1995] with laser Doppler anemometer (LDA) especially for the validation of CFD calculations.

9. References

- Alexandrou C., Hertig J.,A. (1995). Pressure coefficients for buildings in built up environment, Wind tunnel tests report, EPFL, Lausanne
- Allard F. (ed.). URBVENT Handbook on Natural Ventilation in Urban Areas. James & James. London. 2004
- Anon, (1996). A builder's guide to selecting building materials: making informed choices to improve indoor air quality, CANMET Energy Technology Centre, Advanced Houses Program , Draft Technical Note, Canada.
- ASHRAE (2001). Fundamentals Handbook (SI)
- Awbi H.B. (1991). Ventilation of Buildings, Verlag: E & FN Spon, London.
- Baskaran A., Kashef A. (1996). Investigation of air flow around buildings using computational fluid dynamics techniques, Engineering Structures, Vol. 18, No. 11, pp. 861-875, 1996
- Basset M. (1990). Infiltration and leakage paths in single family houses- a multizone infiltration case study, AIVC Technical Note 27
- Bluyssen, P.M., Oliveira Fernandes, E., Molina, J.L (2000). Database for sources of pollution for healthy and comfortable indoor environment (SOPHIE): Status 2000, Healthy Buildings 2000. Espoo (Finland). Materials, Design and Construction. Pp. 385-390. 2000.
- Borchicchio F., McLaughling J.P., Piermattei S. (1995). Radon in indoor air, European collaborative action: Indoor Air quality & its impact on man, Report No 15, EUR 16123 EN
- Bowen, A.J. and N.G. Mortensen (1996). Exploring the limits of WASP: the Wind Atlas Analysis and Application Program. Proceedings of the 1996 European Union Wind Energy Conference and Exhibition, Göteborg, Sweden, May 20-24, 584-587.
- Bulsing P. (2000). Development of low energy ventilation systems. EU Joule TIP-Vent Task 5.2. Project report.
- CEN CR 1752 (1998). Ventilation for buildings – Design criteria for the indoor environment, CEN Report December 1998
- CEN EN 12792 (2003). Ventilation for buildings - Symbols, terminology and graphical symbols
- CEN EN 13141-1 (2004). Ventilation for buildings - Performance testing of components/products for residential ventilation – Part 1: Externally and internally mounted air transfer devices
- CEN EN 13141-5 (2004). Ventilation for buildings – Performance testing of components/products for residential ventilation – Part 5: Cowls and roof outlet terminal devices
- CEN EN 13779 (2004). Ventilation for non-residential buildings-- performance requirements for ventilation and room-conditioning systems.
- CEN EN ISO 7730 (1994). Moderate thermal environments -- Determination of the PMV and PPD indices and specification of the conditions for thermal comfort
- CEN prEN 14788 (2003). Ventilation for buildings - Design and dimensioning of residential ventilation systems, September 2003
- Chand I., Bhargava P.K., Krishak N.L.V (1998). Effect of balconies on ventilation inducing aeromotive force in low rice buildings, Building & Environment 33 No. 6 p 385-396
- Cooper A. (1993). Using CFD techniques to evaluate wind pressure distribution for air infiltration analysis, AIVC AIR Vol. 14 Nr. 2
- Cowan I.R., Castro I.P., Robins A.G. (1997). Numerical considerations for simulations of flow and dispersion around buildings, Journal of Wind Engineering and Industrial Aerodynamics, 67&68 (1997), 535-545
- De Gids W., den Ouden H P L. (1987). Three investigations of the behaviour of Ducts for natural ventilation in which an examination is made of the influence of location an height of the outlet, of the built-up nature of the surroundings and of the form of the outlet. (in Dutch with English translation available). TNO Report 1987 42p, AIVC # 2843
- De Gids W., Phaff H., Knoll B. (2000). The development of low-pressure mechanical ventilation systems LeVent, Proceedings 21st AIVC Annual Conference, „Innovations in Ventilation Technology“, paper 1, September 2000

- Dias Delgado J. F. A., Janeiro Borges A. R., Paixão Conde J. M. (1996). Wind action and temperature difference effects on the ventilation rate of a two-storey building communicating with the outside environment by a chimney, *Journal of Wind Engineering and Industrial Aerodynamics*, Volume 65, Issues 1-3, December 1996, Pages 371-381
- Dorer V., Pfeiffer A. (2002). Energy efficient and demand controlled extract ventilation systems with heat recovery, (in German: Energieeffiziente und bedarfsgerechte Abluftsysteme mit Abwärmenutzung), Final report, EMPA Duebendorf, Switzerland, May 2002.
- Dorer V., Weber A. (2005). Parameters for the performance assessment of residential hybrid ventilation systems, RESHYVENT WP 5 report, RESHVENT CD
- Etheridge D.W. (2000). Unsteady flow effects due to fluctuating wind pressures in natural ventilation design instantaneous flow rates, *Building & Environment* 35 p.321-337
- Fanger O.P. (1988). Introduction of the olf and decipol units to quantify air pollution perceived by humans indoors and outdoors. *Energy and Buildings* 12 p. 7-19
- Feustel H. et al. (2001). COMIS 3.1 - Program for modelling of multizone airflow and pollutant transport in buildings, 2001 CSTB, Sophia-Antipolis, France
- FiSIAQ (2001). Classification of indoor climate 2000, Finnish Society of Indoor Air and Climate
- FLOVENT 3.1 (1999). Computational Fluid Dynamics (CFD) programm for air flow, heat transfer and contamination control simulations within rooms or buildings, Flomerics Ltd.
- Gadilhe A. Y, Fleury B A (1989). Wind pressure coefficients: a comparison between Phoenixics and wind tunnel results. Dubrovnik, 3rd International Phoenixics User Conference, pp 183-197 (AIRBASE #NO 4985)
- Girman J R, Apte M G, Traynor G W et al (1982). Pollutant emission rates from indoor combustion appliances and sidestream cigarette smoke, *Environment International*, 1982, Vol 8, p213-221
- Gonzales M. A. (1984). On the Aerodynamics of Natural Ventilators, *Building and Environment* Vol. 19 No. 3 pp. 179-189
- Grimmond C.S.B., Oke T.R.(1999). Aerodynamic Properties of Urban Areas Derived from Analysis of Surface Form, *Journal of Applied Meteorology*, 38 p 1262-1292
- Grosso M. (1992). Wind Pressure around Buildings: a parametric model, *Energy and Buildings*, 18 101-131
- Grosso M. (1995). CPCALC+, Calculation of wind pressure coefficients on buildings, Software from Polytechnic University of Turin
- Gustén J. (1989). Wind pressures on low-rise buildings : an air infiltration analysis based on full-scale measurements; Gothenburg, Chalmers University of Technology, Division of Structural Design
- Haghighat F. (2000). Modelling air infiltration due to wind fluctuations – a review, *Building & Environment* 35 p.377-337
- Haghighat F., Donnini G. (1993). Emissions of indoor pollutants from building materials - state of the art review, *Architectural Science Review*, Vol.36, No.1, pp.13-22
- Heikkinen J., Kovanen K. et. al. (1993). Evaluation of draught risk from outdoor air intakes above the window, *Proceedings of Indoor Air '93*. Vol. 5 pp 15
- Heiselberg P., Svdt K., Nielsen P.V. (2001). Characteristics of airflow from open windows, *Building & Environment* 36 (2001) 859-869
- Hertig J. A. (1993). Analysis of Meteorological data and main Problems related to the determination of building exposure, LASEN, Lausanne
- Hertig J.A. (1990). Analysis of the influence of the topography to the exposition conditions of buildings, in French : Analyse de l'influence de la topographie sur les conditions d'exposition des batiments (, *Projektbericht ERL-B-2.1*, EPFL-LASEN
- Hoxey R.P., Moran P. (1991). Full scale wind pressure and load experiments – single-span 7.0 x 22.6 m glasshouse, Division Note DN. 1605, AFRC Engineering Research, Silsoe, February 1991
- Huang J. et al. (2004). Modelling contaminant exposure in a Single family House, *Indoor and Built Environment*, Vol. 13, Issue 1, February 2004, Pages 5 - 19

- Jiang Y., Chen Q. (2002). Effect of fluctuating wind direction on cross natural ventilation in buildings from large eddy simulation, *Energy & Building* 37 p 379-386
- Jianming H., Song C.C.S. (1997). A numerical study of wind flow around the TTU building and the roof corner vortex, *Journal of Wind Engineering and Industrial Aerodynamics* 67&68 (1997) 547-558
- Kim J., Kline S.J. and Johnson J.P. (1978). Investigation of separation and reattachment of turbulent shear layer: flow over a backward facing step. Technical Report MD-37, Dept. Mech. Engineering, Stanford University, California, 94a305, 1978
- Klein S.A. et al. (2000). TRNSYS, A Transient System Simulation Program, Solar Energy Laboratory, University of Wisconsin Madison, USA
- Knoll B. (1996). Cp-Generator, Software from TNO
- Knoll B., Phaff J.C., de Gids W.F. (1995). Pressure Simulation Program, 16th AIVC Conference, Palm Springs, USA
- Kronvall J. (1980). Air Flows in Building Components. Lund Institute of Technology, Sweden. Report TVBH-1002.
- Lawson T. (2001). Building aerodynamics, London, Imperial College Press.
- Lee B. E. et al. (1980). A method for the assessment of the wind –induced natural ventilation forces acting on low rise building arrays, *Building Services Engineering Research & Technology*, Vol 1 No.1 1980
- Lien F.S. and M.A. Leschziner M.A. (1994). Assessment of Turbulence-Transport Models Including Non-Linear RNG Eddy-Viscosity Formulation and Second-Moment Closure for Flow over a Backward-Facing Step, *Computers & Fluids*, Vol. 23, pp. 983-1004.
- Mansson LG, Svennberg S. (1992). Demand controlled ventilating systems. Source Book. IEA Annex 18. Swedish Council for Building Research D2. 1993, Stockholm, Sweden.
- Mansson LG. (1995). Evaluation and Demonstration of Domestic Ventilation Systems - State of the Art. IEA Annex 27. Swedish Council for Building Research, A12: 1995, Stockholm, Sweden.
- Meroney R.N., Leitl B.M., Rafailidis S., Schatzmann M. (1999). Wind-tunnel and numerical modelling of flow and dispersion about several building shapes, *Journal of Wind Engineering and Industrial Aerodynamics*, 81 (1999), 333-345
- Meteotest (2002). Meteo meets energy; Geo-Informationssystem for Wind Energy. see also <http://stratus.meteotest.ch/mme/winfo/>
- Mikkelsen A C, Livesey F M. (1995). Evaluation of the numerical k-e model Kameleon II for predicting wind pressures on building surfaces. *Journal of Wind Engineering and Industrial Aerodynamics* 57 (1995) 375-389
- Millet J.R., Villenave J.G., Manson L.G., De Gids W.(1998). Evaluation and Demonstration of Domestic Ventilation Systems- Volume 2: Indoor Air Quality, IEA Annex 27
- Minson A.J., Wood C.J., Belcher R.E. (1995). Experimental velocity measurements for CFD validation, *Journal of Wind Engineering and Industrial Aerodynamics*, 58 (1995), 205-215
- Moor H., (1987). Physics of building aerodynamics for ventilation rate determination. (In German: Physikalische Grundlagen der Gebäudeaerodynamik im Hinblick auf die Berechnung des Luftaustausches). (mostly based on AIC-Notes 13 und 13.1). Dübendorf: EMPA
- Mundt E., Gustavsson M., Leksell P. (2001). Vent-convector – an experimental study, *Building Services Engineering*, KTH, Stockholm, Sweden
- Murakami S. (1997). Current status and future trends in computational wind engineering. *Journal of Wind Engineering and Industrial Aerodynamics* 67&68 (1997), 3-34.
- Murakami S., Ooka R., Mochida A., Yoshida S., Sangjin K. (1999). CFD analysis of wind climate from human scale to urban scale, *Journal of Wind Engineering and Industrial Aerodynamics*, Vol. 81, No. 1-3, pp. 57-81.
- Niachou A., Santamouris M. (2004). RESHYVENT WP 10 : Urban Impact in EU, Final Report, RESHYVENT CD
- Nielsen P.V. (1992). Velocity distribution in the flow from a wallmounted diffuser in rooms with displacement ventilation. *Proceedings 3rd international conference on air distribution in Rooms, ROOMVENT '92*
- Olesen B W, Parsons K C. (2002). Introduction to thermal comfort standards and to the proposed new version of EN ISO 7730, *Energy and Buildings*, Volume 34, Issue 6 (July 2002), Pages 537-548

- Oliveira P.J., Younis B.A. (2000). On the prediction of turbulent flows around full-scale buildings, *Journal of Wind Engineering and Industrial Aerodynamics*, 86 (2000), 203-220
- Orme M., Leksmono N. (2002). Ventilation modelling data guide, AIVC Guide 5, AIVC CD December 2002
- Orme M., Liddament M., Wilson A. (1994). An Analysis and Data Summary of AIVC's Numerical Database, AIVC Technical Note 44
- Orme M., Liddament M., Wilson A. (1998). Numerical Data for Air Infiltration & Natural Ventilation Calculations, Air Infiltration and Ventilation Centre (AIVC), Coventry GB
- Phaff J.C. (1992). Importance of Cp-values in ventilation models, IEA A23, TNO Delft
- Plate E.J., Kiefer H. (2001). Wind loads in urban areas, *Journal of Wind Engineering and Industrial Aerodynamics* 89 1233-1256
- Recknagel H., Sprenger E., Schramek E.R. (2001). Handbook of heating and air conditioning technology, (in German: Taschenbuch für Heizung- und Klimatechnik), Edition 2001/02.
- Reichel D. (1996). Effectivity of air handling units, (in German: Wirksamkeit von Lüftungsgeräten), Fraunhofer IRB Verlag. Bau- und Wohnforschung F2301.
- Reichel D. (1999). Controlled air supply in nearly airtight buildings with decentralized ventilation provisions, (in German: Zur Zuluftsicherung von nahezu fugendichten Gebäuden mittels dezentraler Lüftungseinrichtungen), Dissertation TU Dresden.
- Richter W., Reichel D. (1998). Investigations of the air tightness in solid constructed multifamily buildings, (in German: Untersuchungen zur Luftdichtigkeit von Mehrfamilienhäusern in massiver Bauweise), gi 119 (1998) Heft 5
- Rubinstein, R.Y. (1981). Simulation and the Monte-Carlo Method. Wiley, New York
- Sakamoto H., Arie M. (1982). Flow around a cubic body immersed in a turbulent boundary layer, *Journal of Wind Engineering and Industrial Aerodynamics*, 9 (1982), 275-293
- Santamouris M., Klistikas N., Niachou A. (2001a). Ventilation of street canyons and its impact on passive cooling design, University of Athens, Group buildings environment studies, Athens
- Santamouris M., (2001b). Wind patterns in Urban Environment, Chapter 3 of: Energy and climate in the urban built environment, James & James, London ISBN 1-873936-90-7
- Santamouris M., Asimakopoulous D. (1996). Passive Cooling of Buildings, James & James (Science Publishers), 1996, ISBN 1-873936-47-8
- Santamouris M., et al. (2000). On the impact of the urban environment on the potential of natural ventilation., 21st AIVC Conference, The Hague, Netherlands
- Sawachi T., et.al. (1996). Evaluation of thermal comfort impact of direct air supply in winter. *Proceedings of Indoor Air '96*. Vol. 3. 1996. pp 1087-1092.
- Sawachi T., Hironao S. (1997). Evaluation of thermal comfort impact of direct air supply in winter, part 2. Comparison of different ways of air supply to exhaust only ventilation. 18th Annual AIVC Conference, Athens, Greece, Sept. 1997
- Schälin A., Qingyan C., Moser A., Suter P. (1994). Room air flow atlas, Energy relevant airflows in buildings, (in German: Raumströmungsatlas, Energierrelevante Luftströmungen in Gebäuden (ERL)), Dokumentationsreihe für die Praxis Nr. 4, Swiss Office of Energy and ClimaSuisse.
- Scholze J. (1994). Acoustic and aerodynamic properties of outdoor air transfer devices, (in German: Akustische und strömungstechnische Eigenschaften von Aussenluftdurchlässen), *Bauphysik* 16 (1994), Heft 1
- Smith W.S., Reisner J.M., Kao C.-Y.J. (2000). Simulations of flow around a cubical building: comparison with towing-tank data and assessment of radiatively induced thermal effects, *Atmospheric Environment* 35 (2001) 3811-3821
- Socket H. (1984). Aerodynamics of buildings (in German: Aerodynamik der Bauwerke), Vieweg
- Steinemann U., Tanner C. (1995). Measurements of air tightness in single family houses, terraced houses and multi-family houses, (in German: Messwerte zur Luftdurchlässigkeit von Einfamilienhäusern, Reiheneinfamilienhäusern und Mehrfamilienhäusern), NEFF- Projekt 226 - Phase 3.

- TIP-Vent (2001). Towards Improved Performances of mechanical Ventilation systems.
EU programme: Non Nuclear Energy Programme JOULE IV.
- Vickery B.J., Karakatsanis C. (1987). External wind pressure distributions and induced internal ventilation flow in low-rise industrial and domestic structures, ASHRAE Transactions 1987; 93(2) 2198-2213
- Vollebregt R., Vrans E. (2000). Design pressure difference for self adjusting air inlets, Proceedings 21st AIVC Annual Conference, „Innovations in Ventilation Technology“, paper 49
- Walker I.S. (1993). Pressure coefficients on sheltered buildings, AIVC AIR Vol.13 No.4 1992
- Walker I.S. (1996). Wind shadow model for air infiltration sheltering by upwind obstacles, HVAC&R Research Vol. 2 No. 4 1996
- Walker I.S. Wilson D.J. (1994). Practical Methods for Improving Estimates of Natural Ventilation Rates, 15th AIVC Conference Vol2 p.517
- Welsh P (1995). Flow resistance and wind performance of some common ventilation terminals, BRE, March 1995, BRE Information Paper 6/95, 3pp
- Welsh P (1995). Free-standing ventilation terminals: testing and rating, Building Serv Eng Res Technol, Vol 16, No 4, 1995, pp 189-198
- Welsh P (1995). Testing the performance of terminals for ventilation systems, chimneys and flues, BRE March 1995, BRE Information Paper 5/95, 4pp
- Welsh P. (1994). The testing and rating of terminals used on ventilation systems, proceedings of 15th AIVC Conference, held Buxton, UK, 27-30 September 1994, Volume 1, pp371-380
- Wirén B-G. (1985). Effects of surrounding buildings on wind pressure distributions and ventilation losses for single-family houses, Part 1: 1 ½ -storey detached houses, Part 2:2-Storey terrace houses, The national Swedish institute for building research, Gävle, Sweden 1985/87
- Witthauer J., Horn H., Bischof W. (1993). Indoor air quality, (in German: Raumluftqualität), Verlag C. F. Müller Karlsruhe ISBN 3-7880-7451-5
- Wolfenseher U., Gertis K. (1978). Near ground aerodynamics, presentation of the local wind conditions above built-up and not built-up surfaces based on existing literature, (in German: Bodennahe Aerodynamik, Darstellung der lokalen Windverhältnisse über unbebauten und bebauten Flächen auf Grund vorhandener Literatur, Gesundheits-Ingenieur H.9 S. 259-274, H.11 S. 321-332
- Wong N.H., Chin H.K (2002). An evaluation exercise of a wind pressure distribution model, Energy & Building, 34 p 291-309
- Wouters P., Geerinckx B., Vandaele L. (1993). The calculation of wind pressures around buildings: the determination of the wind speed to be used in the models, IAE A23 Belgian Building Research Institute
- Yongsheng Z., Stathopoulos T. (1997). A new technique for the numerical simulation of wind flow around buildings, Journal of Wind Engineering and Industrial Aerodynamics, 72 (1997), 137-147
- Zang Y. Q., Arya S.P., Snyder W.H. (1996). A comparison of numerical and physical modelling of stable atmospheric flow and dispersion around a cubical building, Atmospheric Environment 30 1327-1345
- Zhou Y., Stathopoulos T. (1997). A new technique for the numerical simulation of wind flow around buildings, Journal of Wind Engineering and Industrial Aerodynamics, Volume 72, Issues 1-3, 12 November 1997, Pages 137-147

The Air Infiltration and Ventilation Centre was inaugurated through the International Energy Agency and is funded by the following seven countries:

Belgium, Czech Republic, France, Greece, the Netherlands, Norway and United States of America.

The Centre provides technical support in air infiltration and ventilation research and application. The aim is to provide an understanding of the complex behaviour of the air flow in buildings and to advance the effective application of associated energy saving measures in both the design of new buildings and the improvement of the existing building stock.

Air Infiltration and Ventilation Centre
Operating Agent and Management
INIVE EEIG
Boulevard Poincaré 79
B -1060 Brussels - Belgium



Tel: +32 2 655 77 11
Fax: +32 2 653 07 29
inive@bbri.be
www.inive.org